WORK FUNCTION TUNING OF ELECTRODE MATERIALS WITH SMALL MOLECULE SURFACE MODIFIERS

A Dissertation
Presented to
The Academic Faculty

By

Hye Kyung Kim

In Partial Fulfillment
Of the Requirements for the Degree
Doctor of Philosophy in the
School of Chemistry and Biochemistry

Georgia Institute of Technology

August 2018

WORK FUNCTION TUNING OF ELECTRODE MATERIALS WITH SMALL MOLECULE SURFACE MODIFIERS

Approved by:

Dr. Seth R. Marder, Advisor
School of Chemistry and Biochemistry
Georgia Institute of Technology

Dr. Christoph Fahrni
School of Chemistry and Biochemistry
Georgia Institute of Technology

Dr. John Reynolds
School of Chemistry and Biochemistry
School of Materials Science and Engineering
Georgia Institute of Technology

Dr. Bernard Kippelen
School of Electrical Engineering
Georgia Institute of Technology

Dr. Elsa Reichmanis
School of Chemical and Biomolecular Engineering
Georgia Institute of Technology

Date Approved: July 19, 2018

To my parents.

ACKNOWLEDGEMENTS

Though the start of this journey began with my desire to pursue advanced education in chemistry, the course of this endeavor to be acknowledged as a Doctoral degree recipient was not on my own. The people that guided me to be able to reach milestones, taught me how to do chemistry, consoled me at my weakest moments, encouraged me to build resilience, and mentored me to question "why", were both near and far, but all reached me deep in my heart. I fully acknowledge and thank these friends, professors, and family for being the sustenance to my Ph.D. life.

First and foremost, I thank my advisor Prof. Dr. Seth Marder for the support and care he has poured upon my academic and personal life, for providing opportunities for growth, and for teaching me that there can be exceptions to rules. I am thankful for the constant reminders not for research progress, but to "eat, drink, sleep, and exercise". Next, I am indebted to Dr. Stephen Barlow for providing scientific insights and for the time and effort spent editing my manuscripts and dissertation. I thank Dr. Timothy Parker for discussing data results and how to optimize reaction conditions. I thank Dr. Denise Bale for her help in all administrative affairs.

I thank the surface modification subgroup who have helped shape my understanding and practice of surface science – Dr. O'Neil Smith, Dr. Anthony Giordano, Dr. Sergio Paniagua, Dr. Rebecca Hill, Dr. Siyuan Zhang, and Federico Pulvirenti. I thank those who have helped me to become a better chemist – Dr. Junxiang Zhang, Dr. Raghunath Dasari, Dr. Yadong Zhang, and Dr. Iryna Davydenko. I also thank the rest of the Marder group members and visiting scholars for support.

I thank Prof. Bernard Kippelen as my committee member and for allowing me to utilize his equipment I thank Prof. Christoph Fahrni as my committee member and collaborator, Dr. Thomas Morgan, and Abraham Jordan for graciously providing me with compounds. I thank Prof. Elsa Reichmanis and Prof. John Reynolds for serving on my committee and providing excellent feedback. I thank Dr. Alexander Hyla and Prof. Jean-Luc Brédas for their collaboration with computational insights. I thank Felipe Larrain and Dr. Canek Fuentes-Hernandez as collaborators, along with the Kippelen group members for useful discussions and helping me use their equipment. I thank Prof. Joseph Perry and the Perry group members for allowing and helping me use their equipment.

Finally, my sincere thanks to friends and family who believed in me and my potential to be more than I aspired to be.

TABLE OF CONTENTS

LIST OF TABLES

LIST OF FIGURES

LIST OF SYMBOLS AND ABBREVIATIONS

EA	Electron Affinity
FTIR	Fourier Transform Infrared Spectroscopy
IR	Infrared
IRRAS	Infrared Reflection-Absorption Spectroscopy
ITO	Indium Tin Oxide
KP	Kelvin Probe
NMR	Nuclear Magnetic Resonance Spectroscopy
OLED	Organic Light Emitting Diode
OP	Oxygen Plasma
SAM	Self-Assembled Monolayer
UHV	Ultra-High Vacuum
UPS	Ultraviolet Photoelectron Spectroscopy
VBM	Valence Band Maximum
WF	Work Function
XPS	X-ray Photoelectron Spectroscopy

SUMMARY

In this thesis, four different classes of compounds were studied as candidates for work function reducing surface modifiers on ITO and gold. Amine containing *N*-oxide and N-heterocyclic carbenes are studied in addition to sulfur containing phosphine sulfide phosphines and N-heterocyclic thiones and selones. Within each study, a group of compounds were selected to compare components such as side groups, backbone – saturated or unsaturated, number of atoms/compound – N/amine oxide, the relative basicity – based on N–C–N bond angle, or P=S units per phosphine, and change of substitution – sulfur versus selenium.

Each study was approached from a top down point of view with the first question being 1) can these compounds bind to the surface and 2) can they reduce the work function of the modified substrate. Once these initial questions were answered, optimization procedures were undertaken in attempts to acquire thin films while retaining low work function. XPS and UPS were heavily utilized to optimize the conditions and examine the relationships stated above.

Three of the studies in this thesis demonstrate the first examples of experimentally measured work function values of planar gold surfaces treated with those classes of compounds, being the N-heterocyclic carbenes, N-heterocyclic thiones and selones, and phosphine sulfide phosphines. These compounds, as will be further highlighted in the respective introduction sections are traditionally metal ligands. Thus, these studies, in part, demonstrate the transition of coordination ligands into surface modifiers to tune electronic properties favorable for metal/organic interfaces.

CHAPTER 1
INTRODUCTION AND BACKGROUND

This chapter aims to outline the field of surface science as it pertains to organic electronic and optoelectronic devices, and relevant to materials chemistry concepts associated with this area. First, a background to the electronic properties of surfaces and the tunable parameters is examined. Then, the motivation for studying and applying surface modifiers on planar metals and metal oxides is discussed. Finally, several key surface analysis techniques and instrumentation background relevant to the thesis are presented.

1.1 Materials Chemistry and Device Operation

1.1.1 Current Organic Based Electronic Technology

Organic based electronic technologies have come a long way from their initial introduction.[1,2] Research and development in the field, in recent years, have resulted in important discoveries and have led to consumer products. Large-panel TV displays,[3] chromogenic smart materials,[4] and flexible clothing and textiles[5] based on organic light emitting diodes (OLEDs) have been demonstrated. The adoption of, and in some cases, transition to OLED displays in the market shows how much the technology has improved to compete with liquid-crystal displays.[6] In addition, organic field effect transistors (OFETs) can be utilized in sensors,[7] and integrated optoelectronic devices such as switching elements in displays.[8]

Organic photovoltaics (OPVs) is also a technology that has been extensively studied over the years, with the promise of low-cost solar energy harvesting due to the compatibility with roll-to-roll printing.[9] To date, while inorganic photovoltaics are still

superior in terms of efficiency, they are fixed to rigid and heavy designs. As opposed to semiconducting devices made from inorganic crystalline materials, organic semiconductors possess benefits such as ease of processability, and flexibility in architecture and design. While the ability to use organic materials also enables a greater diversity in the choice of materials, it in turn breeds new scientific questions when new layers are deposited upon the other. Thus, to improve OPVs for example, understanding the effects of degradation,[10] effects of introducing new acceptor materials,[11] donor materials,[12] and interfacial materials[13] are critical steps in the future of this field.

Specifically, this thesis focuses on understanding the electronic and physical properties at the interface of the electrode and semiconducting material. As will be described in detail in 1.2, the electrode either injects or collects charge carriers (electrons or holes, the latter of which represents an absence of an electron) into or from a semiconducting material and this process needs to be optimized to improve the overall device efficiency. In the following sections, the factors leading to efficient charge injection and collection at interfaces and important terminology to understand the tunable parameters are presented. Finally, the crux of the thesis, how surface modification can help improve the interface energetics, is explained.

1.2 Energy Levels and Photovoltaic Operation

Electronic levels and frontier orbitals govern device behavior because these levels define the electronic structure of materials and their interfaces with other materials (or to the outside world). The relative positions of these energy levels, or interface energetics, also control charge injection/collection and transport across interfaces. Therefore, defining the energy levels and basic concepts pertaining to charge injection/collection and transport

helps to identify the impediments to efficient behavior, and provides an avenue to improve these processes. This section focuses on energy bands, metal-semiconductor contacts, and transport properties to lay the ground for the following discussions.

1.2.1 Electronic Energy Levels

The transport levels, transport gap, vacuum level, work function, electron affinity, and ionization energy are discussed below (Figure 1.1). More extensive discussions of these topics can be found in these references.[14-18]

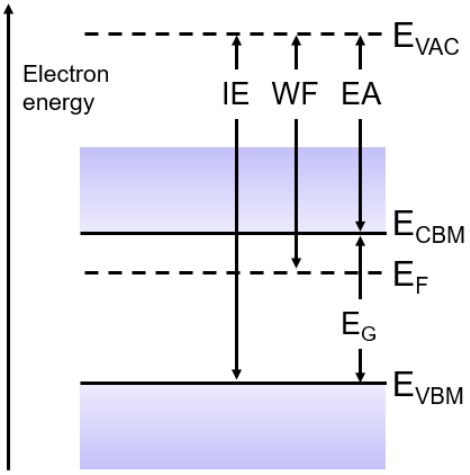

Figure 1.1. Schematic energy diagram of a semiconductor with flat bands to the surface defining the important energy levels in a solid. Pictured are the ionization energy (IE), work function (WF), electron affinity (EA), energy gap (E_G), vacuum level (E_{VAC}), conduction band minimum (E_{CBM}), Fermi level (E_F), and valence band maximum (E_{VBM}). Image is adapted from literature.[18]

1.2.1.1 Transport Levels and Transport Gap

Solid-state materials can be divided into three classes based on their electrical conductivity – metals, semiconductors, and insulators. The available energy states within materials can be modeled to form continuous bands. The lowest energy states that at 0 K

are filled with electrons constitute the valence band and the higher energy states that are unfilled constitute the conduction band. The energy gap (E_G), or transport gap, or band gap, is the difference in energy between the valence band maximum (VBM) and conduction band minimum (CBM). In an ideal crystalline, trap-free semiconductor, no allowed states are found at energies that lie within the band gap.[19]

For metals, the conduction band is partially-filled, and there is no band gap. For insulators, the band gap is large enough (> 5 eV) that room temperature (300 K), the thermal energy is insufficient for having an appreciable density of electrons into the conduction band. In semiconductors, the energy gap between the valence and conduction bands is small enough that at thermal equilibrium, at finite temperature, the conduction band is partially occupied by electrons and the valence band partially occupied by holes. Both carriers can then contribute to electrical conduction.[20]

Absorption of energy to overcome the transport gap leads to promotion of an electron from the valence band to the conduction band, leaving behind a hole, a positive charge carrier, in the valence band. In a molecule, the optical gap (E_{opt}) defines the energy required for a transition from the ground state to the first excited state, where the electron and hole, or exciton, are electrostatically bound by an exciton binding energy (E_B), which is a Coulomb energy of attraction usually on the order of a few tenths of eV in π-conjugated materials.[19] The difference therefore between the transport gap and optical gap will give the exciton binding energy ($E_G = E_{opt} + E_B$).[19] Note that for the case of inorganic semiconductors, the exciton binding energy is small enough that room temperature optical excitation can lead to free charge carriers and that E_{opt} is roughly equivalent to E_G.[19]

In organic compounds, the frontier molecular orbitals are the relevant energy levels where electrons can be accepted into the lowest unoccupied molecular orbital (LUMO) and electrons can be donated from the highest occupied molecular orbital (HOMO).

1.2.1.2 Vacuum Level

The local vacuum level (E_{VAC}) of a solid is defined as the energy of an electron that is at rest just outside the surface, to no longer feel the electrostatic influence of the solid, here on out simply referred to as the vacuum level.[16] This level is sensitive to surface dipoles, atomic structure and the chemical environment of the surface.

1.2.1.3 Electron Affinity and Ionization Energy

Electron affinity (EA), or χ, is a negative quantity that defines the energy gained from an electron falling from the vacuum level to the CBM/LUMO, and ionization energy (IE) is a positive quantity that defines the energy required to remove an electron from the VBM/HOMO to vacuum level.[18] Being able to tune this energy gap via selection of appropriate materials is crucial in the design of light-emitting and light-absorbing materials. With respect to the presently defined energy levels, the transport gap can also be defined by E_G = IP - EA.

1.2.1.4 Fermi Level and Work function

The Fermi-Dirac distribution function gives the probability *f(E)* that a state of energy *E* is occupied by an electron and is given by:

$$f(E) = \frac{1}{e^{(E-E_F)/k_BT} + 1} \qquad \text{Equation 1.1}$$

where k_BT is the thermal energy (the product of the Boltzmann constant and temperature), and E_F the Fermi level. As illustrated in Figure 1.2a and c, at T = 0 K, states below the

Fermi level are filled and states above it are vacant.[20] At T > 0 K, thermal excitation causes states near and below the E_F to lose population and states near and above it to gain population. The Fermi-Dirac distribution in terms of metals and semiconductors is depicted in Figure 1.2. At T > 0 K, the Fermi-Dirac distribution function is no longer a step-like function and broadens as illustrated in Figure 1.2. In a metal, this causes states below and above near the E_F to be partially occupied (Figure 1.2b). In a semiconductor, states in the conduction band might be occupied by electrons, while states in the valence band might be occupied by holes (Fig. 1.2d).

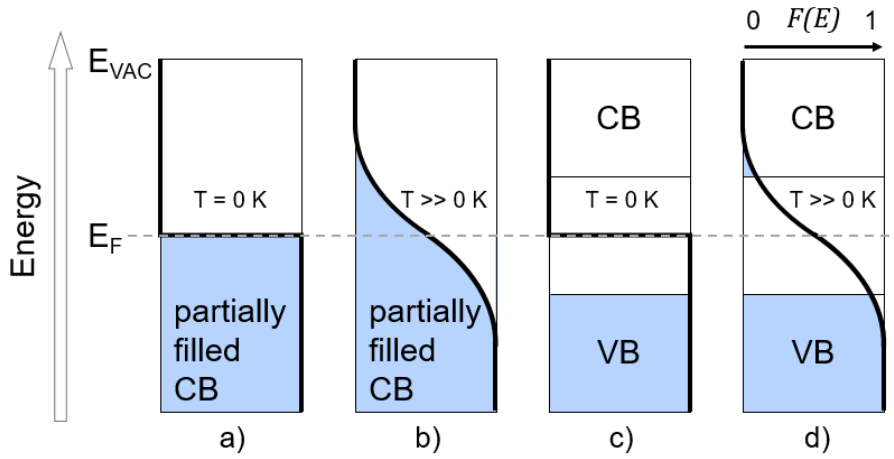

Figure 1.2. Schematic energy diagram of the band structure for metals at T = 0 K (a), at T >> 0 K (b), for semiconductor at T = 0 K (c), and at T >> 0 K (d). The Fermi-Dirac distribution is superimposed on each structure as a bold black line. Blue color represents electrons. Image is adapted from literature.[21]

In semiconductors, the Fermi level generally lies within the band gap (non-degenerate) but can in some cases be within either the conduction/valence band (degenerate) at very high electrical doping (intentionally adding impurities into a semiconductor to add electrons or holes).[22] Doping can result in either added electrons or holes to the system, increasing the number of majority charge carriers, which shifts the

position of the E_F (added electrons will raise the E_F and added holes will lower the E_F). In addition, the Fermi level position depends on other factors, including the density of states, the carrier density and doping concentration.[18]

The work function (Φ) is defined as the minimum energy required to remove an electron from the Fermi level to rest at a point just outside the solid, the vacuum level.[14, 23] The electron, therefore, transitions from being in one state in which it is in the highest occupied level of the neutral ground state to another state in which the solid is singly ionized and the electron is at rest.[24] The definition therefore can be simplified to:

$$\Phi = E_{VAC} - E_F \qquad \text{Equation 1.2}$$

The basic definitions and descriptions of transport levels, vacuum level, EA/IE, and the Fermi level have been presented. Now, these terms will be utilized in full effect to describe the interactions between the metal and organic semiconductor at the interface in the next section.

1.3 Metal/Organic Interfaces and Interface Dipoles

This section serves to outline the surface energetic effects relevant to this thesis. As described earlier in 1.2.1, the energy levels of materials dictate charge injection/collection behavior. The vacuum level and Fermi level are in turn perturbed by several factors including the cleanliness of the surface and induced surface dipoles. These effects are described and broken down to explain the parameters that can be manipulated to alter critical surface properties such as the work function. Further discussion in addition to other electrostatic effects at the interface can be found in the cited reference.[25]

1.3.1 Push-Back and Band Bending

At the interface of the metal and organic semiconductor, assuming no aligned intrinsic dipoles, there are two main interfacial effects. In the case of metals, the vacuum level is naturally raised by the spillage of electronic charge density out of the surface, which results in surface dipoles from the negative potential on the outside and positive potential in the bulk side.[26-27] This spillage can be "pushed-back" into the metal by the presence of any adsorbate. This effect leads to formation of an interfacial dipole and a shift of the virtual vacuum level (VL) Δ at the interface, with Δ defined as the magnitude of the dipole and is a negative quantity when the VL Δ is lowered, as in the case for "push-back".[14-15, 28]

The second interfacial effect occurs when the organic layer in contact with the metal is thick. When a metal and organic material are isolated, they each demonstrate flat band structures, but upon contact, there is a redistribution of charge across the interface, called band bending, to align the Fermi levels to reach electrical equilibrium. The direction of charge redistribution depends on the relative positions of the Fermi levels of the two materials and electrons will "fall" in the direction from the higher Fermi level (closer to vacuum) to lower Fermi level (farther away from vacuum) material. This charge migration leads to a net positive charge on the side where the electrons originated (higher Fermi level material) and a net negative charge on the material that received the electrons (lower Fermi level material).

For example, if the semiconductor had a higher Fermi level than the metal, then upon contact, electrons will move from the semiconductor to the metal, resulting in charge separation at the interface and formation of an electric field in the direction of electron diffusion. This sets up a built-in potential (V_{bi}) of width *W*, called the depletion region,

which is in the opposite direction as the electric field, to oppose any further motion of electrons. The band bends up in the direction of the electric field because of an accumulation of holes in the semiconductor at the interface, and in the above scenario will bend up towards the metal.[21] A diagram portraying the metal spillage and "push-back" effect is simultaneously portrayed with band bending between a metal and semiconducting material in Figure 1.3.

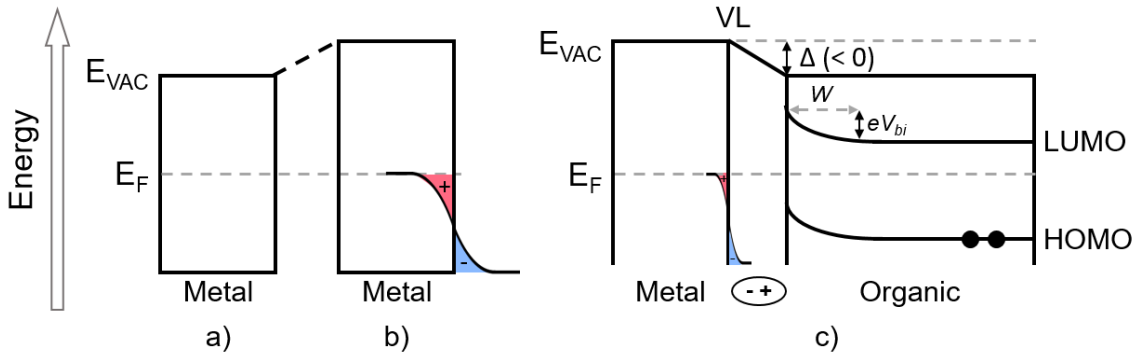

Figure 1.3. Schematic energy diagram of two interfacial effects. In a model of a metal surface without a surface dipole, the electronic states up to the Fermi level are occupied (a), due to abrupt terminations at the surface, electrons leak out of the potential well (blue denotes negative) leaving behind a positive charge (red denotes positive) and thus a surface dipole is created, which raises E_{VAC} (b), when the metal comes in contact with the organic semiconductor, some of the electrons are pushed back into the metal, which reduces the surface dipole and E_{VAC} (c). In addition, the effect of band bending from charge redistribution in the organic layer to reach electrical equilibrium with the metal when the Fermi levels align is shown. There is buildup of built-in potential within a depletion layer of thickness *W*. Image is adapted from literature.[14, 17]

1.3.2 Injection/Collection Barriers

As indicated in section 1.2.1, charge injection/collection and transport are dictated by the energy levels of the materials and their interfaces. When a metal and semiconductor come into contact, the charge redistribution of electrons can go from semiconductor to

metal (to form a Schottky junction), as was described in section 1.3.1, or from metal to semiconductor (to form an Ohmic contact).

In a Schottky junction, the $\Phi_M > \Phi_S$ (M stands for metal and S stands for semiconductor) which leads to a Schottky barrier (Φ_{Bn}). This type of contact is not favorable because there is an energetic barrier that must be overcome for electron flow from the metal to the semiconductor (when an external bias is applied).

In an Ohmic contact, which is a low resistance, non-rectifying junction with a linear IV plot, the $\Phi_M < \Phi_S$. In Ohmic contacts, electrons flow from the metal to the semiconductor upon contact, which creates an electric field in this direction. This leads to an accumulation of electrons in the semiconductor at the interface and the bands bend up in this direction.[29] There is no Schottky barrier in this case. Ohmic and Schottky contacts are illustrated in Figure 1.4. The work function criteria listed in this section are reversed for the hole collecting/injecting contact ($\Phi_M > \Phi_S$ will lead to an Ohmic contact and $\Phi_M < \Phi_S$ will lead to a Schottky junction).

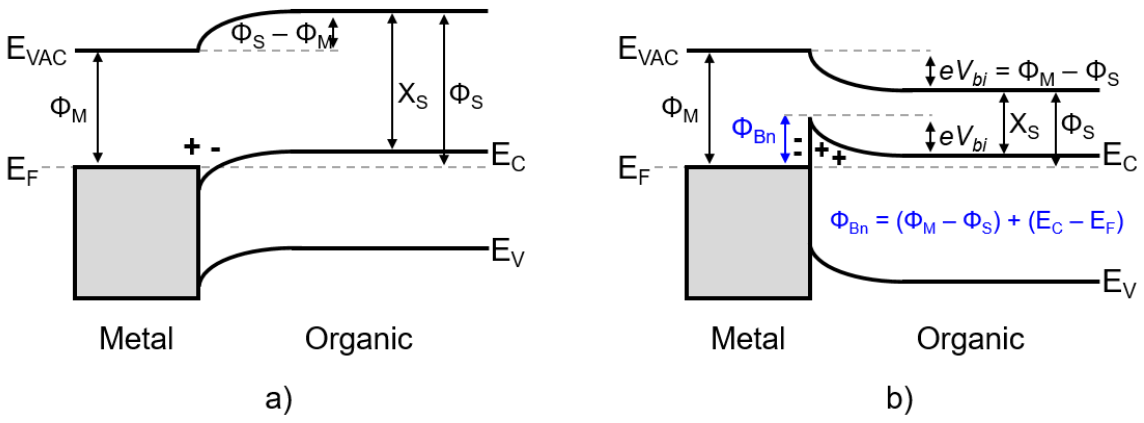

Figure 1.4. Band bending upon contact at a metal and n-type semiconductor interface is shown with an Ohmic contact (a), and Schottky contact (b). The Schottky barrier is highlighted in blue. Unlike Figure 1.3, this figure omits the interfacial dipole between the metal and semiconductor. Image was adapted from literature.[21, 30]

Therefore, at any metal/semiconductor interface, there can be a Schottky junction with an energy barrier or Ohmic contact without an energy barrier, depending on the relative work functions of the two materials. When there is a barrier, the barrier heights can be described in relation to the work function of the metal and the EA or IE of the semiconducting material. The electron-injection/collection barrier height (Φ_{Bn}) is the difference in energy between the work function of the electron-injection/collection electrode and the EA of the semiconductor (Φ_M - X_S), where WF > EA, or can also be described as (Φ_M - Φ_S) + (E_C - E_F) (Figure 1.4).[14, 31] The hole-injection/collection barrier height (Φ_{Bp}) is defined as the difference in energy between the IE of the semiconductor and the work function of the hole-injection/collection electrode, where IE > WF (not explicitly shown in any figure here but can be rationalized from the above explanations).

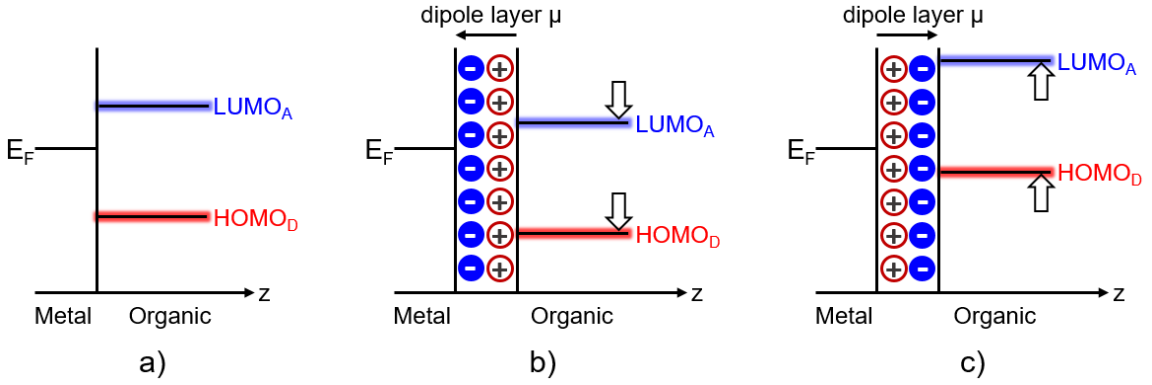

Figure 1.5 Schematic flat band energy diagram of metal/organic semiconductor contact showing the LUMO of the acceptor and HOMO of the donor (a), adding a dipolar organic layer with negative pole towards metal optimizes electron injection/collection (b). away from metal optimizes hole injection/collection. The effect of band bending and pillow effect explained earlier is omitted for clarity. Image is adapted from literature.[25]

Taking the push-back and band bending effects into account, the final positions of the transport levels of the semiconductor and the metal Fermi level will be where charge

injection/collection occurs (Figure 1.5a). Without changing either the metal or semiconductor, the charge injection/collection can be improved by introducing a dipolar interlayer in between, examples of which will be discussed in section 1.4 (Figure 1.5bc)

The dipolar interfacial materials must be thin and conducting enough to not hinder charge transport across the interface altogether. The metal work function must also be as low as possible for the electron injection/collection metal and as high as possible for the hole injection/collection metal. Thus, the energy alignment at the interface of metals and semiconductors have been discussed in addition to the potential barriers for charge transport that exist depending on the final alignment. In the next section, the types of surface dipoles that are formed at this junction will be detailed.

1.3.3 Types of Surface Dipoles

The interface dipole at the metal/semiconductor, or metal/modifier (see 1.4.2), interface can be broken down into three main components defined in Equation 1.3, where Φ symbolizes work function.[15, 32]

$$\Delta\Phi = \Delta V_{int\ dip} + \Delta V_{mol} + \Delta V_{geom} \qquad \text{Equation 1.3}$$

(1) $\Delta V_{int\ dip}$ refers to the chemical dipole induced by a partial charge transfer from the molecular layer to the surface, the potential energy step induced due to the bonding of a molecule to the surface called the bond dipole (BD), the push-back (or pillow) effect [33-34], and other charge reorganization depending on the nature of surface interactions. Also, the amount the surface dipole (from the metal spilling out electrons) that is reduced from physisorbed material is termed the interface dipole.

(2) ΔV_{mol} refers to the electrostatic potential energy change across an isolated molecular layer in vacuum (also referred to as ΔV_{vac}), due to its intrinsic dipole moment when aligned on surface.

(3) ΔV_{geom} refers to the geometric relaxations that take place when the surface interacts with the molecular layer (also referred to as $\Delta \Phi_M$). For surfaces with chemisorbed adsorbents, the surface geometry of the metal modified and these modifications induce a large shift of the electron distribution of the modified surface and can be calculated by taking the difference of the work function of a virtual surface of the bare substrate in a geometry that is produced with the adsorbents (but with the adsorbents removed) and the work function of the optimized bare substrate.

1.3.4 Metal and Metal Oxide Electrode Materials

This section introduces two materials that are used as the electron injection/collection electrode in this thesis. As described in section1.3.2, this electrode in devices requires a low work function. Examples of low work function metals include alkali earth metals such as Ca (2.9 eV)[35], Ba (2.7 eV)[36], Mg (3.68 eV)[35], and moderately high work function metals include coinage metals such as Cu (4.7 eV)[35], Ag (4.26 eV)[37], and Au (4.8 eV) [38]. However, widely used low WF metals are sensitive to moisture and oxygen. Therefore, high WF metals and metal oxides can be used in lieu of the unstable metals, and their WF can be reduced to make them suitable as electron injection/collection electrodes.

1.3.4.1 Properties of Gold (Au) as an Electrode Material

Gold is a noble metal with high resistance to corrosion that can serve as a high work function electrode in organic device platforms. It has a low electrical resistivity at 2.44 μΩ cm at 20 °C and is highly reflective.[35] Because of these properties, gold is often used in

electronics and as electrodes. Sputtered gold films that are commonly used for experimental tests may have some roughness.[39] In contrast, gold surfaces used for computational study can be chosen from any plane in the crystal lattice, which are labeled by their Miller indices. Some examples are shown in Figure 1.6, with Au(111) being the most prevalent due to its planarity.[40]

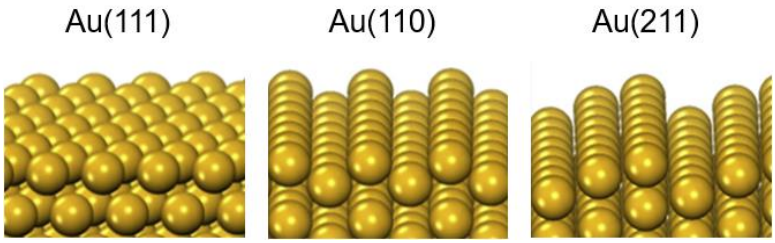

Figure 1.6. Structures of Au(111), Au(110), Au(211) surfaces. Adapted with permission from ref.[40]. Copyright 2015 Elsevier.

1.3.4.2 Properties of Indium Tin Oxide (ITO) as an Electrode Material

ITO is a transparent conducting oxide with attractive optical and electrical properties and are also used as moderately high work function electrodes. It has a low resistivity (order of 10^{-4} Ω cm) and is over 90% transparent in the visible region (for a 170 nm thick ITO film).[41] The composition of the oxide films are heterogeneous and can vary based on the deposition parameters but typically consists of polycrystalline In_2O_3 doped with 10% Sn and various oxide forms of the two metals. When In_2O_3 is annealed, oxygen vacancy sites (V_o) can form, and the neighboring In 5s orbitals at each vacancy form shallow donor states below the conduction band minimum (CBM) that trap two electrons per oxygen vacancy.[42] At low levels of oxygen vacancies, the position of the Fermi level is estimated to be 0.03 eV below the conduction band minimum and at high levels, an impurity band that overlaps with the bottom of the conduction band may form (Figure 1.7).

In addition, Sn substitution for In leads to a one electron donor level just below the conduction band. Therefore, both V_o and Sn 5s levels contribute to electron conduction.

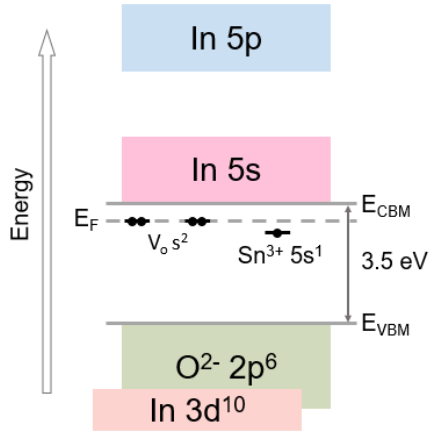

Figure 1.7. Schematic energy diagram for ITO films. Oxygen vacancy sites within the crystal structure result in doping, which creates new donor levels close to the conduction band minimum. Sn doping also introduces additional donor levels. Image is adapted from literature.[42]

As for the surface of ITO, Armstrong et al. have characterized the surface of clean ITO films that have become hydroxylated from surface reactions with water that was present in the atmosphere.[43] A schematic of the cross-section of this type of film is presented below (Figure 1.8). Therefore, the clean ITO films that are used in this thesis can be assumed to have this type of hydroxylated surface.

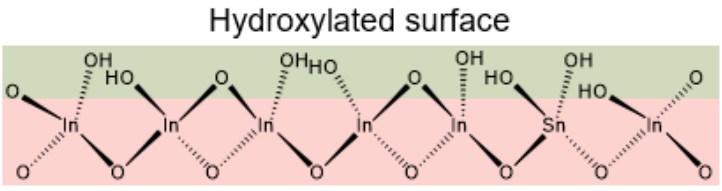

Figure 1.8. Cartoon of the cross-section of hydroxylated ITO. Image is adapted from literature.[43]

1.4 Surface Modification

1.4.1 Surface Cleanliness

Given the sensitivity of the surface in probing the electronic state, it is important to ensure pristine surfaces during analysis. In doing so, many studies have been devoted to cleaning protocol utilizing both wet and dry techniques.[44-46] Depending on the surface to be cleaned, the appropriate procedure and environment must be selected and one must be cognizant of the possible side effects. For example, abrasion of metallic surfaces such as gold or silver will lead to delamination from the glass/plastic backing. Oxidative pretreatments can be realized through UV/ozone, oxygen plasma, electrochemical oxidation, or piranha treatment to increase (or introduce) the surface hydroxyl content of metal oxides (and metals).[47-50] Therefore, it is critical to control the cleanliness of the surface and facilities dedicated to ensuring clean environments with low particulate levels and controlled airflow are widely used in the semiconductor manufacturing industry.

1.4.2 Interface Materials

Alignment of the energy levels at the metal/organic interface is directly related to device performance.[51] To control these interfacial properties, new interlayers have been introduced, which have led to enhanced wettability or modification of the materials' electronic structure.[13] Specifically, surface energy and work function can be modulated to improve the charge carrier injection/collection in such devices. In this thesis, work function reducing interface materials, specifically surface modifiers are studied and therefore, a short summary of work function reducing electron transport materials (ETM) from the literature will be detailed below. However, before the details, first, two modes of surface interactions are described.

1.4.2.1 Physisorption versus Chemisorption

Organic adsorbents can interact with the surface through physical van der Waals/dipole forces (physisorption) or through chemical hybridization in the form of covalent, metallic or ionic bonds (chemisorption).[52] Typically, physisorption is characterized by large adsorption distance, distance between the surface and the chemical, (> 3 Å) and a small adsorption energy (several tens of meV per atom), while chemisorption is characterized by small adsorption distance (< 3 Å) and a relatively larger adsorption energy (hundreds of meV or eVs per atom). In addition, the electronic structure of physisorbed material on the surface is similar to when it is in the gas phase, while for chemisorbed material, the electronic structure is strongly affected from the formation of chemical bonds to the surface. In the context of surface modifiers, physisorbed materials may form multilayers on the surface, which are less likely to form ordered monolayers and dipoles, while chemisorbed materials are limited to a monolayer but ordered formation.

1.4.2.2 Work function Reducing Transport Interlayers

Intrinsic dipoles of the interfacial materials and formation of surface interfacial dipoles can lead to vacuum-level shifting at the organic/electrode interface[53-55] Electron donating interfacial layers have been synthesized by incorporation of polar amine, phosphonate, or ethylene glycol groups on cores such as non-fullerene oligomers[56-58], fullerene derivatives[59-62], polymers[53, 63-64], and polyelectrolytes[65] (Figure 1.9).

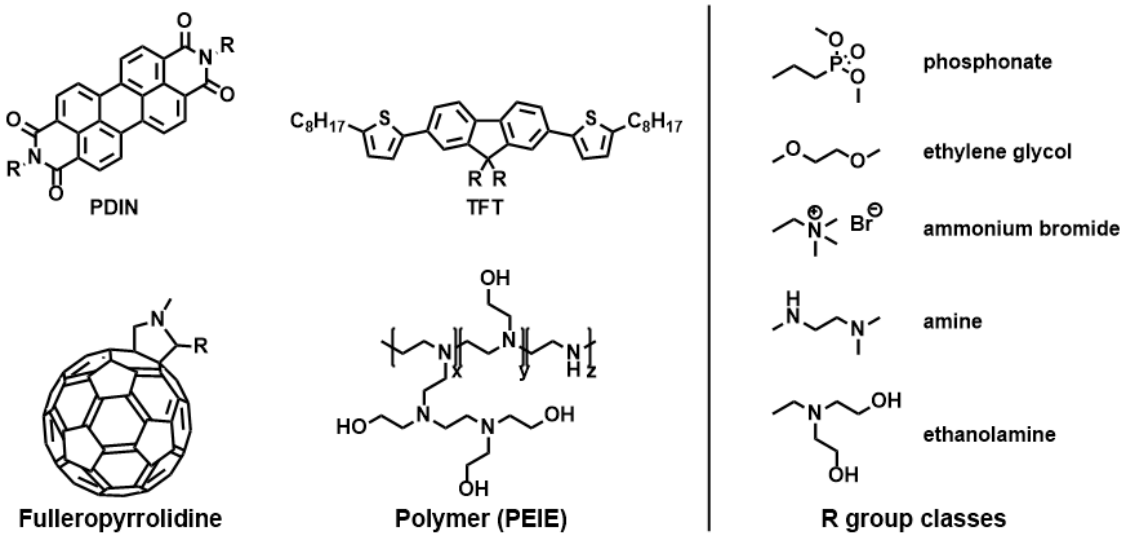

Figure 1.9. Examples of generic core structures used in electron donating interfacial layers with examples of types of R groups.[53, 57-58, 62]

In addition to these organic interlayers, transparent metal oxides (TMOs) such as TiO_2 and ZnO, and various functionalized derivatives have been incorporated as ETMs as well.[66] These types of ETMs, besides aiding energy level alignment, serve to block holes from reaching the electron injection/collection electrode.

1.4.2.3 Work function Reducing Self-Assembled Monolayers

In contrast to the ETMs described above, self-assembled monolayers (SAMs) are dipolar materials that align by highly ordered interactions, which enable scientists to effectively design structures for specific purposes.[67-69] They are usually processed on top of the electrode to be modified, whereas ETMs can be processed on top of the semiconducting organic layer and the electrode deposited on top of the ETM. The structure of a SAM is described next and examples of SAMs will be covered in section 1.4.4.

1.4.3 Self-Assembled Monolayers

As described in 1.3.2, dipolar molecular layers when deposited on a metal or metal oxide, can tune the work function to reduce the barrier heights if they exist. A common way to prepare SAMs is by immersing a clean substrate into a solution (1–10 mM) of the modifier for 12–18 h. In some cases, the SAMs are even capable of removing previously adsorbed adventitious materials from the surface. In the case of SAMs, thin films of 1–3 nm, depending on the standing height of the modifier are formed. Because the modifier is specifically oriented with one end facing the substrate and the other the organic, surface wetting at each interface must be compatible. The basic design of a SAM and the wetting improvement are pictured below (Figure 1.10).

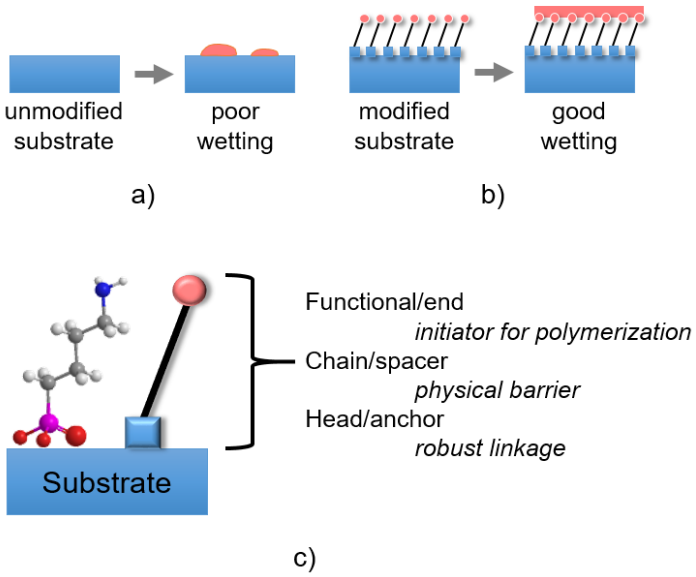

Figure 1.10. Cartoon of wetting improvement with surface modification. An unmodified substrate displays poor wetting with an organic semiconducting material (orange) (a), whereas a SAM-modified substrate displays good wetting (b). The structure of a representative SAM molecule (butylamine phosphonic acid) juxtaposed with a generic SAM molecule with the three components of head, chain and end is shown (c). Image is adapted from literature.[67, 70]

1.4.3.1 Binding Groups, Spacers, and Tails

The binding group or head/anchor group of the SAM molecule typically forms a covalent bond with (or is simply physisorbed to) the substrate (refer to 1.4.2.1). Well-studied and utilized head groups in the literature include thiols,[69, 71] silanes,[72-74] carboxylic acids,[75-76] and phosphonic acids, [70, 77-78] (see section 1.4.4). The chain or spacer serves as a physical separation between the substrate to the end/tail group. It is typically a flexible or rigid alkyl chain, saturated or unsaturated, respectively, or conjugated rings.[79-83] The tail or functional/end group of the SAM dictates the wettability of the modified substrate and it may be a dipolar group or a reactive group such as azide, that can be "clicked" to new groups and enable late stage functionalization to the surface post SAM formation.[84-86]

In this way, SAMs can provide a means to alter the work function of the modified metal/metal oxide to serve as an electrode in optoelectronic devices by introducing a surface dipole. This dipole can be broken down into the components introduced in section 1.3.3, with the covalent bond between the head group and surface constituting the bond dipole, and the spacer and/or tail (if there is a dipolar moiety in this region) with surface interaction constituting the molecular dipole. The net dipole will determine whether the work function of the modified electrode will increase or decrease.

1.4.4 Review of Monolayer Forming Materials

Although relevant SAMs and ETM for each chapter will be introduced in the beginning of each chapter, a short overview of representative monolayer forming materials on ITO and gold is presented in this section. A review of phosphonic acids (PAs) on ITO, which were heavily studied by the Marder group, can be found in the cited reference and a few key findings are presented below.[87] Second, background on thiols on gold is presented.

Phosphonic acids form robust bonds, mostly in a bidentate binding mode to ITO,[77, 88] which require harsh conditions to remove (basic wash or plasma etching),[78] and depending on the substitution pattern can either raise or lower the work function of the modified surface, thus are versatile for modifying either electrode (Figure 1.11).[87] ITO modified with benzyl phosphonic acids immersed in 10 mM ethanolic solutions for 24 h led to experimental WFs (measured by UPS) of 5.5 eV from a PA with electron withdrawing trifluoro group in the para position and 4.1 eV from a PA with two fluoro groups in the ortho positions, from oxygen plasma treated ITO (5.0 eV).[89] While the molecular dipole largely directs the overall net shift of the WF from the pretreated surface (in this case), the bond dipole from the PA anchoring groups, based on DFT calculations on ITO, increases the WF, which opposes the molecular dipoles in the opposite direction.[32] Therefore, PAs are more suitable candidates thus far for hole injection/collection electrodes.

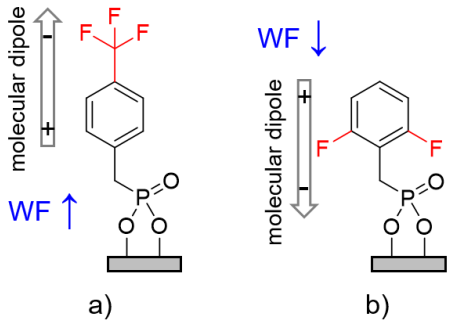

Figure 1.11. Schematic of two phosphonic acids attached to ITO and the direction of the work function change from the molecular dipole depicted with a 4-(trifluoromethyl) (benzyl)phosphonic acid (*p*-CF_3BPA), leading to an increase in WF (a) and (2,6-difluorobenzyl)phosphonic acid (*o*-F_2BPA), leading to a decrease in WF (b). Image is adapted from literature (general conformations above are from computed geometry).[87]

In addition, to control the surface energy of the modified ITO, which can aid homogeneous film formation and reduce pinhole formation, a range of PAs composed of hydrophilic or hydrophobic tails can be utilized. Large contact angles of over 100° have been recorded for ITO modified with PAs with hydrophobic tails: octylphosphonic acid with a work function of 4.6 eV and tridecafluorooctylphosphonic acid (FOPA) with 5.3 eV.[90] This shows that PA-modified ITO with different work functions can result in similar wettabilities. In the same vein, the high work function of unmodified ITO (air plasma treated 5.4 eV) can be retained while changing the wettability (from <10°) through FOPA modification (to 108°).[90]

Thiols and sulfides on gold have been studied intensively since the 1980s.[67, 91-93] SAMs with thiol and sulfide head groups have been characterized to form well packed monolayers, depending on the chain length, on gold and in the case of thiols, the reaction mechanism leading to chemisorption can be described as an oxidative addition of the S–H bond to the gold, followed by reductive elimination of the hydrogen.[67] Adsorption energy for alkanethiolates on gold have been calculated to be -5.5 kcal/mol by electrochemistry.[94]

Compared to sulfur, oxygen has been theoretically calculated to only weakly adsorb on Au(111) requiring coordination to multiple gold atoms.[95] This aligns well with the "hard" and "soft" classification of Lewis bases.[96] Bases with N, O, F donor atoms are classified as "hard" because of their high electronegativity, low polarizability, and are harder to oxidize than "soft" bases, which are of low electronegativity, high polarizability, and are easier to oxidize, which contain P, S, I, Br, Cl donor atoms. Metal atoms and bulk metal are classified as "soft" acids and they prefer to bind to "soft" bases. Therefore, even

though oxygen is in the same family as sulfur, SAMs based on alcohol head groups have not been determined to form robust bonds to gold.

Therefore, knowing that sulfur and polarizable atoms have high affinities for gold, sulfur containing compounds that were not of alkanethiolate nature were utilized as new head groups in this thesis.

1.5 Analytical Techniques

Surface sensitive techniques that can resolve the fine structures of approximately a few angstroms must be utilized to meaningfully study the surface. Below are the basic principles of the function of each technique that is utilized in this thesis. Note that physical methods such as scanning electron microscopy and atomic force microscopy were not utilized but serve as important tools that can provide morphological data.

1.5.1 X-ray Photoelectron Spectroscopy

X-ray photoelectron spectroscopy (XPS) is a surface sensitive analytical technique used to characterize and quantify the elemental composition and chemical states of a surface.[97] Physical characteristics such as film uniformity and thickness can also be studied based on the intensities of the signals. The system is under ultrahigh vacuum (UHV) with the surface being analyzed, X-ray source, and analyzer housed within (Figure 1.12). XPS utilizes the photoelectric effect by irradiating a surface with photons ($h\nu$) from a soft X-ray energy source, typically Al Kα (1486.6 eV) or Mg Kα (1253.6 eV), to eject low energy photoelectrons out of core energy levels of the atoms present on the surface (from the modifier and/or the bulk). The photoelectrons are collected by the analyzer and are separated by their kinetic energies (KE), that depend on the binding energies of the parent element and atomic energy level. The relationship is given by:

$$BE = h\upsilon - KE - \Phi_{spectrometer}$$ Equation 1.4

where BE and KE are the binding and kinetic energy of the electron, hν is the photon energy, and $\Phi_{spectrometer}$ is the work function of the spectrometer, which is used for calibration. Figure 1.13 shows a simplified view of the process, up to the electron ejection.

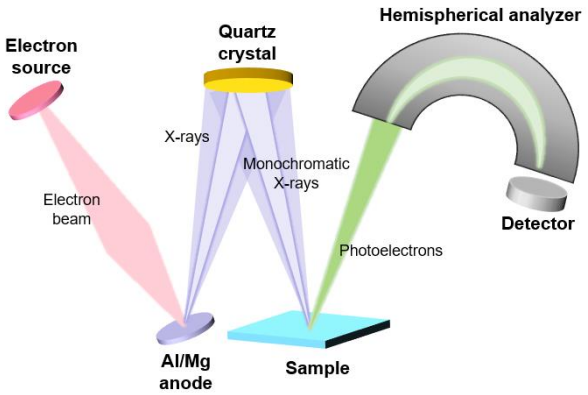

Figure 1.12. Diagram of XPS instrumentation. Electrons from the source are irradiated onto the anode, which produces X-rays. The X-rays are beamed into a quartz crystal to produce monochromatic X-rays, according to Snell's law, which are in turn irradiated on the sample. Photoelectrons ejected from the sample travel through the hemispherical analyzer to the detector. Image is adapted from literature.[97]

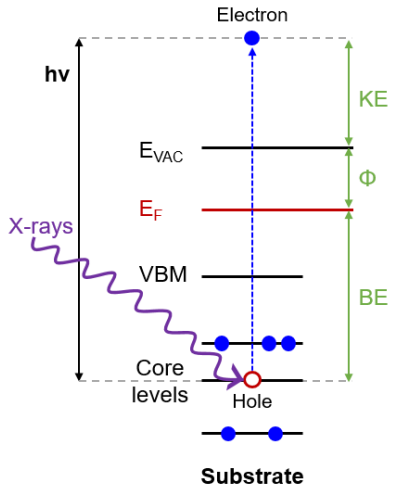

Figure 1.13. Band diagram of X-ray excitation of substrate leading to electron ejection from a core level to vacuum, leaving behind a hole. Image is adapted from literature.[97]

Due to the specific nature of binding energy, changes to the chemical environment, such as new oxidation states can be easily detected from shifts of tenths of one eV. The C 1s region for example is commonly probed to determine the presence and atomic percentages of C–C, C–O, C=O, O–C=O, and O–(C=O)–O groups. As listed, the relative binding energies increase with increased oxidation because of increased coulombic interactions between the positive nucleus and core electrons.

The depth of analysis for XPS is determined by the attenuation length (λ) of the electrons, which is related to the inelastic mean free path (IMFP). The Beer-Lambert relationship takes into account this attenuation length to provide depth (d) information given the intensity of the emitted electrons (*I*), also taking into account the angle of the surface normal (θ) by the following expression:

$$I = I_0 \exp\left(\frac{-d}{\lambda cos\theta}\right) \qquad \text{Equation 1.5}$$

where I_0 is the intensity from an infinitely thick, uniform substrate.

Accordingly, 65% of the observed signal originates from depths of < λ, 85% from < 2λ, and 95% from < 3λ. This calculates to a total detection depth limit of ~10 nm by XPS for typical core energies and hν.

1.5.2 Ultraviolet Photoelectron Spectroscopy

Ultraviolet photoelectron spectroscopy (UPS) is another UHV analytical technique and is used to determine the electronic structure of the surface through ejection of electrons from states with relatively low BEs.[97] Typically, low energy ultraviolet photons from He I (21.2 eV) or He II (40.8 eV) emission lines, discharged from a helium arc, are used to determine the work function, Fermi level, valence band maximum of the surface, and potentially valence band or filled orbital structure (Figure 1.14).

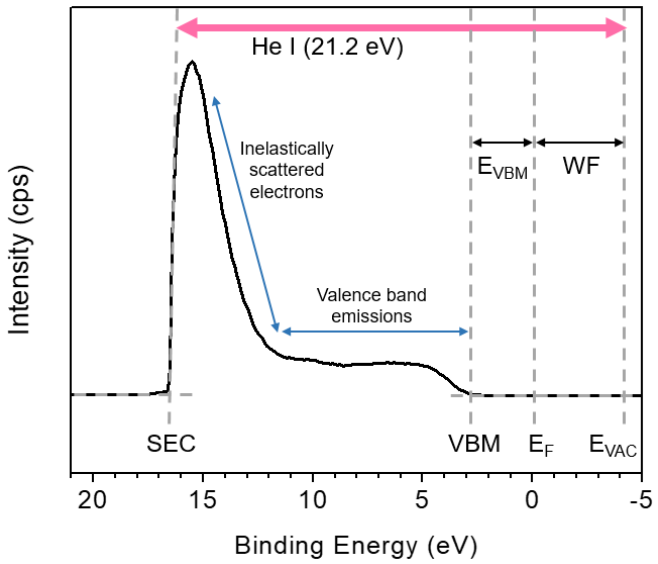

Figure 1.14. UPS spectrum of ITO with electronic energy labels. The intersection of the secondary electron cutoff (SEC) and background marks the deepest electrons released, which is equal to the vacuum level minus the source (SEC = E_{VAC} - hν); the emission of intermediate binding energy is characteristic of inelastically scattered electrons, and the valence band emissions mark the lowest binding energy electrons. The energy cutoff at the lower BE end marks the valence band maximum (VBM) with the Fermi level calibrated to 0 eV. $E_{VBM} = E_F$ - VBM and the WF = $E_{VAC} - E_F$. Image is adapted from literature.[98]

The signal depends on the density of states in the material and the binding energy, and inelastically scattered secondary electrons comprise the background. Following the same expression to determine depth (Equation 1.5) from the previous section, UPS only penetrates 2–3 nm.

1.5.3 Kelvin Probe

Kelvin probe (KP) is another technique that can be used to measure the work function of materials and can be performed in air or under inert conditions, but does not require UHV. By this technique the contact potential difference (V_{CPD}) between two materials, the probing tip and substrate, is measured. This technique does not utilize UV

rays, unlike UPS, and therefore substrates measured by KP would not be subject to the WF lowering effect that UV-exposed samples demonstrated in a study by Kippelen et al.[99]

Isolated materials with different work functions have their local vacuum levels aligned, but not their Fermi levels. When the two come near and are electrically connected, the Fermi levels will proceed to align with current flowing from the material with lower WF to the one with higher WF. This causes charge buildup on each surface and an electrostatic force to develop due to the potential difference. In the actual setup, a capacitive plate-probe is vibrated at a specific frequency ω over the sample and a steady-state AC current develops. The DC bias (counter potential) that must be applied for the current to be nullified, and the system to reach a charge-free state, is the quantifiable negative V_{CPD} (Figure 1.15).[100]

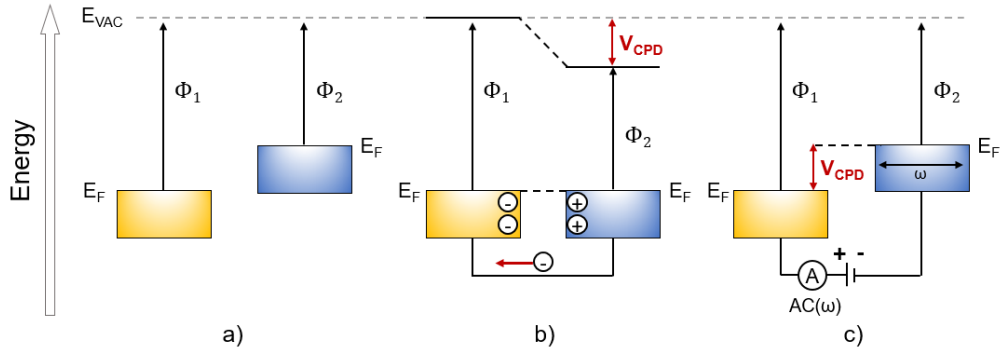

Figure 1.15. Diagram of Kelvin probe instrumentation. Two surfaces with different work function (Φ) before contact (a), electrons flow from low Φ to high Φ material after contact to align Fermi levels, leading to electrostatic force (b), nullifying potential applied through external bias with a magnitude equal to negative the contact potential difference (V_{CPD}) (c). Image is adapted from literature.[101]

Since KP measures a V_{CPD} and not actual WF, the measurements must be calibrated to a reliable standard with a known WF, such as highly ordered pyrolytic graphene

(HOPG). HOPG, with a WF of 4.5 eV, is inert and surface dipoles do not tend to develop from typical ambient contaminants such as water or hydrocarbons.

1.5.4 Infrared Reflection Absorption Spectroscopy

Infrared reflection absorption spectroscopy (IRRAS), also referred to as reflection absorption infrared spectroscopy (RAIRS) is a highly sensitive IR technique used to study thin films down to a submonolayer.[102] A polarized IR beam reflects off of an IR reflective surface at a grazing angle of incidence (between 65° and 85°) and detects vibrational modes with dipole moments in the same plane as the incident light (*p*-polarized) (Figure 1.16). This is because at large angles of incidence, *p*-polarized light leads to an enhanced electric field component at this axis.[103] If one chooses to probe the dipole moments that are parallel to the surface, polarization modulation (PM) IRRAS can be used to acquire *s*-polarized reflections. Obtaining both *p*-polarized and *s*-polarized reflections can increase the sensitivity of the measurement.[104] For a molecule to be IR active and thus capable of being detected by IR spectroscopy, it must have a change in dipole moment at a vibration that is associated within the IR range.

Structural information such as the tilt angle of the modifiers on the surface can also be derived by comparing the vibrations expected from modeling. More details can be read in this reference.[105] Also, when comparing IRRAS with the transmission IR from the powder form, new vibrational signals, a shift, or loss of signal can be detected and used to determine surface binding.

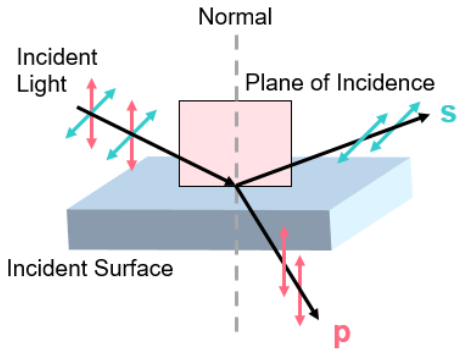

Figure 1.16. Diagram of reflection of IR beam at a grazing angle to a modified gold surface from IRRAS. Image is adapted from literature.[106]

1.6 Organization of the Thesis

From the introduction and pointed references, the reader should now be equipped with the fundamental background knowledge to understand the research presented in the forthcoming chapters. To briefly summarize, interfacial engineering by introducing an interlayer to control the interface energetics has seen significant progress in recent years with a range of materials for both electron and hole transport layers. Transport materials can be classified into two general categories of interlayers and self-assembled monolayers. Among other roles, they serve to reduce the charge collection barrier, and to improve wetting. This thesis describes the study of a range of (electron) interfacial materials that are SAM or SAM-like, that could either form monolayers or a few multilayers on the surface of gold or ITO to lower the work function of the metal/metal oxides.

Chapter 2 presents a work based on water/alcohol soluble modifiers that form multilayer thickness on the surface of ITO. We investigated the effect of a dipolar amine *N*-oxide on the WF of ITO compared to unoxidized amines. We hypothesized that a stronger dipole from the dipolar *N*-oxides would lead to a greater reduction in WF. The stability of the work-function and physical adsorption on exposure to ambient conditions,

and polar/nonpolar solvents were tested and the resulting surfaces were compared to the prior state to quantify the changes. Previous studies with water/alcohol soluble modifiers with amine *N*-oxides typically utilized this functional group as an appendage to a conjugated core but did not study the effect of the functional group on its own.

Chapter 3 demonstrates a combined experimental and computational study in collaboration with Dr. Alexander Hyla and the Jean-Luc Brédas group, Bernard Kippelen group, and Joseph Sadighi group at Georgia Tech. This chapter focuses on quantifying and understanding the effect of N-heterocyclic carbenes on the work function of the modified planar gold surfaces. We hypothesized that a more basic carbene would lead to a greater reduction in WF. The carbenes were synthesized by the author, Dr. Chelsea Wyss, and Abraham Jordan of the Sadighi group. We attempted to determine the effect that N,N' substituent size would have to the overall binding and electronic effect of the modifiers. The experimental coverage was determined and compared with DFT calculated results, the latter of which was performed by Dr. Alexander Hyla. Previous works demonstrated the robustness of the N-heterocyclic carbene-Au bond, but this study demonstrated for the first time, the effect to the work function of the modified surface. Diodes using the N-heterocyclic carbene on the electron injecting contact were fabricated and tested by Felipe Larrain of the Kippelen group. This work was published in Chemistry of Materials in April 2017.

Chapter 4 portrays a work in collaboration with Dr. Thomas Morgan and the Christoph Fahrni group at Georgia Tech. The Fahrni group provided their new class of Cu binding ligands, synthesized by Dr. Thomas Morgan,[107] which they have found have excellent affinity for Cu, for study on Au planar surfaces. These phosphine-sulfide

phosphines (PSPs) were investigated to determine the role of phosphine-sulfide versus phosphine in coordination to planar gold and the effect to the WF. We hypothesized that a greater density of P=S groups oriented with its dipoles perpendicular to the surface would lead to a greater reduction in WF. This was tested by using PSPs of different conformational flexibility. Most of the work focuses on quantifying the work function and coverage through spectroscopic techniques in addition to testing the robustness and stability of this new type of binding group.

Chapter 5 outlines a work in collaboration with Abraham Jordan from the Joseph Sadighi group at Georgia Tech. The Sadighi group provided their N-heterocyclic thione and selone (NHT/NHSe) ligands that were originally used for synthesizing organometallic particles, for study on Au planar surfaces. These ligands were also studied to introduce a new type of binding group and to determine the effect of changing the head group and R groups of the NHTs/NHSe's on the work function and coverage on gold. We hypothesized that the greater magnitude and proximity of the aligned dipole to the surface would lead to a greater reduction in WF. This was tested by using compounds with either a sulfur or selenium head group and R groups of different sterics around the head group. The robustness of the surface modifiers to adhere to the surface and stability of the WF modification were also studied.

Chapter 6 discusses the results from each chapter to put into context among the chapters and with outside applications. Suggested future work for those who wish to continue the trajectory in the study of work function reducing surface modifiers in relation to this thesis are presented.

Appendix A lists the findings of a published study in collaboration with the Sukbok Chang group from KAIST, South Korea. A practical route to 8-aminoquinolines, a useful backbone in various applications, was demonstrated by using readily installable and easily deprotectable amidating reagents.

Appendix B briefly reviews work carried out in collaboration with the author's IGERT fellowship classmates. An economic analysis of a combined residential PV/lithium ion battery storage system in the United States is examined and has recently been published to Renewable and Sustainable Energy Reviews.

1.7 References

[1] Tang, C. W.; VanSlyke, S. A., Organic Electroluminescent Diodes. *Appl. Phys. Lett.* **1987,** *51* (12), 913.

[2] Walzer, K.; Maennig, B.; Pfeiffer, M.; Leo, K., Highly Efficient Organic Devices Based on Electrically Doped Transport Layers. *Chem. Rev.* **2007,** *107*, 1233-1271.

[3] Noh, J. Y.; Han, D. M.; Jeong, W. C.; Kim, J. W.; Cha, S. Y., Development of 55" 4K UHD OLED TV Employing the Internal Gate IC with High Reliability and Short Channel Igzo Tfts. *J. Soc. Inf. Disp.* **2018,** *26* (1), 36-41.

[4] Lampert, C. M., Chromogenic Smart Materials. *Mater. Today* **2004,** *7* (3), 28-35.

[5] Cochrane, C.; Meunier, L.; Kelly, F. M.; Koncar, V., Flexible Displays for Smart Clothing: Part I - Overview. *Indian J. Fibre Text. Res.* **2011,** *36*, 422-428.

[6] Chen, H.-W.; Lee, J.-H.; Lin, B.-Y.; Chen, S.; Wu, S.-T., Liquid Crystal Display and Organic Light-Emitting Diode Display: Present Status and Future Perspectives. *Light Sci. Appl.* **2018,** *7*, 17168.

[7] Facchetti, A., Semiconductors for Organic Transistors. *Mater. Today* **2007,** *10* (3), 28-37.

[8] Huitema, H. E. A.; Gelinck, G. H.; van der Putten, J. B. P. H.; Kuijk, K. E.; Hart, C. M.; Cantatore, E.; de Leeuw, D. M., Active-Matrix Displays Driven by Solution-Processed Polymeric Transistors. *Adv. Mater.* **2002,** *14* (17), 1201-1204.

[9] Holliday, S.; Li, Y.; Luscombe, C. K., Recent Advances in High Performance Donor-Acceptor Polymers for Organic Photovoltaics. *Prog. Polym. Sci.* **2017,** *70*, 34-51.

[10] Mateker, W. R.; McGehee, M. D., Progress in Understanding Degradation Mechanisms and Improving Stability in Organic Photovoltaics. *Adv. Mater.* **2016,** *29* (10), 1603940.

[11] Yan, C.; Barlow, S.; Wang, Z.; Yan, H.; Jen, A. K. Y.; Marder, S. R.; Zhan, X., Non-Fullerene Acceptors for Organic Solar Cells. *Nat. Rev. Mater.* **2018,** *3*, 18003.

[12] Collins, S. D.; Ran, N. A.; Heiber, M. C.; Nguyen, T. Q., Small Is Powerful: Recent Progress in Solution-Processed Small Molecule Solar Cells. *Adv. Energy Mater.* **2017,** *7* (10), 1602242.

[13] Chueh, C.-C.; Li, C.-Z.; Jen, A. K. Y., Recent Progress and Perspective in Solution-Processed Interfacial Materials for Efficient and Stable Polymer and Organometal Perovskite Solar Cells. *Energy Environ. Sci.* **2015,** *8* (4), 1160-1189.

[14] Ishii, H.; Sugiyama, K.; Ito, E.; Seki, K., Energy Level Alignment and Interfacial Electronic Structures at Organic/Metal and Organic/Organic Interfaces. *Adv. Mater.* **1999,** *11* (8), 605-625.

[15] Crispin, X.; Geskin, V.; Crispin, A.; Cornil, J.; Lazzaroni, R.; Salaneck, W. R.; Brédas, J.-L., Characterization of the Interface Dipole at Organic Metal Interfaces. *J. Am. Chem. Soc.* **2002,** *124*, 8131-8141.

[16] Cahen, D.; Kahn, A., Electron Energetics at Surfaces and Interfaces: Concepts and Experiments. *Adv. Mater.* **2003,** *15* (4), 271-277.

[17] Heimel, G.; Romaner, L.; Zojer, E.; Brédas, J.-L., The Interface Energetics of Self-Assembled Monolayers on Metals. *Acc. Chem. Res.* **2008,** *41* (6), 721-729.

[18] Kahn, A., Fermi Level, Work Function and Vacuum Level. *Mater. Horiz.* **2016,** *3* (1), 7-10.

[19] Bredas, J.-L., Mind the Gap! *Mater. Horiz.* **2014,** *1* (1), 17-19.

[20] Serway, R. A.; Jewett, J. W., *Physics for Scientists and Engineers*. Cengage Learning: 2010; Vol. 5.

[21] Sze, S. M.; Ng, K. K., *Physics of Semiconductor Devices*. 3 ed.; John Wiley & Sons: Hoboken, New Jersey, 2007.

[22] Laurendeau, N. M., *Statistical Thermodynamics: Fundamentals and Applications*. Cambridge University Press: 2005.

[23] Wandelt, K., The Local Work Function: Concept and Implications. *Appl. Surf. Sci.* **1997,** *111*, 1-10.

[24] Wandelt, K., *Thin Metal Films and Gas Chemisorption*. Elsevier: Amsterdam, 1987.

[25] Heimel, G., Introduction to the Theory of Metal/Organic Interfaces. In *The WSPC Reference on Organic Electronics: Organic Semiconductors*, World Scientific: 2016; pp 131-158.

[26] Lang, N. D.; Kohn, W., Theory of Metal Surfaces: Charge Density and Surface Energy. *Phys. Rev. B* **1970,** *1* (12), 4555-4568.

[27] Lang, N. D.; Kohn, W., Theory of Metal Surfaces: Work Function. *Phys. Rev. B* **1971,** *3* (4), 1215-1223.

[28] Bagus, P. S.; Staemmler, V.; Wöll, C., Exchangelike Effects for Closed-Shell Adsorbates: Interface Dipole and Work Function. *Phys. Rev. Lett.* **2002,** *89* (9), 096104.

[29] Kippelen, B., Organic Photovoltaics: Physical Concepts Behind Device Operation. In *The WSPC Reference on Organic Electronics: Organic Semiconductors*, World Scientific: 2016; pp 115-157.

[30] Sah, C.-T., *Fundamentals of Solid State Electronics*. World Scientific Publishing Company: 1991.

[31] Kahn, A.; Koch, N.; Gao, W., Electronic Structure and Electrical Properties of Interfaces between Metals and Π-Conjugated Molecular Films. *J. Polym. Sci. Part B: Polym. Phys* **2003,** *41* (21), 2529-2548.

[32] Li, H.; Paramonov, P.; Brédas, J.-L., Theoretical Study of the Surface Modification of Indium Tin Oxide with Trifluorophenyl Phosphonic Acid Molecules: Impact of Coverage Density and Binding Geometry. *J. Mater. Chem.* **2010,** *20* (13), 2630.

[33] Chen, Y. C.; Cunningham, J. E.; Flynn, C. P., Dependence of Rare-Gas-Adsorbate Dipole Moment on Substrate Work Function. *Phys. Rev. B* **1984,** *30* (12), 7317-7319.

[34] Hwang, J.; Wan, A.; Kahn, A., Energetics of Metal–Organic Interfaces: New Experiments and Assessment of the Field. *Mater. Sci. Eng., R* **2009,** *64* (1), 1-31.

[35] Hodgman, C. D., *Handbook of Chemistry and Physics*. 40th ed.; Chemical Rubber Publishing: Cleveland, Ohio, 1959.

[36] Gupta, V.; Kyaw, A. K. K.; Wang, D. H.; Chand, S.; Bazan, G. C.; Heeger, A. J., Barium: An Efficient Cathode Layer for Bulk-Heterojunction Solar Cells. *Sci. Rep.* **2013,** *3*, 1965.

[37] Dweydari, A. W.; Mee, C. H. B., Work Function Measurements on (100) and (110) Surfaces of Silver. *Phys. Status Solidi A* **1975,** *27* (1), 223-230.

[38] Anderson, P. A., Work Function of Gold. *Phys. Rev.* **1959,** *115* (3), 553-554.

[39] Schug, C.; Schempp, S.; Lamparter, P.; Steeb, S., Surface Roughness of Sputter-Deposited Gold Films: A Combined X-Ray Technique and AFM Study. *Surf. Interface Anal.* **1999,** *27* (7), 670-677.

[40] Li, J.; Liu, W.; Wu, X.; Gao, X., Mechanism of Ph-Switchable Peroxidase and Catalase-Like Activities of Gold, Silver, Platinum and Palladium. *Biomaterials* **2015,** *48*, 37-44.

[41] Kim, H.; Gilmore, C. M.; Piqué, A.; Horwitz, J. S.; Mattoussi, H.; Murata, H.; Kafafi, Z. H.; Chrisey, D. B., Electrical, Optical, and Structural Properties of Indium–Tin–Oxide Thin Films for Organic Light-Emitting Devices. *J. Appl. Phys.* **1999,** *86* (11), 6451-6461.

[42] Fan, J. C. C.; Goodenough, J. B., X-Ray Photoemission Spectroscopy Studies of Sn-Doped Indium-Oxide Films. *J. Appl. Phys.* **1977,** *48* (8), 3524-3531.

[43] Brumbach, M.; Veneman, P. A.; Marrikar, F. S.; Schulmeyer, T.; Simmonds, A.; Xia, W.; Lee, P.; Armstrong, N. R., Surface Composition and Electrical and Electrochemical Properties of Freshly Deposited and Acid-Etched Indium Tin Oxide Electrodes. *Langmuir* **2007,** *23*, 11089-11099.

[44] Clark, P. G.; Wagener, T. J., 16 - Removal of Particles by Chemical Cleaning. In *Developments in Surface Contamination and Cleaning*, Kohli, R.; Mittal, K. L., Eds. William Andrew Publishing: Norwich, NY, 2008; pp 873-888.

[45] Durkee, J. B., 15 - Cleaning with Solvents. In *Developments in Surface Contamination and Cleaning*, Kohli, R.; Mittal, K. L., Eds. William Andrew Publishing: Norwich, NY, 2008; pp 759-871.

[46] McDermott, W. T.; Butterbaugh, J. W., 19 - Cleaning Using Argon/Nitrogen Cryogenic Aerosols. In *Developments in Surface Contamination and Cleaning*, Kohli, R.; Mittal, K. L., Eds. William Andrew Publishing: Norwich, NY, 2008; pp 951-986.

[47] Finklea, H. O.; Avery, S.; Lynch, M.; Furtsch, T., Blocking Oriented Monolayers of Alkyl Mercaptans on Gold Electrodes. *Langmuir* **1987,** *3*, 409-413.

[48] Ron, H.; Rubinstein, I., Alkanethiol Monolayers on Preoxidized Gold. Encapsulation of Gold Oxide under an Organic Monolayer. *Langmuir* **1994,** *10*, 4566-4573.

[49] Ron, H.; Rubinstein, I., Self-Assembled Monolayers on Oxidized Metals. 3. Alkylthiol and Dialkyl Disulfide Assembly on Gold under Electrochemical Conditions. *J. Am. Chem. Soc.* **1998,** *120*, 13444-13452.

[50] Carvalhal, R. F.; Freire, R. S.; Kubota, L. T., Polycrystalline Gold Electrodes: A Comparative Study of Pretreatment Procedures Used for Cleaning and Thiol Self-Assembly Monolayer Formation. *Electroanalysis* **2005,** *17*, 1251-1259.

[51] Ma, H.; Yip, H.-L.; Huang, F.; Jen, A. K. Y., Interface Engineering for Organic Electronics. *Adv. Func. Mater.* **2010,** *20* (9), 1371-1388.

[52] Lazic, P., Physisorption at Surfaces. In *Physics of Surface, Interface and Cluster Catalysis*, IOP Publishing: 2016; pp 2-1-2-25.

[53] Zhou, Y.; Fuentes-Hernandez, C.; Shim, J.; Meyer, J.; Giordano, A. J.; Li, H.; Winget, P.; Papadopoulos, T.; Cheun, H.; Kim, J.; Fenoll, M.; Dindar, A.; Haske, W.; Najafabadi, E.; Khan, T. M.; Sojoudi, H.; Barlow, S.; Graham, S.; Brédas, J.-L.; Marder, S. R.; Kahn, A.; Kippelen, B., A Universal Method to Produce Low-Work Function Electrodes for Organic Electronics. *Science* **2012,** *336* (6079), 327-32.

[54] Lee, B. H.; Jung, I. H.; Woo, H. Y.; Shim, H. K.; Kim, G.; Lee, K., Multi-Charged Conjugated Polyelectrolytes as a Versatile Work Function Modifier for Organic Electronic Devices. *Adv. Func. Mater.* **2013,** *24* (8), 1100-1108.

[55] Kang, R.; Oh, S. H.; Kim, D. Y., Influence of the Ionic Functionalities of Polyfluorene Derivatives as a Cathode Interfacial Layer on Inverted Polymer Solar Cells. *ACS Appl. Mater. Interfaces* **2014,** *6* (9), 6227-36.

[56] Zhang, Z.-G.; Qi, B.; Jin, Z.; Chi, D.; Qi, Z.; Li, Y.; Wang, J., Perylene Diimides: A Thickness-Insensitive Cathode Interlayer for High Performance Polymer Solar Cells. *Energy Environ. Sci.* **2014,** *7* (6), 1966-1973.

[57] Russ, B.; Robb, M. J.; Popere, B. C.; Perry, E. E.; Mai, C.-K.; Fronk, S. L.; Patel, S. N.; Mates, T. E.; Bazan, G. C.; Urban, J. J.; Chabinyc, M. L.; Hawker, C. J.; Segalman, R. A., Tethered Tertiary Amines as Solid-State n-Type Dopants for Solution-Processable Organic Semiconductors. *Chem. Sci.* **2016,** *7* (3), 1914-1919.

[58] Chen, L.; Liu, X.; Wei, Y.; Wu, F.; Chen, Y., Alcohol-Soluble Interfacial Fluorenes for Inverted Polymer Solar Cells: Sequence Induced Spatial Conformation Dipole Moment. *Phys. Chem. Chem. Phys.* **2016,** *18* (3), 2219-29.

[59] Zhang, Z.-G.; Li, H.; Qi, Z.; Jin, Z.; Liu, G.; Hou, J.; Li, Y.; Wang, J., Poly(Ethylene Glycol) Modified [60]Fullerene as Electron Buffer Layer for High-Performance Polymer Solar Cells. *Appl. Phys. Lett.* **2013,** *102* (14), 143902.

[60] Zhang, Z.-G.; Li, H.; Qi, B.; Chi, D.; Jin, Z.; Qi, Z.; Hou, J.; Li, Y.; Wang, J., Amine Group Functionalized Fullerene Derivatives as Cathode Buffer Layers for High Performance Polymer Solar Cells. *J. Mater. Chem. A* **2013,** *1* (34), 9624-9629.

[61] Ma, D.; Lv, M.; Lei, M.; Zhu, J.; Wang, H.; Chen, X., Self-Organization of Amine-Based Cathode Interfacial Materials in Inverted Polymer Solar Cells. *ACS Nano* **2014,** *8* (2), 1601-1608.

[62] Xu, W.; Yan, C.; Kan, Z.; Wang, Y.; Lai, W.-Y.; Huang, W., High Efficiency Inverted Organic Solar Cells with a Neutral Fulleropyrrolidine Electron-Collecting Interlayer. *ACS Appl. Mater. Interfaces* **2016,** *8* (22), 14293-14300.

[63] He, Z.; Zhang, C.; Xu, X.; Zhang, L.; Huang, L.; Chen, J.; Wu, H.; Cao, Y., Largely Enhanced Efficiency with a PFN/Al Bilayer Cathode in High Efficiency Bulk Heterojunction Photovoltaic Cells with a Low Bandgap Polycarbazole Donor. *Adv. Mater.* **2011,** *23* (27), 3086-3089.

[64] Xu, X.; Han, B.; Chen, J.; Peng, J.; Wu, H.; Cao, Y., 2,7-Carbazole-1,4-Phenylene Copolymers with Polar Side Chains for Cathode Modifications in Polymer Light-Emitting Diodes. *Macromol.* **2011,** *44* (11), 4204-4212.

[65] Guan, X.; Zhang, K.; Huang, F.; Bazan, G. C.; Cao, Y., Amino N-Oxide Functionalized Conjugated Polymers and Their Amino-Functionalized Precursors: New Cathode Interlayers for High-Performance Optoelectronic Devices. *Adv. Func. Mater.* **2012,** *22* (13), 2846-2854.

[66] Chen, S.; Manders, J. R.; Tsang, S.-W.; So, F., Metal Oxides for Interface Engineering in Polymer Solar Cells. *J. Mater. Chem.* **2012,** *22* (46), 24202-24212.

[67] Ulman, A., Formation and Structure of Self-Assembled Monolayers. *Chem. Rev.* **1996,** *96*, 1533-1554.

[68] Schreiber, F., Structure and Growth of Self-Assembling Monolayers. *Prog. Surf. Sci.* **2000,** *65* (5-8), 151-257.

[69] Love, J. C.; Estroff, L. A.; Kriebel, J. K.; Nuzzo, R. G.; Whitesides, G. M., Self-Assembled Monolayers of Thiolates on Metals as a Form of Nanotechnology. *Chem. Rev.* **2005,** *105* (4), 1103-1170.

[70] Hotchkiss, P. J.; Jones, S. C.; Paniagua, S. A.; Sharma, A.; Kippelen, B.; Armstrong, N. R., The Modification of Indium Tin Oxide with Phosphonic Acids: Mechanisms of Binding, Tuning Surface Properties, and Potential for Use in Organic Electronic Applications. *Acc. Chem. Res.* **2012,** *45* (3), 337-346.

[71] Laibinis, P. E.; Whitesides, G. M.; Allara, D. L.; Tao, Y. T.; Parikh, A. N.; Nuzzo, R. G., Comparison of the Structures and Wetting Properties of Self-Assembled Monolayers of N-Alkanethiols on the Coinage Metal Surfaces, Copper, Silver, and Gold. *J. Am. Chem. Soc.* **1991,** *113* (19), 7152-7167.

[72] Parikh, A. N.; Schivley, M. A.; Koo, E.; Seshadri, K.; Aurentz, D.; Mueller, K.; Allara, D. L., N -Alkylsiloxanes: From Single Monolayers to Layered Crystals. The Formation of Crystalline Polymers from the Hydrolysis of n-Octadecyltrichlorosilane. *J. Am. Chem. Soc.* **1997,** *119* (13), 3135-3143.

[73] Haensch, C.; Hoeppener, S.; Schubert, U. S., Chemical Modification of Self-Assembled Silane Based Monolayers by Surface Reactions. *Chem. Soc. Rev.* **2010,** *39* (6), 2323-2334.

[74] Toworfe, G. K.; Composto, R. J.; Shapiro, I. M.; Ducheyne, P., Nucleation and Growth of Calcium Phosphate on Amine-, Carboxyl- and Hydroxyl-Silane Self-Assembled Monolayers. *Biomaterials* **2006,** *27* (4), 631-642.

[75] Laibinis, P. E.; Hickman, J. J.; Wrighton, M. S.; Whitesides, G. M., Orthogonal Self-Assembled Monolayers: Alkanethiols on Gold and Alkane Carboxylic Acids on Alumina. *Science* **1989,** *245* (4920), 845-847.

[76] Chen, F.; Li, X.; Hihath, J.; Huang, Z.; Tao, N., Effect of Anchoring Groups on Single-Molecule Conductance: Comparative Study of Thiol-, Amine-, and Carboxylic-Acid-Terminated Molecules. *J. Am. Chem. Soc.* **2006,** *128* (49), 15874-15881.

[77] Paniagua, S. A.; Hotchkiss, P. J.; Jones, S. C.; Marder, S. R.; Mudalige, A.; Marrikar, F. S.; Pemberton, J. E.; Armstrong, N. R., Phosphonic Acid Modification of Indium−Tin Oxide Electrodes: Combined XPS/UPS/Contact Angle Studies. *J. Phys. Chem.* **2008,** *112* (21), 7809-7817.

[78] Queffélec, C.; Petit, M.; Janvier, P.; Knight, D. A.; Bujoli, B., Surface Modification Using Phosphonic Acids and Esters. *Chem. Rev.* **2012,** *112* (7), 3777-3807.

[79] Sachs, S. B.; Dudek, S. P.; Hsung, R. P.; Sita, L. R.; Smalley, J. F.; Newton, M. D.; Feldberg, S. W.; Chidsey, C. E. D., Rates of Interfacial Electron Transfer through π-Conjugated Spacers. *J. Am. Chem. Soc.* **1997,** *119* (43), 10563-10564.

[80] Imahori, H.; Norieda, H.; Nishimura, Y.; Yamazaki, I.; Higuchi, K.; Kato, N.; Motohiro, T.; Yamada, H.; Tamaki, K.; Arimura, M.; Sakata, Y., Chain Length Effect on the Structure and Photoelectrochemical Properties of Self-Assembled Monolayers of Porphyrins on Gold Electrodes. *J. Phys. Chem.* **2000,** *104* (6), 1253-1260.

[81] Tamada, K.; Ishida, T.; Knoll, W.; Fukushima, H.; Colorado, R.; Graupe, M.; Shmakova, O. E.; Lee, T. R., Molecular Packing of Semifluorinated Alkanethiol Self-Assembled Monolayers on Gold: Influence of Alkyl Spacer Length. *Langmuir* **2001,** *17* (6), 1913-1921.

[82] Liu, H.; Bhushan, B., Investigation of Nanotribological Properties of Self-Assembled Monolayers with Alkyl and Biphenyl Spacer Chains (Invited). *Ultramicroscopy* **2002,** *91* (1-4), 185-202.

[83] Ishida, T.; Mizutani, W.; Aya, Y.; Ogiso, H.; Sasaki, S.; Tokumoto, H., Electrical Conduction of Conjugated Molecular Sams Studied by Conductive Atomic Force Microscopy. *J. Phys. Chem.* **2002,** *106* (23), 5886-5892.

[84] Faucheux, N.; Schweiss, R.; Lützow, K.; Werner, C.; Groth, T., Self-Assembled Monolayers with Different Terminating Groups as Model Substrates for Cell Adhesion Studies. *Biomaterials* **2004,** *25* (14), 2721-2730.

[85] Collman, J. P.; Devaraj, N. K.; Chidsey, C. E. D., "Clicking" Functionality onto Electrode Surfaces. *Langmuir* **2004,** *20* (4), 1051-1053.

[86] Binder, W. H.; Sachsenhofer, R., 'Click' Chemistry in Polymer and Materials Science. *Macromol. Rapid Commun.* **2007,** *28* (1), 15-54.

[87] Paniagua, S. A.; Giordano, A. J.; Smith, O. N. L.; Barlow, S.; Li, H.; Armstrong, N. R.; Pemberton, J. E.; Brédas, J.-L.; Ginger, D.; Marder, S. R., Phosphonic Acids for Interfacial Engineering of Transparent Conductive Oxides. *Chem. Rev.* **2016,** *116* (12), 7117-7158.

[88] Paramonov, P. B.; Paniagua, S. A.; Hotchkiss, P. J.; Jones, S. C.; Armstrong, N. R.; Marder, S. R.; Brédas, J.-L., Theoretical Characterization of the Indium Tin Oxide Surface and of Its Binding Sites for Adsorption of Phosphonic Acid Monolayers. *Chem. Mater.* **2008,** (20), 5131-5133.

[89] Ratcliff, E. L.; Garcia, A.; Paniagua, S. A.; Cowan, S. R.; Giordano, A. J.; Ginley, D. S.; Marder, S. R.; Berry, J. J.; Olson, D. C., Investigating the Influence of Interfacial

Contact Properties on Open Circuit Voltages in Organic Photovoltaic Performance: Work Function Versus Selectivity. *Adv. Energy Mater.* **2013,** *3* (5), 647-656.

[90] Sharma, A.; Kippelen, B.; Hotchkiss, P. J.; Marder, S. R., Stabilization of the Work Function of Indium Tin Oxide Using Organic Surface Modifiers in Organic Light-Emitting Diodes. *Appl. Phys. Lett.* **2008,** *93* (16), 163308.

[91] Nuzzo, R. G.; Allara, D. L., Adsorption of Bifunctional Organic Disulfides on Gold Surfaces. *J. Am. Chem. Soc.* **1983,** *105*, 4481-4483.

[92] Nuzzo, R. G.; Zegarski, B. R.; Dubois, L. H., Fundamental Studies of the Chemisorption of Organosulfur Compounds on Gold(111). Implications for Molecular Self-Assembly on Gold Surfaces. *J. Am. Chem. Soc.* **1987,** *109* (3), 733-740.

[93] Porter, M. D.; Bright, T. B.; Allara, D. L.; Chidsey, C. E. D., Spontaneously Organized Molecular Assemblies. 4. Structural Characterization of N-Alkyl Thiol Monolayers on Gold by Optical Ellipsometry, Infrared Spectroscopy, and Electrochemistry. *J. Am. Chem. Soc.* **1987,** *109* (12), 3559-3568.

[94] Schlenoff, J. B.; Li, M.; Ly, H., Stability and Self-Exchange in Alkanethiol Monolayers. *J. Am. Chem. Soc.* **1995,** *117*, 12528-12536.

[95] Shi, H.; Stampfl, C., First-Principles Investigations of the Structure and Stability of Oxygen Adsorption and Surface Oxide Formation at Au(111). *Phys. Rev. B* **2007,** *76*, 075327-1-14.

[96] Pearson, R. G., Hard and Soft Acids and Bases, HSAB, Part 1: Fundamental Principles. *Journal of Chemical Education* **1968,** *45* (9), 581.

[97] Watts, J. F.; Wolstenholme, J., *An Introduction to Surface Analysis by XPS and AES*. John Wiley & Sons: England, 2003.

[98] Giordano, A. J.; Pulvirenti, F.; Khan, T. M.; Fuentes-Hernandez, C.; Moudgil, K.; Delcamp, J. H.; Kippelen, B.; Barlow, S.; Marder, S. R., Organometallic Dimers: Application to Work-Function Reduction of Conducting Oxides. *ACS Appl. Mater. Interfaces* **2015,** *7* (7), 4320-6.

[99] Zhou, Y.; Shim, J. W.; Fuentes-Hernandez, C.; Sharma, A.; Knauer, K. A.; Giordano, A. J.; Marder, S. R.; Kippelen, B., Direct Correlation between Work Function of Indium-Tin-Oxide Electrodes and Solar Cell Performance Influenced by Ultraviolet Irradiation and Air Exposure. *Phys. Chem. Chem. Phys.* **2012,** *14* (34), 12014-12021.

[100] Vilarinho, P. M.; Rosenwaks, Y.; Kingon, A., *Scanning Probe Microscopy: Characterization, Nanofabrication and Device Application of Functional Materials*. Kluwer Academic Publishers: Dordrecht, 2002.

[101] Kalinin, S. V.; Gruverman, A., *Scanning Probe Microscopy*. Springer-Verlag New York: 2007.

[102] Gauglitz, G.; Moore, D. S., *Handbook of Spectroscopy*. Wiley-VCH Verlag GmbH & Company KGaA: 2014.

[103] Fringeli, U. P., Atr and Reflectance Ir Spectroscopy, Applications A2 - Lindon, John C. In *Encyclopedia of Spectroscopy and Spectrometry*, Elsevier: Oxford, 1999; pp 58-75.

[104] Tolstoy, V. P.; Chernyshova, I.; Skryshevsky, V. A., *Handbook of Infrared Spectroscopy of Ultrathin Films*. Wiley: 2003.

[105] Flach, C. R.; Gericke, A.; Mendelsohn, R., Quantitative Determination of Molecular Chain Tilt Angles in Monolayer Films at the Air/Water Interface: Infrared Reflection/Absorption Spectroscopy of Behenic Acid Methyl Ester. *J. Phys. Chem. B* **1997,** *101* (1), 58-65.

[106] Hubbard, A. T., *The Handbook of Surface Imaging and Visualization*. CRC Press: 1995.

[107] Morgan, M. T.; Yang, B.; Harankhedkar, S.; Nabatilan, A.; Bourassa, D.; McCallum Adam, M.; Sun, F.; Wu, R.; Forest Craig, R.; Fahrni Christoph, J., Stabilization of Aliphatic Phosphines by Auxiliary Phosphine Sulfides Offers Zeptomolar Affinity and Unprecedented Selectivity for Probing Biological Cu(I). *Angew. Chem. Int. Ed.* **2018,** *57*, 9711-9715.

CHAPTER 2
REDUCTION OF THE WORK FUNCTION OF INDIUM TIN OXIDE BY WATER/ALCOHOL SOLUBLE ALIPHATIC AMINE N-OXIDES

2.1 Literature Precedents

2.1.1 Purpose of Modification Layer

As described in the introduction chapter, for many organic electronic applications, low-work function (WF) electrodes are required for efficient electron injection or collection. Intrinsically low work function (WF) metals such as Ca and Ba can be used, but are highly moisture or air sensitive.[1-3] Using high WF, but stable, metals such as Al, Ag, or Au leads to large electron-injection barriers into low-electron affinity organic semiconductors, for example in OLEDs, and can compromise open-circuit voltage when used for electron collection in solar cells. Interfacial layers can be introduced to reduce the WF of high WF metals or metal oxides to transform them into low WF electrodes.

2.1.2 Water/alcohol Soluble Conjugated Polymers

Recently, water/alcohol soluble conjugated polymers (WSCPs), which consist of a π-conjugated backbone with polar side chains, have been used as surface modifiers in many devices because of its orthogonal solvent compatibility.[4-7] In addition, even without the conjugated backbone, structures with the presence of the characteristic side chains have also been classified as WSCPs. Examples of WSCP backbones include polyfluorenes,[8] polythiophene,[9] fullerene derivatives,[10-11] non-conjugated polymers like poly(ethylene oxide) (PEO)[12] and PEI/PEIE,[13] and small molecules like Rhodamine 101.[14] The classes of polar side groups include amino-functionalized quaternized derivatives (with mobile counterions),[8-9] neutral compounds (diethanolamine and phosphonates),[15-16] amino *N*-

oxides,[4, 17-20] and zwitterionic (sulfobetaines)[21-22] with no mobile ions (Figure 2.1). With the advantage of orthogonal solvent processability, which means that the solvent in which the surface modifier is deposited from has a contrasting polarity from the solvent that contains the active material that is sequentially deposited, roll-to-roll processing methods becomes more feasible.

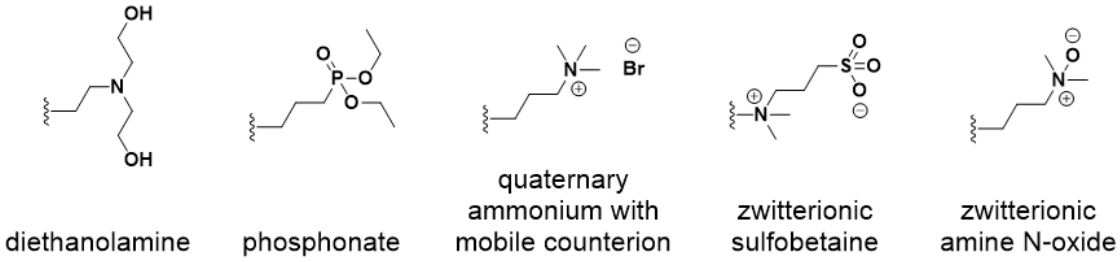

Figure 2.1. Structures of typical polar side groups of WSCPs.[4, 8-9, 15-22]

2.1.2.1 Amine *N*-oxide Functionalized Polymer PFN

In 2012, Guan *et al*. introduced the first class of amino *N*-oxide functionalized polyfluorene polymers (PFNO)[4] as surface modifiers, and contrasted its performance with the amino functionalized counterparts (PFN), which had been widely used as a surface modifier previously (Figure 2.2).[8, 23-25] These compounds were of special interest because of their excellent solubility in polar solvents, large dipole moments, and the absence of mobile counterions, which have been reported to be problematic.[26] Furthermore, the researchers showed that PCDTBT:$PCB_{71}BM$ based polymer solar cells (PSCs) with top Al electron-collecting electrodes had higher power conversion efficiency (PCE) for the PFNO modified devices compared with the PFN modified.[4]

The utility of these types of *N*-oxide functionalized polymers[4] as surface modifiers was demonstrated in a tandem PSC structure with polymer-modified MoO_x, to improve the contact with TiO_2. These solution processed metal oxide/dipole layer/metal oxide interconnecting layers showed enhanced current density versus voltage (*J–V*) characteristics in homo-tandem P3HT:$PC_{60}BM$ and PBDTTT-C-T:$PC_{70}BM$ device architectures.[27]

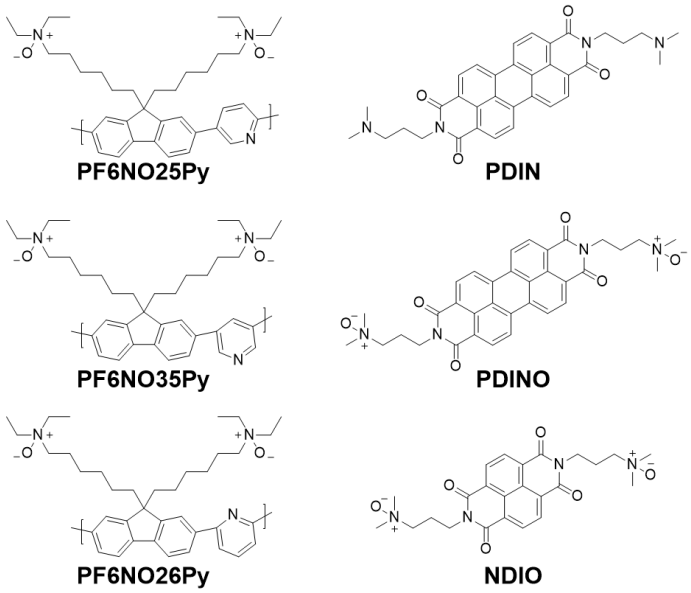

Figure 2.2. Structures of amine *N*-oxide functionalized polymers and small molecule surface modifiers.[4, 17-18]

2.1.2.2 Amine *N*-oxide Functionalized Small Molecule PDI and NDI

Shortly after, non-polymeric conjugated *N*-oxides were used as surface modifiers based on a perylene diimide (PDINO)[17] and naphthalene diimide (NDIO)[18] cores. Structures with these cores are notable for their high photochemical stability, high electron affinities, easy functionalization and high conductivities owing to their extended

conjugated structures.[28-31] In addition, small molecules offer the advantage of relative ease of synthesis and precise molecular structure compared with polymers. PDINO-based devices demonstrated thickness-insensitivity of the surface modifier and were successfully incorporated within a wide range of thicknesses (6–25 nm) in functional PSCs.[17] The electronic properties of PDI-interlayers were investigated on Al, Ag, and Au electrodes and in each case, the surface modifiers lowered the WF of the metals by a few meV. NDIO-coated ITO was reported to have a WF of 3.96 eV compared with untreated ITO (4.49 eV) measured by UPS, which led to a decrease in energy mismatch between the WF of ITO and the EA of $PC_{71}BM$ (3.91 eV), the acceptor material in the inverted PSC (Table 2.1).[18]

Table 2.1. WF of WSCP, PDIN, PDINO, and NDIO.[4, 17-18]

Modifier/Substrate	WF (eV)
MoO_x	5.42
Al (UPS)	4.3
Ag (UPS)	4.3
ITO (UPS)	5.1
ITO (UPS)	4.49
PF6NO26Py/MoO_x	4.71
PF6NO35Py/MoO_x	4.43
PF6N25Py/MoO_x	4.18
PDIN/Al	3.50
PDIN/Ag	3.94
PDIN/Au	3.93
PDINO/Al	3.49
PDINO/Ag	3.60
PDINO/Au	3.62
NDIO/ITO	3.96

2.1.3 Motivation for Studying Aliphatic Amine *N*-oxides

Currently WSCPs show promise as surface modifiers on a variety of electrodes for several reasons: they have conjugated backbones that ensure conductivity (although successful examples of non-conjugated polymers have been reported)[13], polar side chains

that allow for water/alcohol solubility, and orthogonal solvent processing, which in turn allows for low temperature solution processing of devices. In the literature thus far, the aforementioned backbones have been decorated with the various polar side groups and variations based on exchange of counterions in the case of quaternized derivatives have been studied. There has also been an example with the polar side group that has traditionally been pendant, to be within the main chain, alternating with the conjugated PDI.[32] In the literature, the polar/ionic derivatives have usually been compared with the neutral/precursor materials. However, the polar side chains have not been studied isolated from the conjugated main chains as small molecule derivatives.

Herein, we report the behavior of aliphatic amine *N*-oxides as small-molecule surface modifiers for ITO. The modifiers are easily synthesized by exposure of the corresponding amine to aqueous hydrogen peroxide, and are readily soluble in water and methanol. They demonstrate better adhesion to the ITO cathode than the non-oxidized amine precursors based on a comparison of the N 1s signals of substrates modified under the same conditions measured by XPS, and are although partially removed by washing with dichlorobenzene, a typical solvent for organic semiconductor deposition, the remaining material is in some cases sufficient to maintain a low WF. The *N*-oxides show modest reductions to the WF of ITO, with the magnitude of the reduction increasing with increasing thickness.

2.2 Selection of Amines and *N*-oxides

Figure 2.3 represents the chemical structures of the amines and the corresponding *N*-oxide compounds studied in this paper. *N,N*-Dimethylhexylamine (DMHA/1N), tetramethylethylenediamine (TMEDA/2N), pentamethyldiethylenetriamine (PMDETA/

3N) and their respective *N*-oxides were studied to understand the effect of the number of amine moieties per molecule and the effect of amine oxidation.

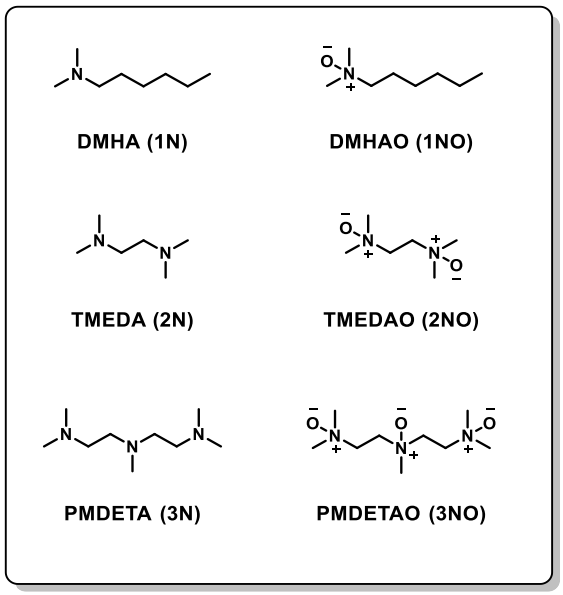

Figure 2.3. Structure of amines/*N*-oxides.

In this study, ITO surfaces were treated by spin-coating different concentrations of amine/*N*-oxide in methanol to produce films of varying thicknesses. These films were characterized by measuring the resulting WF (by UPS and KP) and by estimating the resulting thicknesses and percent monolayers using the ratio of XPS intensities of core signals associated with the modifier atoms to those arising from the bulk substrate (refer to 2.4.4 for method). The thicknesses were derived by assuming a uniform coverage of modifier with a density of 1 g cm^{-3} and known density of 6.65 g cm^{-3},[33] and the percent monolayers were estimated by assuming that all the polar side groups of each modifier are oriented towards the surface with a conformation that results in the maximum footprint.

2.2.1 Surface Oriented Assumptions

2.2.1.1 Binding Orientation

The cartoon in Figure 2.4 illustrates the proposed orientation of the end groups of 2NO on the surface of ITO of a monolayer.

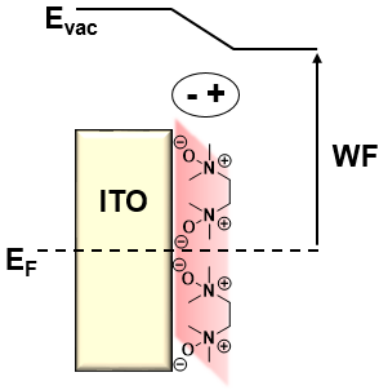

Figure 2.4. Sketch of metal oxide/interface layer and interface dipole formed from modification by 2NO leading to a reduction in work function.

2.3 Analysis of Modified ITO Surfaces

2.3.1 Coverage and Workfunction Modification Analysis

When dilute concentrations (0.5 to 2.0 mM) were used, films of thicknesses on the order of a few nm were deposited (for 2NO and 3NO), with the corresponding WF decreasing with increasing thickness (Figure 2.5). There is a linear correlation between the workfunction and thickness, with a similar trend between 2NO and 3NO. Separate plots of the workfunction change versus percent monolayer can be found in Figure 2.6.

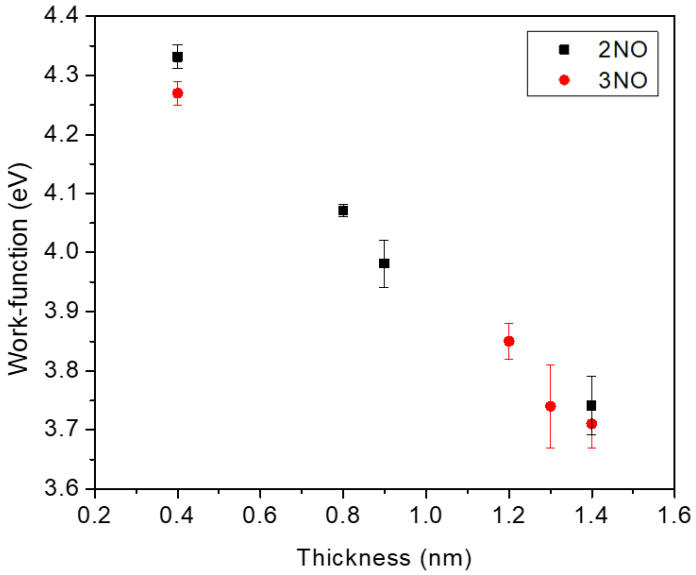

Figure 2.5. Workfunction (by UPS) versus thickness of 2NO and 3NO on ITO processed from spin coating different concentrations (0.5, 1.0, 1.5, 2.0 mM) of the amine *N*-oxides. The x-error is 0.1 nm for all data points.

When compared with films deposited from more concentrated 10 mM solutions, the latter resulted in thicknesses of several nm but the same WF reduction as a 1.4 nm thick film (Table 2.2). This indicated that less than 2 nm of a modification layer was sufficient to reduce the WF of ITO to low levels (3.7 eV). Since these surface modifiers are non-conjugated and expected, thicker layers are likely essentially insulating in nature, ultrathin layers would presumably allow charge carriers to more easily tunnel between the modified electrode and an organic semiconducting layer in a device. In the case of 1NO, regardless of the concentration of the spin coating solution, approximately the same thicknesses were achieved, although the less dilute solution resulted in a slightly lower workfunction (by 0.11 eV) (Table 2.2).

Table 2.2. Tabulation of Workfunction, Molecular Coverage and Thickness Estimation of Amine *N*-oxides on ITO derived from XPS signals.

System	footprint (Å^2)		coverage (10^{14} molecules cm^{-2})		% ideal monolayer	thickness (nm)[d]
	estim	exptl[a]	ideal[b]	exptl[c]		
1NO-1.0 mM	26	23.5 ± 1.9	3.85	4.3 ± 0.3	100	0.7
1NO-10.0 mM	26	23.8 ± 2.2	3.85	4.2 ± 0.4	100	0.7
2NO-0.5 mM	51	45.5 ± 15.3	1.96	2.0 ± 0.5	100	0.4
2NO-1.0 mM	51	22.1 ± 1.6	1.96	4.5 ± 0.3	200	0.8
2NO-1.5 mM	51	19.6 ± 2.8	1.96	5.2 ± 0.7	300	0.9
2NO-2.0 mM	51	11.2 ± 1.4	1.96	9.0 ± 1.0	500	1.4
2NO-10.0 mM	51	1.7 ± 0.3	1.96	60.3 ± 10.9	3100	4.7
3NO-0.5 mM	70	67.5 ± 12.6	1.43	1.5 ± 0.3	100	0.4
3NO-1.0 mM	70	21.1 ± 1.7	1.43	4.8 ± 0.4	300	1.2
3NO-1.5 mM	70	18.6 ± 1.2	1.43	5.4 ± 0.3	400	1.3
3NO-2.0 mM	70	17.2 ± 1.4	1.43	5.9 ± 0.5	400	1.4
3NO-10.0 mM	70	1.7 ± 0.2	1.43	58.8 ± 7.4	4100	6.1

[a] The ideal coverage is estimated as the reciprocal of the estimated footprint. Note that the footprint is based on an ellipse of a simple model of each modifier if all amines were facing the same direction and interacting with the surface. [b] The experimental average coverage was estimated from XPS data as described in section 2.4.4; the error bars are estimated based on spot-to-spot variation of XPS peaks, but do not take into account approximations made in converting XPS ratios to atomic ratios. The footprint given is the reciprocal of the coverage. [c] The percentage ideal monolayer compares the experimental coverage to the ideal coverage and rounded to the nearest hundreds place. [d] These were assuming density of 1 g cm^{-3} as described in section 2.4.4.

Table 2.2 also lists the approximate percent monolayers of each modifier, which were calculated as described in 2.4.4 by assuming that for each modifier, all the polar side groups are oriented towards the surface and assuming a conformation that results in the maximum footprint. To arrive at an estimated percent monolayer, the expected footprint was compared to the experimental footprint and the corresponding values are found in Table 2.2

2.3.2 Percent Monolayer Analysis

Since 1NO only contains one oxidized amine group, if that unit were to anchor to the surface, it would result in a 40° tilt for the hexyl chain. This corresponds to a standing height of 0.7 nm, which matches the experimental thickness that was derived from the XPS signals. Both treatment conditions (1 mM and 10 mM) resulted in a monolayer of 1NO.

This can be rationalized that as there is only one anchoring group and a hydrophobic tail, additional layers would be electrostatically difficult to form. For 2NO and 3NO however, which contain higher N/C ratios and have two and three oxide moieties, respectively, using a concentrated 10 mM solution resulted in estimated thicknesses of greater than 5 nm and several thousand percent monolayers. From these findings, it can be assumed that the dipole-dipole intermolecular interactions are strong enough to overcome the volatility of the modifiers in ultrahigh vacuum (UHV). This type of relationship can be rationalized by comparing with hydrogen bonding, where if compounds contain the same hydrogen bonding capable groups (for example –OH), the compound with more (three –OH groups) will have the strongest intermolecular forces (glycerol b.p. 290 °C, ethylene glycol b.p. 197 °C, ethanol b.p. 78 °C). Given that the ITO surface post oxygen plasma treatment is highly polar and rich in metal oxides,[34] it is reasonable that the N–O polar bonds is acting as a Lewis base towards any low-coordinate surface metal ions, or displace water from surface metal ions, and us able to adhere well (under UHV).

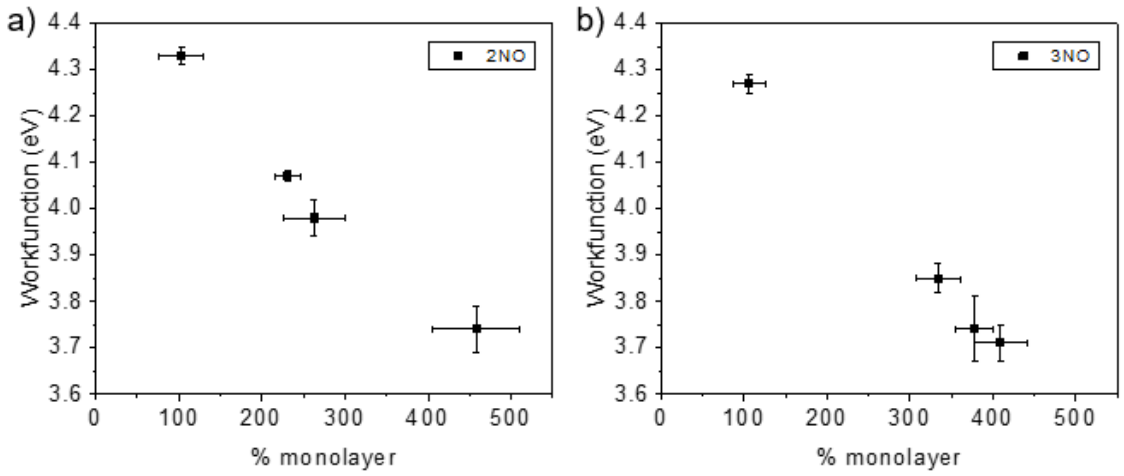

Figure 2.6. Graph of Workfunction (measured by UPS) versus % monolayer of 2NO and 3NO on ITO spin coated from different concentrations.

2.3.3 Comparison with Amine Precursors

To compare the effect of a dipolar functional group, the non-oxidized precursors were also used to modify plasma treated ITO (with 10 mM solutions) and the resulting WF and N/In ratios were measured (by UPS and XPS). The amines were unable to reduce the WF as significantly as the oxidized counterparts (lowest value was for 3N at 4.33 eV), which may be in part due to the low N/In ratios (of N 1s and In 3d) for these surfaces, which correlate to low coverage (Table 2.3).

Table 2.3. Experimental (UPS) workfunction of the amine/*N*-oxide modified ITO surfaces and corresponding N/In ratios from XPS signals.

System	UPS Φ (eV)[ab]	N/In ratios[ab]
ITO (OP)	5.11 ± 0.06	n/a
1N	4.80 ± 0.04	0
1NO	4.22 ± 0.03	0.063 ± 0.005
2N	4.65 ± 0.03	0.042 ± 0.010
2NO	3.77 ± 0.02	1.891 ± 0.307
3N	4.33 ± 0.04	0.064 ± 0.006
3NO	3.69 ± 0.04	2.638 ± 0.229

[a] The error bars are the standard deviations derived by measurement of five samples over three different surfaces. [b] All films were processed from 10 mM solutions.

The high resolution (HR) core ionization spectra of the amines on ITO can be found in Figure 2.7. Even though solutions of the same concentration were used, the resulting N/In ratios were drastically different between the two sets (oxidized and non-oxidized). The *N*-oxide-modified surfaces had higher N/In ratios than the amine-modified, and 1N was not detected at all by XPS. Considering that the substrates were processed under the same conditions, we assume that the intermolecular interactions among the amines were not as strong as among the *N*-oxides and, therefore, the amines were more easily lost under

ultrahigh vacuum (UHV) upon pumping of the chamber. Also 1NO and 2NO are solids with m.p. at ca. 88 °C and 3NO is a viscous liquid, whereas all the precursor amines are non-viscous liquids at room temperature.

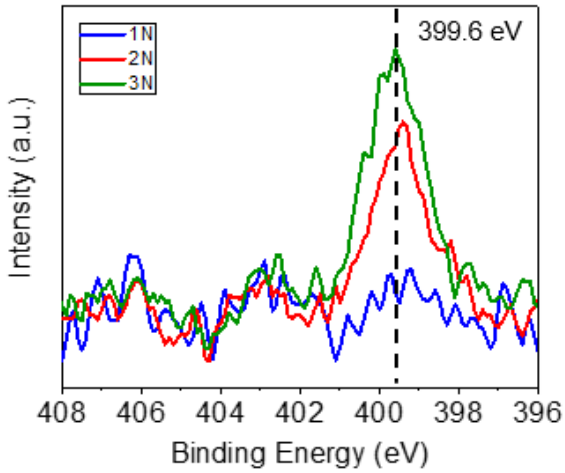

Figure 2.7. N 1s high resolution core ionization spectra of amines (1N, 2N, 3N) measured by XPS. The BE of the peak maxima is about 399.6 eV. No 1N is detected at all by XPS under these processing conditions (from 10 mM dilution, same parameters as in experimental).

Although the films in Table 2.3 cannot be directly compared due to the difference in thicknesses, more dilute solutions were not used to process the amine modifiers because of their relatively higher volatility. Thus, the advantage of oxidation to the amines includes the ability to control thickness (stable to UHV) and a WF below 4 eV for thin layers (ca. 3.7 eV at 1.4 nm for 2NO and 3NO).

2.3.4 XPS Analysis

2.3.4.1 Setting a Reference

To analyze the change to the electronic environment of the surface of ITO upon deposition of amine *N*-oxides, HR spectra of the nitrogen 1s core ionization were analyzed.

First, the spectra obtained from the films deposited from 10 mM solutions are compared against films of thicknesses greater than the detection depth limit of XPS (10 nm) to represent nitrogen signals from solely the compound without surface interactions (Figure 2.8). The absence of the strong In 3d signals that would arise from the bulk substrate confirm the success of the deposition of 2NO and 3NO. No matter how concentrated the 1NO solution was, only an estimated thickness of 6 nm could be achieved for 1NO.

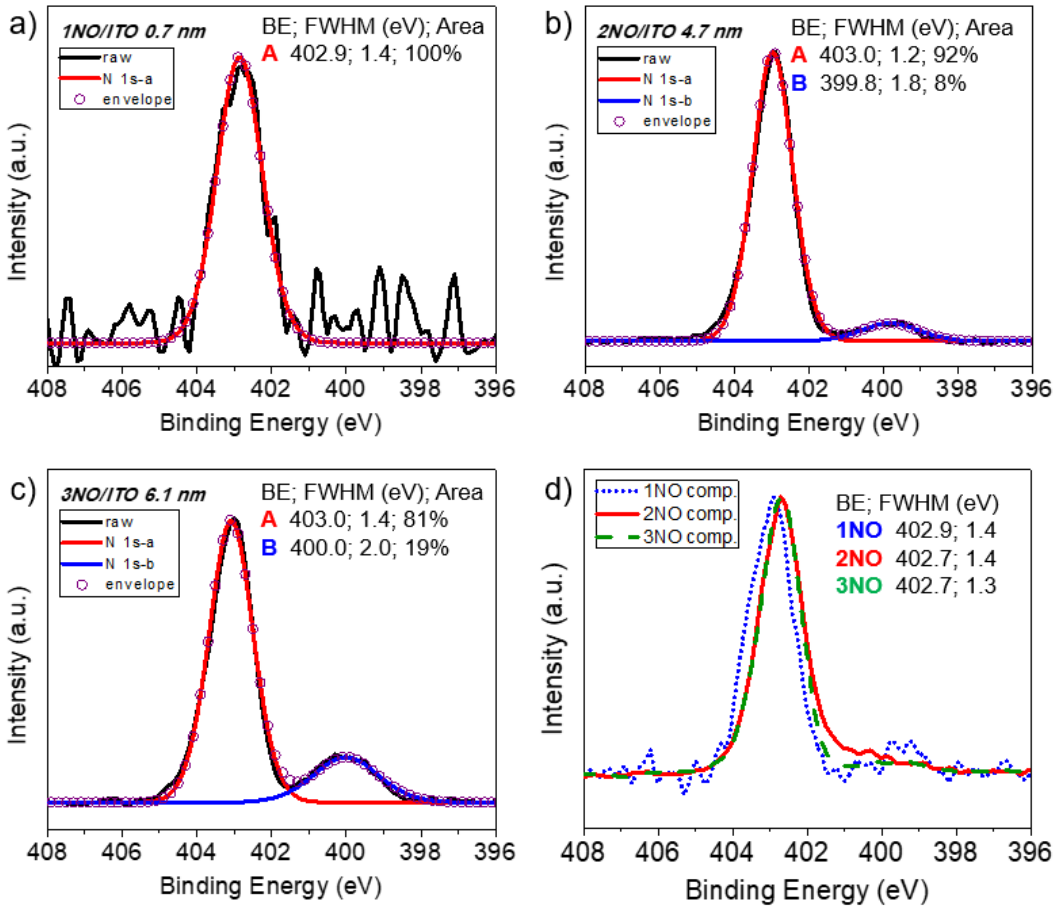

Figure 2.8. Peak components of N 1s core ionization (XPS) (from 10 mM dilutions), 1NO-(0.7 nm) (a)[a], 2NO-(4.7 nm) (b), 3NO-(6.1 nm) (c), and of films of >10 nm thickness (d)[b].

[a] This spectrum is similar to that deposited from 1 mM solution. [b] These were calibrated by setting the C 1s scanned for the same spot to 284.8 eV (1NO), and 286.0 eV (2NO) and (3NO), which are the average C 1s detected for each compound when treated in a more dilute solution. The 1NO deposited film (1NO-comp.) is not greater than 10 nm.

However, because of the assumptions taken to calibrate the spectra in Figure 2.8d where little to no In 3d was present, Figure 2.8a–c were used instead as reference peaks (calibrated to the corresponding In 3d). To validate this approach, it can be noted that due to the thickness of the overlayers in Figure 2.8a–c, a large majority of the signal comes from the compounds themselves, as opposed to those strongly interacting with the ITO surface. Therefore, sufficient peak positions and widths could be derived with these spectra.

Each of the major peak components from each spectrum is assumed to be composed of one component with a binding energy (BE) and a full width at half maximum (FWHM) listed on the figures (Figure 2.8). All the major components were positioned at 402.9–403 eV with a FWHM range of 1.2–1.4 eV, which allows for some flexibility in the peak analysis. This component most likely refers to the amine oxide functionality and the lower BE component found in Figure 2.8a,b is consistent with an unoxidized amino group. Since 2NO and 3NO do not contain this type of amino group, this finding suggests that a reaction may occur that leads to a loss of an oxide upon interaction with ITO.

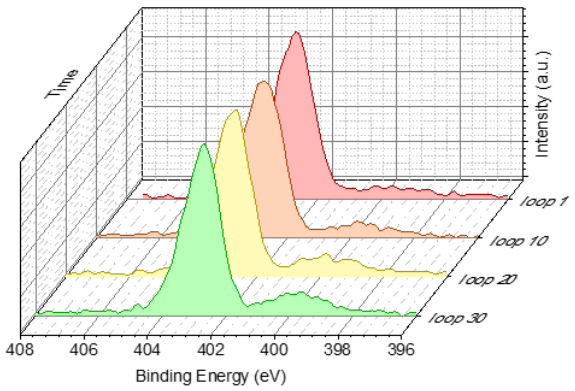

Figure 2.9. The degradation of a thick overlayer of 3NO on ITO was tested by sweeping the same N 1s spot 30 times, without averaging the results. Sweeps 1, 10, 20, and 30 are shown and labeled as loops.

In addition, this peak grows in intensity on increasing exposure of a thick 3NO film on ITO to the X-ray beam (Figure 2.9), suggesting it may at least partly be due to X-ray damage.

2.3.4.2 Analysis of Few Multilayers

The N 1s HR spectra from the films that resulted in about a monolayer of estimated coverage are shown in Figure 2.10. Similar to the spectra in Figure 2.8, only one major component can be seen and the positions (with FWHM in parentheses) were at 402.9 (1.4), 403.1 (1.4), and 403.1 (1.5) eV for the three compounds 1NO, 2NO, and 3NO, respectively. These positions and peak widths are similar to those of the reference spectra, which may indicate that the local nitrogen environment in an unbound amine oxide is similar to that when it is interacting with the surface in either a hydrogen bonding or Lewis basic manner. Although there is asymmetry in the peak in Figure 2.8c and the FWHM of 0.1 eV is larger than the set range, it is difficult to fit significant components into this peak. The N 1s of each of the films deposited from the other solutions (1.0, 1.5, 2.0 mM) are shown in Figure 2.11 and tabulated in Table 2.4.

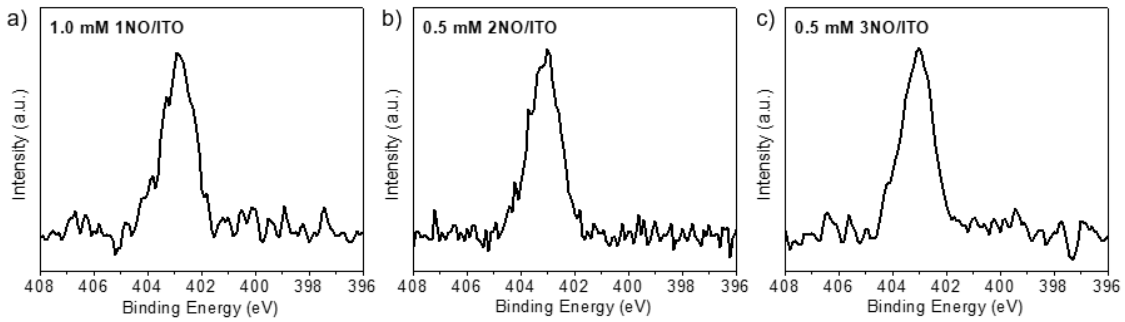

Figure 2.10. XPS N 1s of amine *N*-oxide/ITO for close to monolayer coverage, 1NO (a), 2NO (b), 3NO (c).

Table 2.4. N 1s peak positions of the multilayers of amine *N*-oxides on ITO.

System	Binding Energy (eV)	FWHM (eV)
1NO-1.0 mM	402.9	1.4
2NO-0.5 mM	403.1	1.4
2NO-1.0 mM	403.2	1.4
2NO-1.5 mM	403.1	1.3
2NO-2.0 mM	403.0	1.4
3NO-0.5 mM	403.1	1.5
3NO-1.0 mM	403.0	1.4
3NO-1.5 mM	403.0	1.3
3NO-2.0 mM	403.1	1.4

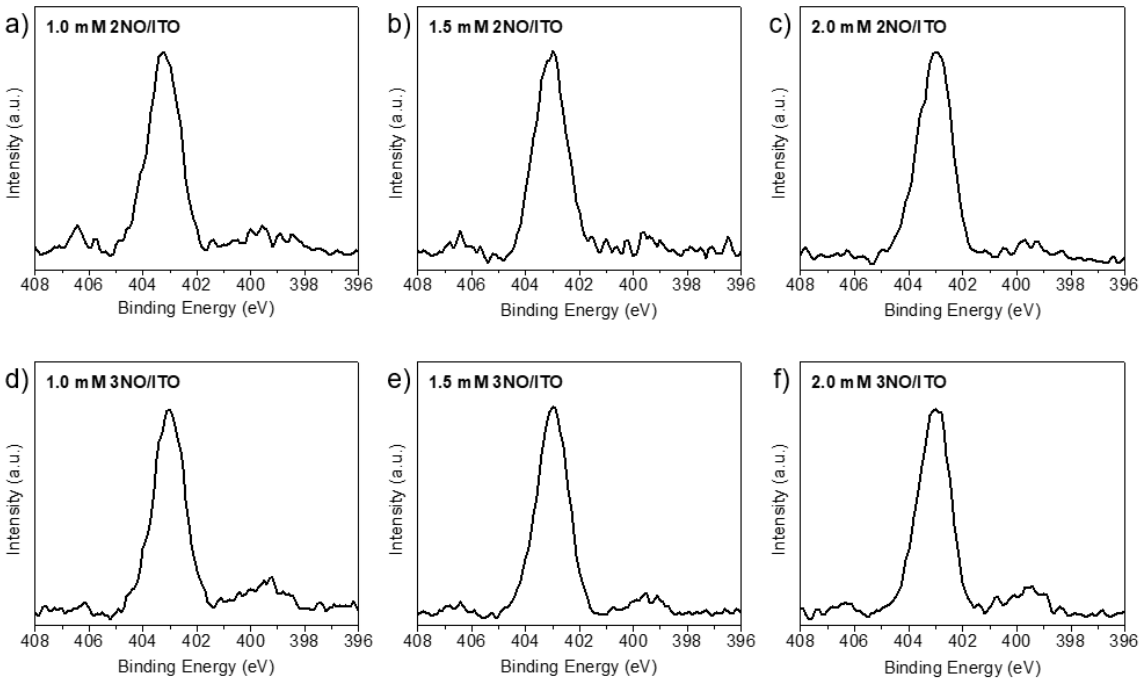

Figure 2.11. N 1s XPS signal from monolayers of amine *N*-oxide on ITO (from 0.5 or 1 mM dilutions), 1NO-0.5 (a), 2NO-0.5 (b), 3NO-0.5 (c). N 1s of 2NO and 3NO on ITO processed from spin coating different concentrations (0.5, 1.0, 1.5, 2.0 mM) of the amine *N*-oxides. The graphs were normalized and do not represent the relative intensities.

2.3.5 Washing Tests

To determine the robustness of the surface modifiers to processing conditions, two washing tests were performed on modified substrates (from 10 mM solutions).

2.3.5.1 Methanol Washing Test

Rinsing an amine oxide modified substrate with methanol, a polar solvent, results in little to no retention of the modifier on the surface (Table 2.5).

2.3.5.2 1,2-Dichlorobenzene Washing Test

In contrast, to verify the resistance to non-polar solvents, a washing test with 1,2-dichlorobenzene (DCB), a common solvent in depositing active layers in photovoltaics, was performed. In this test, modified substrates were measured for the WF and elemental compositions (by UPS/XPS) and then the same substrates were "washed" (by spin coating DCB at the same parameters listed in the experimental) and remeasured for the change.

Table 2.5. Work function values of washed substrates, under two different conditions, and the average N/In ratios (from N 1s and In 3d) of the sensitivity corrected intensities of the remaining modifiers after the washing condition. After substrates were modified according to the experimental (from 10 mM dilutions), they were washed (3 x 1 mL) with methanol (a), or with 1,2-dichlorobenzene* (spin coated at 3000 rpm, 1100 acceleration, for 30 sec., followed by annealing for 10 min at 70 °C) (b).

System	UPS Φ (eV)		XPS (N/In ratios)	
	[a]MeOH wash	[b*]1,2-DCB wash	[a]MeOH wash	[b*]1,2-DCB wash
ITO (OP)	4.81 ± 0.07	4.82 ± 0.07	–	
1NO	4.58 ± 0.04	4.40 ± 0.03	0.001	0.036 ± 0.005
2NO	4.75 ± 0.02	3.65 ± 0.03	0.001	0.870 ± 0.132
3NO	4.58 ± 0.03	3.62 ± 0.06	0.001	1.194 ± 0.210

* These substrates were measured prior to this wash, then washed by this method and re-measured. The control sample, ITO (OP) was not washed with 1,2-dichlorobenzene and represents the WF reduction over 6 h time.

As illustrated in Figure 2.12, the WF of ITO after 6 h, which was the time interval between when the substrate was first plasma treated to when the DCB-washed substrates were measured, reduced to 4.82 eV. The WF reduction of the control sample over time was expected as carbonaceous contaminants and particles from the atmosphere may have adhered to the surface. When 1NO-modified ITO was washed with DCB, the WF was similar to that of the control sample and increased from the original WF value (prior to the wash) by 0.18 eV. The resulting N/In ratios (listed in Table 2.2) also indicate that the surface modifiers were washed away to a degree, 40% for 1NO (Figure 2.12). The UPS spectra in Figure 2.12 also illustrate, however, that even with a DCB-wash, 2NO- and 3NO-modified ITO retain the large WF reduction from pre-wash, even though they both encountered a 52% and 55% reduction of the N/In ratio evident in the XPS spectra, respectively (Figure 2.12c). This implies that the DCB-washed surfaces are half the thickness as previously, which would result in ~2.4 nm and ~3 nm for 2NO and 3NO, respectively. This supports the previous result that thicknesses of at least 1.4 nm for either compound is required to reduce the WF of ITO to ~3.7 eV.

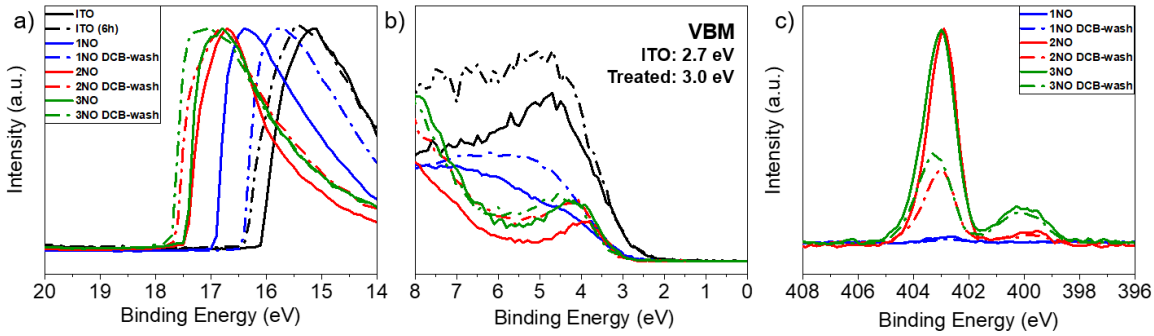

Figure 2.12. UPS spectra showing minimal WF shift after washing with DCB (a)[a], onset of ionization (b), corresponding reduction in nitrogen content for each modified surface (by XPS)[b]. [a] Values for WF and N/In ratios can be found in Table S3. [b] These spectra were normalized to the respective In 3d peak.

The onset of ionization, which gives insight to the band bending contribution versus the surface dipole contribution to the WF reduction, illustrates that the valence band maxima shift away from vacuum upon modification of ITO by ca. 0.3 eV (Figure 2.12b). This implies that the contribution to the WF reduction from the surface dipole (SD) generated from the modifiers is 0.59 eV (for 1NO), 1.04 eV (for 2NO), and 1.12 eV (for 3NO) (Figure 2.13). It is evident that there is a larger SD effect for 2NO and 3NO than for 1NO, which may be due to a net dipole from the two and three N–O groups per molecule that is larger than the dipole from 1 N–O group in 1NO, if the groups were oriented in a way that would lead to positive summation of the two vectors.

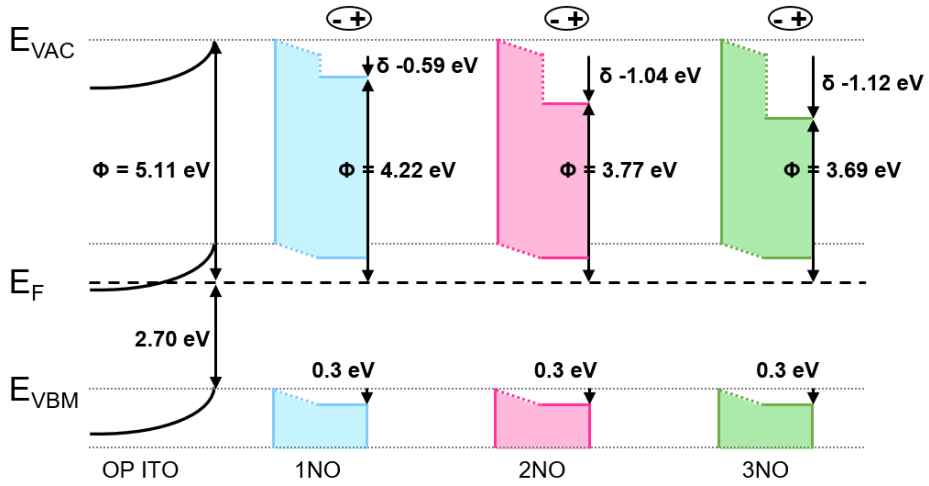

Figure 2.13. Schematic energy band diagrams, from UPS measurements, comparing the amine *N*-oxide modified ITO with OP ITO. Taking the shift in the valence band maxima, VBM, into account, the respective surface dipole contributions (δ) are indicated.

2.3.6 Contact Angle and Surface Energy

The surface of plasma treated ITO is very hydrophilic and addition of surface modifiers could alter that property depending on the nature of the surface modifier. To

determine the change in wettability of the amine *N*-oxide modified-ITO relative to just methanol-washed ITO, water contact-angle measurements were performed by changing the concentration of the solution from which the modifiers were spin coated.[35] The results show that with a methanol wash, the contact angle of oxygen plasma treated ITO increases from 21.4° to 41.6° (Figure 2.14).

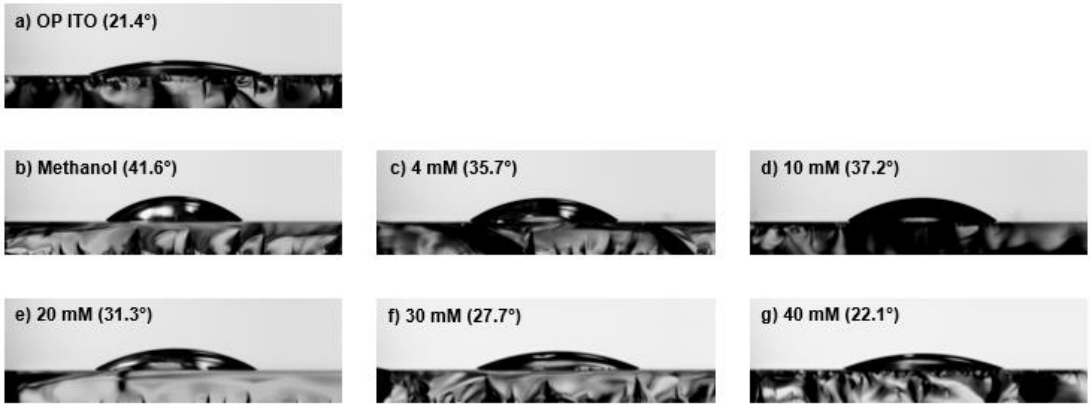

Figure 2.14. Contact angles with water, of OP ITO (21.4 ± 1.9°) (a), and OP ITO modified with various solvents and dilutions: methanol (41.6 ± 1.4°) (b), 4 mM 2NO in methanol (35.7 ± 1.0°) (c), 10 mM 2NO in methanol (37.2 ± 1.6°) (d), 20 mM 2NO in methanol (31.3° ± 1.8) (e), 30 mM 2NO in methanol (27.7 ± 1.4°) (f), 40 mM 2NO in methanol (22.1 ± 0.9°) (g).

As 2NO is introduced into methanol from 0.5 mM to 40 mM, the contact angle of the modified surface is initially similar to OP ITO at 20.1° and then increases to 35.7° (4 mM), and then decreases to 22.1° (40 mM). This indicates that at low concentration, the surface is hydrophilic and becomes hydrophobic with increasing thickness of surface modifier, then becomes hydrophilic again. The initial hydrophilicity of the modified substrate may indicate that the multilayers are oriented with the polar groups facing upwards (0.5 mM–2 mM) until a point at which the orientation becomes more randomized with increasing backbone facing upwards (4 mM–10 mM), which would increase

hydrophobicity and result in an increased contact angle. The final decrease back to the hydrophilicity of the unmodified surface may be due to the excess modifier dissolving in the probe liquid, which would spread the droplet horizontally and lead to a decreased contact angle.

2.3.7 Stability of Modified Substrates

2.3.7.1 Effect of UHV to the WF

To mitigate against loss of the modifier under UHV, the WF of the *N*-oxides were also measured by Kelvin Probe under nitrogen and remeasured after one week of exposure to ambient conditions (Figure 2.15). The results showed a similar trend to the UPS results, and the WF remained constant over one week, though with lower fluctuations within and among the substrates.

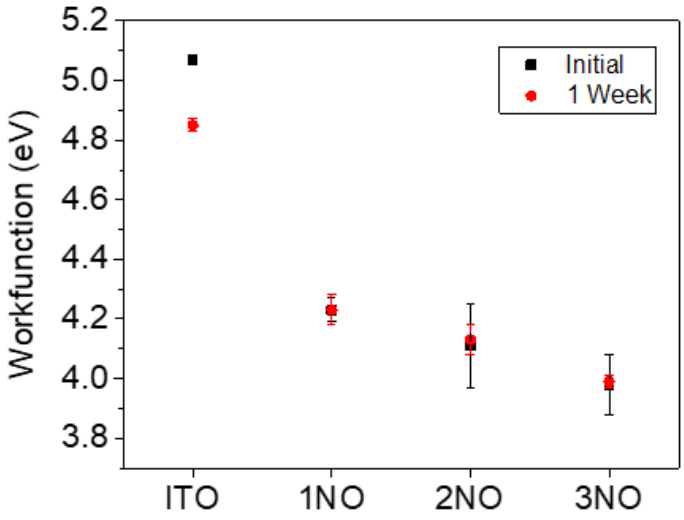

Figure 2.15 Work function values measured by Kelvin Probe under nitrogen for amine *N*-oxide modified ITO substrates (modified using the same procedure as the UPS measured samples in Table 2.3, from 10 mM dilutions) and the values after one week in ambient conditions.

2.3.7.2 Effect of UV Exposure to the WF

To determine whether the modified substrates would be affected by UV-exposure, the WF of 2NO-modified ITO substrates (from 2 mM, 3 mM and 4 mM solutions) were tracked with increasing exposure from 0, 10, to 30 min by Kelvin Probe in the glovebox.

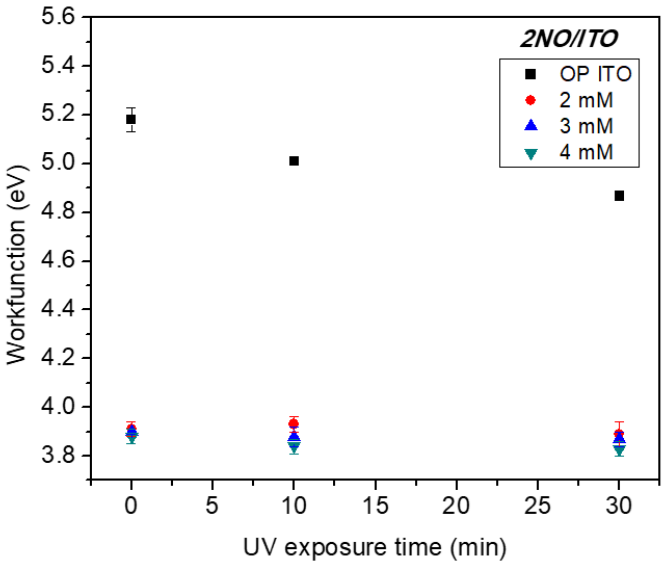

Figure 2.16. Work function values measured by Kelvin Probe under nitrogen for 2NO-modified ITO spin coated from different solutions, and under increasing amount of UV exposure.

According to Zhou et al., ITO substrates under UV illumination over several minutes experienced a reduction to the WF from 4.7 eV to 4.2 eV with reversibility upon exposure to ambient oxygen.[36] As displayed in Figure 2.16 and Table 2.6, while the WF of oxygen plasma treated ITO decreases from 5.2 to 4.9 eV with 30 min of UV exposure, the WF of the treated substrates remain constant.

Table 2.6. WF Values of UV-exposed 2NO-modified ITO measured by KP for Figure 2.16.

	UV exposure time		
	0 min	10 min	30 min
1 (OP ITO)	5.18 ± 0.05	5.01 ± 0.01	4.87 ± 0.02
2 (2 mM)	3.91 ± 0.03	3.93 ± 0.03	3.89 ± 0.05
3 (3 mM)	3.90 ± 0.01	3.88 ± 0.04	3.87 ± 0.03
4 (4 mM)	3.88 ± 0.03	3.84 ± 0.03	3.83 ± 0.03

2.3.7.3 Effect of Mixing with Non-Fullerene Acceptor

To determine whether an amine *N*-oxide would react with a popular non-fullerene acceptor, m-ITIC (3,9-bis(2-methylene-(3-(1,1-dicyanomethylene)-indanone))-5,5,11,11-tetrakis(4-hexylphenyl)-dithieno[2,3-d:2',3'-d']-s-indaceno[1,2-b:5,6-b']dithiophene) synthesized by Dr. Junxiang Zhang of the Marder group, within a device architecture, UV-vis absorption measurements of mixtures of the two compounds were taken. According to Zhou et al., PEI/PEIE, which contain aliphatic amine groups, react with ITIC and renders devices made with these two materials juxtaposed to each other, detrimental.[37] Since the amine *N*-oxides do not have aliphatic amine groups but all are in an oxidized state, it would be unlikely that they would react in the same manner proposed by other Zhou et al.[37]

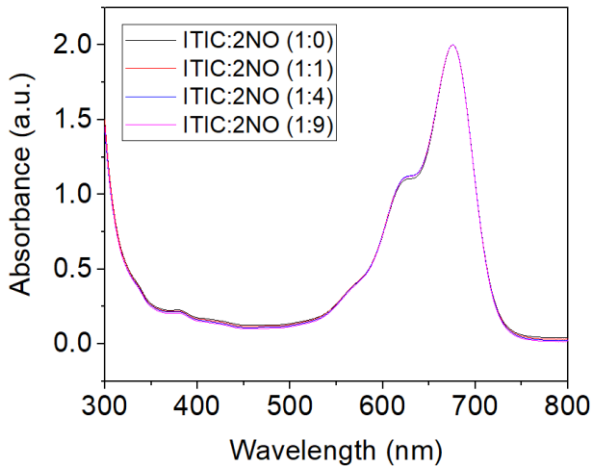

Figure 2.17. UV-vis absorption of mixtures of ITIC and 2NO in different ratios. The concentration of ITIC was fixed with increasing concentrations of 2NO introduced with the same final total volume for each measurement in chloroform and a drop of methanol.

As can be observed from Figure 2.17, the spectra with mixtures of the two compounds (1:1, 1:4, 1:9) all appear identical to the spectrum with only ITIC. This indicates that the structure of ITIC does not change in the presence of 2NO and that this likely indicates that there was no reaction between the two compounds. Therefore, 2NO is compatible to be used in a device adjacent to ITIC.

2.3.8 Conclusions

We have demonstrated for the first time the usage of aliphatic amine *N*-oxides without a conjugated backbone as surface modifiers on ITO. Compared to the non-oxidized amine precursors, the amine *N*-oxides demonstrate better adhesion to the surface and can lower the WF of ITO to values as low as 3.7 eV. Evaluation by XPS of the modified surface reveals that the nitrogen component on the surface-confined spectra does not differ significantly from the signal arising from the compound itself, but regardless, leads to an environment that causes a reduced WF. Washing with DCB led to about half of the surface

modifiers stripped from the surface, but a retention of the WF reduction due to the sufficient thickness. Contact angle studies showed that modified surfaces were as hydrophilic as plasma treated ITO at low concentrations.

We hypothesized that the dipoles from the amine *N*-oxide dipolar polar functional group would be more effective than the dipoles from amines in reducing the WF of ITO if aligned perpendicular to the surface. We indeed observed a greater WF reduction for ITO surfaces modified with the former. We can also conclude the amine *N*-oxides had stronger intermolecular interactions than amines from the observation that multilayers of the amine *N*-oxides could coat ITO. Increasing thicknesses of the surface modifier, except for 1NO, resulted in increasing WF reductions up to the saturation thickness of 1.4 nm. This observation suggests that the dipoles from the additional layers of surface modifier were largely in the direction of the surface, leading to increased molecular dipole and a greater reduction in WF.

2.4 Experimental

All chemicals were used as received from commercial sources without any further purification. ^{1}H and ^{13}C NMR spectra were recorded on a Varian Mercury Vx 300 spectrometer. Chemical shifts are reported in delta (δ) units, expressed in parts per million (ppm) vs. tetramethylsilane using the solvent as an internal standard (D_2O, 4.76 ppm for ^{1}H and 1,4-dioxane, 66.0 ppm for ^{13}C NMR).

2.4.1 Materials

2.4.1.1 *N*,*N*-dimethylhexan-1-amine oxide hydrate (1NO) [38]

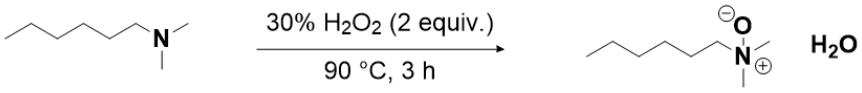

N,*N*-dimethylalkyl amine (2.7 mL, 1 mmol) was placed in a sealed tube and dissolved in 2 mL of methanol. Hydrogen peroxide (3.4 mL, 2 mmol, 30%) was added dropwise with vigorous stirring. The reaction was heated at 90 ºC for 3 h. The reaction crude was concentrated under reduced pressure and further dried under high vacuum. Finally, the oily residue was passed through a plug of basic alumina eluting first with dichloromethane and then dichloromethane:methanol 95:5 to afford a white solid 1NO•H_2O (1.23 g, 49%). ^{1}H NMR (300 MHz, D_2O, δ) 3.32 – 3.19 (m, 2H), 3.14 (s, 6H), 1.85 – 1.65 (m, 2H), 1.38 – 1.13 (m, 6H), 0.86 (t, *J* = 6 Hz, 3H). ^{13}C{^{1}H} NMR (75 MHz, D_2O, dioxane reference): 70.65, 57.20, 30.70, 25.43, 22.92, 21.86, 13.31. HRMS (ESI): Calcd for $C_8H_{20}NO$ (MH^+) 146.1539; found 146.1537 Anal. Calcd for $C_8H_{19}NO•H_2O$: C, 58.86; H, 12.97; N, 8.58. Found: C: 59.34; H: 12.95; N: 8.51.

2.4.1.2 *N*^{1},*N*^{1},*N*^{2},*N*^{2}-tetramethylethane-1,2-diamine dioxide trihydrate (TMEDAO/2NO)[39]

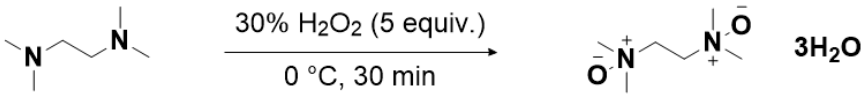

Hydrogen peroxide (9.0 mL, 90 mmol, 30%) was added to a wide necked round bottom flask and cooled to 0 °C. Tetramethylethylenediamine (2.7 mL, 18 mmol) was added dropwise over 5 min and then the mixture was stirred at 0 °C for 30 min. The solution was cooled to room temperature before being concentrated under reduced pressure (60 °C, 20 Torr). Water (3.0 mL) was added and the reaction mixture was again concentrated under reduced pressure, followed by drying under high vacuum, providing TMEDAO•3H_2O as a white solid (3.88 g, 98%). ^{1}H NMR (300 MHz, D_2O, δ): 3.85 (s, 4H, –C*H*$_2$), 3.25 (s, 12H, –C*H*$_3$); ^{13}C{^{1}H} NMR (75 MHz, D_2O, dioxane reference): 63.08 (CH_2), 58.68 (CH_3). These values match those in the literature. HRMS (ESI): Calcd for $C_6H_{17}N_2O_2$ (MH^+)

149.1285; found 149.1281. Anal. Calcd for $C_6H_{16}N_2O_2$•$3H_2O$: C, 35.63; H, 10.96; N, 13.85. Found: C: 35.24; H: 10.68; N: 13.74.

2.4.1.3 N^1-(2-(dimethyloxidoazanyl)ethyl)-N^1,N^2,N^2-trimethylethane-1,2-diamine dioxide pentahydrate (PMDETAO/3NO) [39]

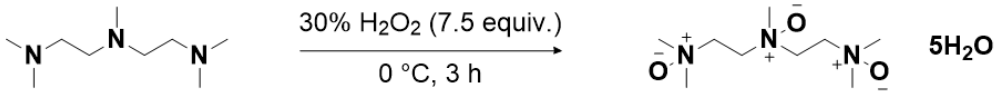

Hydrogen peroxide (9.0 mL, 90 mmol, 30%) was added to a round bottom flask and cooled to 0 °C. Pentamethyldiethylenetriamine (2.5 mL, 12 mmol) was added dropwise over 5 min and the reaction was stirred at 0 °C for 3 h. The solution was cooled to room temperature before being concentrated under reduced pressure. Water (3.0 mL) was added and the reaction mixture again concentrated under reduced pressure, followed by drying under high vacuum, providing PMDETAO•$5H_2O$ (3.43 g, 87%) as a white viscous oil. ^{1}H NMR (300 MHz, D_2O, δ): 3.93 (m, 8H, –CH_2), 3.27 (s, 6H, –CH_3), 3.26 (s, 6H, –CH_3), 3.22 (s, 3H, –CH_3); ^{13}C{^{1}H} NMR (75 MHz, D_2O, dioxane reference): 63.13, 62.74, 58.88, 58.58, 55.99. HRMS (ESI): Calcd for $C_9H_{23}N_3O_3Na$ (MNa^+) 244.1632; found 244.1637. Anal. Calcd for $C_9H_{23}N_3O_3$•$5H_2O$: C, 34.72; H, 10.68; N, 13.50; O, 41.11. Found: C: 34.77; H: 10.37; N: 13.51.

2.4.2 ITO Surface Cleaning and Modification

Commercially available ITO substrates (Eagle-XG, Thin Film Devices, Anaheim, CA) were cut into 0.5” × 0.5” squares and subjected to detergent-solvent cleaning. Substrates were first scrubbed with a 5% solution of Triton X-100 detergent in DI water, and immersed in sequential 10 min sonication baths in the diluted detergent, DI water, and ethanol, and dried under a flow of nitrogen. The DSC ITO were etched with oxygen plasma

(OP) with a PE-50 XL Plasma System for 5 min prior to any additional surface treatment. Substrates were modified by spin coating freshly prepared dilutions of amine in methanol at 3000 or 5000 rpm, 1100 acceleration, for 30 or 60 sec followed by annealing at 70 °C for 10 min. Samples were immediately taken for X-ray photoelectron spectroscopy /ultraviolet photoelectron spectroscopy (XPS/UPS) analysis.

2.4.3 Surface Characterization

2.4.3.1 UPS and XPS and KP

All UPS and XPS measurements were conducted in a Kratos Axis Ultra spectrometer with an average base pressure of 10^{-9} Torr. UPS spectra were collected prior to XPS spectra with a 21.2 eV He (I) excitation and a pass energy of 5 eV using a 27 μm spot size. XPS spectra were collected with a monochromatic Al Kα source using a 400 μm spot size and a pass energy of 160 eV for survey acquisition and 20 eV for high-resolution spectra. XPS was performed with a normal take-off angle (0°). Data were analyzed using Vision Processing software 2.2.8. The binding energies of all XPS spectra were calibrated and normalized to the In 3d line at 443.9 eV and processed with a Shirley background subtraction and Savitzky-Golay smoothing unless otherwise stated. The method for estimating the experimental coverage/thickness from XPS data was adapted from other works.[40-45] Kelvin Probe (KP) WF data were obtained using Besocke Delta Phi Kelvin Probe system in a nitrogen atmosphere. The measurements were calibrated to a freshly cleaved highly ordered pyrolytic graphite with a known work function of 4.50 eV.[36] All XPS, UP, and KP data points represent multiple samples scanned on multiple spots; standard deviation is reported among different samples.

2.4.4 Method for Experimental Estimation of Coverage and Thickness

The method for determining experimental coverage was detailed in previous work but of an amine on a gold surface. In this work, the same assumptions were considered and appropriate variables replaced as needed.[40]

Equation 8 from the above reference when considering an ITO surface, using In 3d as the line of interest from the bulk surface can be modified as such:

$$I_{\mathrm{In(total)}}/A = \lambda_{\mathrm{In}} \cdot k \cdot N_{\mathrm{In}}/V \qquad (1)$$

when considering a surface containing 28 In atoms/1180 Å^3 (model of 222 surface)[41] and an inelastic mean free path (IMFP) of 2.81 nm for In $3d_{5/2}$ at a 443.9 eV binding energy (whose kinetic energy is 1042.1 eV), when using Al Kα radiation ($h\nu$ = 1486 eV) derived from $\lambda = B(\mathrm{KE})^{0.5}$, the expression that can be used to estimate IMFP for photoelectrons with KE > 150 eV, where B for In is 0.087 nm,[43] which, inserting values of λ_{In} and N_{In}/V from above gives a value of:

$$I_{\mathrm{In(total)}}/A = k \cdot 0.67\ \text{Å}^{-2} = k \cdot (0.67 \times 10^{16}\ \mathrm{cm}^{-2}) \qquad (2)$$

replacing k with N_{N}/A (number of N atoms per unit area) leads to:

$$N_{\mathrm{N}}/A = (I_{\mathrm{N}}/I_{\mathrm{In(total)}}) \cdot (0.67 \times 10^{16}\ \mathrm{cm}^{-2}) \qquad (3)$$

by taking the intensities of the N 1s and In 3d that have been corrected for photoionization cross-section and detector sensitivity, we can arrive at a footprint of amine compound from experimental data (if the number of N atoms per compound is greater than one, the above equation must be multiplied by that factor to yield the footprint of the entire compound.

The method for determining experimental thickness was first detailed in a work by Carlson in determining the thickness of tungsten oxide on tungsten and Strohmeier to determine the thickness of aluminum oxide on aluminum.[44-45] For the aluminum oxide on

aluminum, the Al 2p signal from each layer was compared, and thus the expressions could be simplified further given only one IMFP. In our system however, the appropriate modifications were inputted in the expressions.

Assuming a uniform overlayer of oxide (2) on metal (1), the relative intensities of the peaks from XPS can be used in the following expression to determine the thickness (*d*) of the overlayer:

$$\frac{I_1}{I_2} = \frac{N_1\lambda_1}{N_2\lambda_2}\frac{\exp[-d/\lambda_2 \sin\theta]}{1-\exp[-d/\lambda_2 \sin\theta]} \quad (4)$$

where I_1 and I_2 refer to the intensities of the peaks of the metal and overlayer, respectively; N_1 refers to the volume density of metal atoms in the metal (in our case, In atoms in ITO), and N_2 refers to the volume density of metal atoms in the oxide (in our case, N atoms in the overlayer) (or in other terms, the atoms per unit volume), λ_1 and λ_2 refer to the IMFP of the appropriate photoelectrons in the metal and oxide, respectively (in nm), and θ refers to the electron take-off angle (with respect to the sample surface). The expression can be simplified and rearranged in terms of *d*:

$$d = \lambda_2 \sin\theta \ln\left[\frac{N_1\lambda_1}{N_2\lambda_2}\frac{I_2}{I_1} + 1\right] \quad (5)$$

where the expression for the atomic number density of our system is given by:

$$\frac{N_{In,ITO}}{N_{N,overlayer}} = \frac{\rho_{ITO}F_{overlayer}}{\rho_{overlayer}F_{ITO}} \quad (6)$$

where ρ_x is the density of material x and F_x is the formula weight of x. The formula weight of ITO, F_{ITO} should be divided by the number of atoms present of the element that we are obtaining the number density for ITO (in this case In). We are assuming ITO to represent In_2O_5Sn, thus the value for F_{ITO} must be divided by 2 to give the formula weight for 1 mole of In atoms. To obtain $F_{overlayer}$, the molecular weight of each anhydrous amine *N*-oxide

was divided by the number of N atoms per compound. The density of these were also assumed to be 1 g cm^{-3}, which is an underestimation given that the compounds were solids or viscous liquid. The IMFP for the compounds was also calculated by the method given by Cumpson.[42]. In our case, $\theta = 90°$ and the sin term was simplified to equal 1.

The following parameters were used:

$\rho_{ITO} = 6.65\ g\ cm^{-3}$

$\rho_{overlayer} = 1.0\ g\ cm^{-3}$

$F_{ITO} = 428.34\ au$

$F_{overlayer} = MW/N_x\,; F_{1NO} = 145.25\ au, F_{2NO} = 74.11\ au, F_{3NO} = 73.77\ au$

$\lambda_1 = 2.81\ nm$

λ_2: $\lambda_{1NO} = 3.53\ nm,\ \lambda_{2NO} = 3.46\ nm,\ \lambda_{3NO} = 3.40\ nm$

by taking the intensities of the N 1s and In 3d that have been corrected for photoionization cross-section and detector sensitivity (same inputs as for determination of coverage), we can arrive at a thickness of overlayer on ITO.

2.5 References

[1] Rivaton, A.; Chambon, S.; Manceau, M.; Gardette, J.-L.; Lemaître, N.; Guillerez, S., Light-Induced Degradation of the Active Layer of Polymer-Based Solar Cells. *Polym. Degrad. Stab.* **2010,** *95* (3), 278-284.

[2] Voroshazi, E.; Verreet, B.; Buri, A.; Müller, R.; Di Nuzzo, D.; Heremans, P., Influence of Cathode Oxidation Via the Hole Extraction Layer in Polymer:Fullerene Solar Cells. *Org. Electron.* **2011,** *12* (5), 736-744.

[3] Norrman, K.; Gevorgyan, S. A.; Krebs, F. C., Water-Induced Degradation of Polymer Solar Cells Studied by H2(18)O Labeling. *ACS Appl. Mater. Interfaces* **2009,** *1* (1), 102-112.

[4] Guan, X.; Zhang, K.; Huang, F.; Bazan, G. C.; Cao, Y., Amino N-Oxide Functionalized Conjugated Polymers and Their Amino-Functionalized Precursors: New Cathode Interlayers for High-Performance Optoelectronic Devices. *Adv. Func. Mater.* **2012,** *22* (13), 2846-2854.

[5] Duan, C.; Zhang, K.; Zhong, C.; Huang, F.; Cao, Y., Recent Advances in Water/Alcohol-Soluble Π-Conjugated Materials: New Materials and Growing Applications in Solar Cells. *Chem. Soc. Rev.* **2013,** *42* (23), 9071-9104.

[6] He, Z.; Wu, H.; Cao, Y., Recent Advances in Polymer Solar Cells: Realization of High Device Performance by Incorporating Water/Alcohol-Soluble Conjugated Polymers as Electrode Buffer Layer. *Adv. Mater.* **2014,** *26* (7), 1006-1024.

[7] Hu, Z.; Zhang, K.; Huang, F.; Cao, Y., Water/Alcohol Soluble Conjugated Polymers for the Interface Engineering of Highly Efficient Polymer Light-Emitting Diodes and Polymer Solar Cells. *Chem. Commun.* **2015,** *51* (26), 5572-5585.

[8] Huang, F.; Wu, H.; Wang, D.; Yang, W.; Cao, Y., Novel Electroluminescent Conjugated Polyelectrolytes Based on Polyfluorene. *Chem. Mater.* **2004,** *16* (4), 708-716.

[9] Seo, J. H.; Gutacker, A.; Sun, Y.; Wu, H.; Huang, F.; Cao, Y.; Scherf, U.; Heeger, A. J.; Bazan, G. C., Improved High-Efficiency Organic Solar Cells Via Incorporation of a Conjugated Polyelectrolyte Interlayer. *J. Am. Chem. Soc.* **2011,** *133* (22), 8416-8419.

[10] Ma, D.; Lv, M.; Lei, M.; Zhu, J.; Wang, H.; Chen, X., Self-Organization of Amine-Based Cathode Interfacial Materials in Inverted Polymer Solar Cells. *ACS Nano* **2014,** *8* (2), 1601-1608.

[11] Page, Z. A.; Liu, Y.; Duzhko, V. V.; Russell, T. P.; Emrick, T., Fulleropyrrolidine Interlayers: Tailoring Electrodes to Raise Organic Solar Cell Efficiency. *Science* **2014,** *346* (6208), 441-444.

[12] Zhang, F.; Ceder, M.; Inganäs, O., Enhancing the Photovoltage of Polymer Solar Cells by Using a Modified Cathode. *Adv. Mater.* **2007,** *19* (14), 1835-1838.

[13] Zhou, Y.; Fuentes-Hernandez, C.; Shim, J.; Meyer, J.; Giordano, A. J.; Li, H.; Winget, P.; Papadopoulos, T.; Cheun, H.; Kim, J.; Fenoll, M.; Dindar, A.; Haske, W.; Najafabadi, E.; Khan, T. M.; Sojoudi, H.; Barlow, S.; Graham, S.; Brédas, J.-L.; Marder, S. R.; Kahn, A.; Kippelen, B., A Universal Method to Produce Low-Work Function Electrodes for Organic Electronics. *Science* **2012,** *336* (6079), 327-32.

[14] Sun, K.; Zhao, B.; Murugesan, V.; Kumar, A.; Zeng, K.; Subbiah, J.; Wong, W. W. H.; Jones, D. J.; Ouyang, J., High-Performance Polymer Solar Cells with a Conjugated Zwitterion by Solution Processing or Thermal Deposition as the Electron-Collection Interlayer. *J. Mater. Chem.* **2012,** *22* (45), 24155-24165.

[15] Huang, F.; Niu, Y. H.; Zhang, Y.; Ka, J. W.; Liu, M. S.; Jen, A. K. Y., A Conjugated, Neutral Surfactant as Electron-Injection Material for High-Efficiency Polymer Light-Emitting Diodes. *Adv. Mater.* **2007,** *19* (15), 2010-2014.

[16] Xu, X.; Han, B.; Chen, J.; Peng, J.; Wu, H.; Cao, Y., 2,7-Carbazole-1,4-Phenylene Copolymers with Polar Side Chains for Cathode Modifications in Polymer Light-Emitting Diodes. *Macromol.* **2011,** *44* (11), 4204-4212.

[17] Zhang, Z.-G.; Qi, B.; Jin, Z.; Chi, D.; Qi, Z.; Li, Y.; Wang, J., Perylene Diimides: A Thickness-Insensitive Cathode Interlayer for High Performance Polymer Solar Cells. *Energy Environ. Sci.* **2014,** *7* (6), 1966-1973.

[18] Zhao, K.; Ye, L.; Zhao, W.; Zhang, S.; Yao, H.; Xu, B.; Sun, M.; Hou, J., Enhanced Efficiency of Polymer Photovoltaic Cells Via the Incorporation of a Water-Soluble Naphthalene Diimide Derivative as a Cathode Interlayer. *J. Mater. Chem. C* **2015,** *3* (37), 9565-9571.

[19] Chakravarthi, N.; Park, H.-Y.; Aryal, U. K.; Kim, J.; Gal, Y.-S.; Song, M.; Cho, Y.-R.; Jin, S.-H., Phosphine Oxide and Amino N-Oxide Functionalized Phenylquinoline-Based Small Molecules: New Cathode Interfacial Layers for High-Performance Inverted Organic Solar Cells. *Org. Electron.* **2018,** *58*, 111-118.

[20] Liu, J.; Zhang, L.; Xu, H.; Ding, Z.; Hu, J.; Liu, Y., Amino N-Oxide Functionalized Graphene Quantum Dots as Cathode Interlayer for Inverted Polymer Solar Cells. *J. Mater. Chem. C* **2018**.

[21] Duan, C.; Wang, L.; Zhang, K.; Guan, X.; Huang, F., Conjugated Zwitterionic Polyelectrolytes and Their Neutral Precursor as Electron Injection Layer for High-Performance Polymer Light-Emitting Diodes. *Adv. Mater.* **2011,** *23* (14), 1665-1669.

[22] Liu, F.; Page, Z. A.; Duzhko, V. V.; Russell, T. P.; Emrick, T., Conjugated Polymeric Zwitterions as Efficient Interlayers in Organic Solar Cells. *Adv. Mater.* **2013,** *25* (47), 6868-6873.

[23] He, Z.; Zhong, C.; Huang, X.; Wong, W.-Y.; Wu, H.; Chen, L.; Su, S.; Cao, Y., Simultaneous Enhancement of Open-Circuit Voltage, Short-Circuit Current Density, and Fill Factor in Polymer Solar Cells. *Adv. Mater.* **2011,** *23* (40), 4636-4643.

[24] He, Z.; Zhang, C.; Xu, X.; Zhang, L.; Huang, L.; Chen, J.; Wu, H.; Cao, Y., Largely Enhanced Efficiency with a PFN/Al Bilayer Cathode in High Efficiency Bulk Heterojunction Photovoltaic Cells with a Low Bandgap Polycarbazole Donor. *Adv. Mater.* **2011,** *23* (27), 3086-3089.

[25] Zhang, W.; Zhao, B.; He, Z.; Zhao, X.; Wang, H.; Yang, S.; Wu, H.; Cao, Y., High-Efficiency Ito-Free Polymer Solar Cells Using Highly Conductive PEDOT:PSS/Surfactant Bilayer Transparent Anodes. *Energy Environ. Sci.* **2013,** *6* (6), 1956-1964.

[26] Tordera, D.; Kuik, M.; Rengert, Z. D.; Bandiello, E.; Bolink, H. J.; Bazan, G. C.; Nguyen, T.-Q., Operational Mechanism of Conjugated Polyelectrolytes. *J. Am. Chem. Soc.* **2014,** *136* (24), 8500-8503.

[27] Lu, S.; Guan, X.; Li, X.; Sha, W. E. I.; Xie, F.; Liu, H.; Wang, J.; Huang, F.; Choy, W. C. H., A New Interconnecting Layer of Metal Oxide/Dipole Layer/Metal Oxide for Efficient Tandem Organic Solar Cells. *Adv. Energy Mater.* **2015,** *5* (17), 1500631.

[28] Wurthner, F., Perylene Bisimide Dyes as Versatile Building Blocks for Functional Supramolecular Architectures. *Chem. Commun.* **2004,** (14), 1564-1579.

[29] Weil, T.; Vosch, T.; Hofkens, J.; Peneva, K.; Müllen, K., The Rylene Colorant Family—Tailored Nanoemitters for Photonics Research and Applications. *Angew. Chem. Int. Ed.* **2010,** *49* (48), 9068-9093.

[30] Huang, C.; Barlow, S.; Marder, S. R., Perylene-3,4,9,10-Tetracarboxylic Acid Diimides: Synthesis, Physical Properties, and Use in Organic Electronics. *J. Org. Chem.* **2011,** *76* (8), 2386-2407.

[31] Chen, L.; Li, C.; Mullen, K., Beyond Perylene Diimides: Synthesis, Assembly and Function of Higher Rylene Chromophores. *J. Mater. Chem. C* **2014,** *2* (11), 1938-1956.

[32] Hu, Z.; Xu, R.; Dong, S.; Lin, K.; Liu, J.; Huang, F.; Cao, Y., Quaternisation-Polymerized N-Type Polyelectrolytes: Synthesis, Characterisation and Application in High-Performance Polymer Solar Cells. *Mater. Horiz.* **2017,** *4* (1), 88-97.

[33] Program, N. T. Chemical Information Profile for Indium Tin Oxide. https://ntp.niehs.nih.gov/ntp/noms/support_docs/ito060309_508.pdf (accessed March 28, 2018).

[34] Kim, J. S.; Ho, P. K. H.; Thomas, D. S.; Friend, R. H.; Cacialli, F.; Bao, G. W.; Li, S. F. Y., X-Ray Photoelectron Spectroscopy of Surface-Treated Indium-Tin Oxide Thin Films. *Chem. Phys. Lett.* **1999,** *315* (5), 307-312.

[35] Lee, B. R.; Jung, E. D.; Nam, Y. S.; Jung, M.; Park, J. S.; Lee, S.; Choi, H.; Ko, S. J.; Shin, N. R.; Kim, Y. K.; Kim, S. O.; Kim, J. Y.; Shin, H. J.; Cho, S.; Song, M. H., Amine-Based Polar Solvent Treatment for Highly Efficient Inverted Polymer Solar Cells. *Adv. Mater.* **2014,** *26* (3), 494-500.

[36] Zhou, Y.; Shim, J. W.; Fuentes-Hernandez, C.; Sharma, A.; Knauer, K. A.; Giordano, A. J.; Marder, S. R.; Kippelen, B., Direct Correlation between Work Function of Indium-Tin-Oxide Electrodes and Solar Cell Performance Influenced by Ultraviolet Irradiation and Air Exposure. *Phys. Chem. Chem. Phys.* **2012,** *14* (34), 12014-12021.

[37] Hu, L.; Liu, Y.; Mao, L.; Xiong, S.; Sun, L.; Zhao, N.; Qin, F.; Jiang, Y.; Zhou, Y., Chemical Reaction between an Itic Electron Acceptor and an Amine-Containing Interfacial Layer in Non-Fullerene Solar Cells. *J. Mater. Chem. A* **2018,** *6* (5), 2273-2278.

[38] Galan, A.; Espelt, M.; Ballester, P., Intermittent Compression of N-Alkyl-N,N-Dimethylamine N-Oxides Encapsulated in a Container with Bis[2]Catenane Topology. *Supramol. Chem.* **2016,** *28* (5-6), 455-463.

[39] Read, C. D. G.; Moore, P. W.; Williams, C. M., N,N,N',N'-Tetramethylenediamine Dioxide (TMEDAO2) Facilitates Atom Economical/Open Atmosphere Ley-Griffith (Tpap) Tandem Oxidation-Wittig Reactions. *Green Chem.* **2015,** *17* (9), 4537-4540.

[40] Kim, H. K.; Hyla, A. S.; Winget, P.; Li, H.; Wyss, C. M.; Jordan, A. J.; Larrain, F. A.; Sadighi, J. P.; Fuentes-Hernandez, C.; Kippelen, B.; Brédas, J.-L.; Barlow, S.; Marder, S. R., Reduction of the Work Function of Gold by N-Heterocyclic Carbenes. *Chem. Mater.* **2017,** *29* (8), 3403-3411.

[41] Paramonov, P. B.; Paniagua, S. A.; Hotchkiss, P. J.; Jones, S. C.; Armstrong, N. R.; Marder, S. R.; Brédas, J.-L., Theoretical Characterization of the Indium Tin Oxide Surface and of Its Binding Sites for Adsorption of Phosphonic Acid Monolayers. *Chem. Mater.* **2008,** (20), 5131-5133.

[42] Cumpson, P. J., Estimation of Inelastic Mean Free Paths for Polymers and Other Organic Materials Use of Quantitative Structure-Property Relationships. *Surf. Interface Anal.* **2001,** *31*, 23-34.

[43] Seah, M. P.; A., D. W., Quantitative Electron Spectroscopy of Surfaces: A Standards Data Base for Electron Inelastic Mean Free Path in Solids. *Surf. Interface Anal.* **1979,** *1* (1), 2-11.

[44] Carlson, T. A.; McGuire, G. E., Study of the X-Ray Photoelectron Spectrum of Tungsten—Tungsten Oxide as a Function of Thickness of the Surface Oxide Layer. *J. Electron Spectrosc. Relat. Phenom.* **1972,** *1* (2), 161-168.

[45] Strohmeier, B. R., An ECSA Method for Determining the Oxide Thickness on Aluminum Alloys. *Surf. Interface Anal.* **2004,** *15* (1), 51-56.

CHAPTER 3
REDUCTION OF THE WORK FUNCTION OF GOLD BY N-HETEROCYCLIC CARBENES

3.1 Introduction

For many electronic devices, including organic light-emitting diodes, photovoltaics, and n-channel transistors, at least one low-work function (WF) electrode material is required to facilitate electron injection or collection at the organic semiconductor/electrode interface. Intrinsically low-WF metals such as calcium, however, are highly reactive to oxygen and moisture. Their use can be circumvented by using high-WF materials coated with surface modifiers that lead to a dipole at the surface, which induces a shift in the vacuum level and a reduction of the WF. This chapter is the result of a collaboration and all calculations were performed by Dr. Alexander Hyla.

3.1.1 Reductants on Gold Surfaces

Gold has a high WF (ca. 5.2 eV for clean surfaces) and is widely used for electronics applications due to its conductivity and excellent stability in a variety of chemical environments. Its WF can be significantly lowered using molecular reductants that, when deposited on gold from either solution or vacuum, give rise to a surface dipole through electron transfer to the gold. Reductants that have been examined include tetrakis(dimethylamino)ethylene,[1] neutral methyl viologen,[2] acridine orange base,[3] and the organometallic dimeric sandwich complexes $(MCp^*Cp)_2$ {M = Rh, Ir; Cp* = C_5Me_5; Cp = C_5H_5};[4-5] the lowest WF value obtained is 2.7 eV, measured using UV photoelectron spectroscopy (UPS) for a 15 Å film of $(RhCp^*Cp)_2$ vacuum deposited on clean Au(111).[5] Another method to significantly lower the WF of Au is the use of

polyethylenimine (PEI) or its ethoxylated derivative (PEIE), which are only processable from solution; a WF of 3.4 eV was measured using UPS for PEIE-treated gold, whereas either polymer affords WFs of ca. 3.9 eV as measured by Kelvin probe (KP) *in air*.[6] This WF reduction is thought to originate from both the dipole resulting from coordination of multiple amine groups in the polymer to the surface and the resulting alignment of the C–N bonds in the polymer and their dipoles. In contrast to most of the reductants and reductant-treated gold surfaces mentioned above, both the polymers and the modified surfaces are stable in air; on the other hand, the exact composition on the surface is challenging to determine, layers are not necessarily of uniform thickness, and the water present in the commercially available reagents may adversely affect stability for some applications.

Self-assembled monolayers (SAMs) are yet another class of surface modifiers that can be used to lower WF. Since their first use by Nuzzo and Allara,[7] thiolates have become the most widely used components for SAMs on gold; alkanethiolate monolayers typically reduce the WF of gold to ca. 4 eV, with the exact value depending on the alkyl chain and the measurement technique.[8-10] A very low WF of 1.6 eV has recently been determined using the field emission properties of Au-coated nanowires with a [121]tetramantane-2-thiolate SAM; however, this value is attributable to formation of the radical cation of the modifier at the tip of the nanowires, and a typical alkylthiolate SAM WF value of ca. 4 eV was found by UPS.[10]

Thiolate-based SAMs offer the possibility of combining WF reduction with other properties through synthetic thiol chemistry. SAMs of simple alkyl thiols are thermally and oxidatively unstable;[11-12] however, more stable monolayers can be attained using, for

example, [13] or multidentate thiols,[14] although the fluoroalkyl thiols are not effective at lowering the WF.[9]

3.1.2 N-Heterocyclic Carbenes

N-Heterocyclic carbenes (NHCs) have been widely used as ligands in transition-metal chemistry[15-19] and have increasingly been used as ligands for gold nanoparticles.[20-22] In the past few years, they have been used as SAM-forming modifiers on planar surfaces of various metals, [20] including gold.[23-27] Many precursor salts and free NHCs are commercially available or can be obtained through fairly simple synthetic procedures.[28] The ligand characteristics of NHCs can be altered through saturation/unsaturation and variation of ring size and through heteroatom substituents,[29-30] whereas additional characteristics can be imparted through derivatization of their backbones (for example, NHC SAMs on Au have been functionalized by "click" chemistry using azide functionalities[23] and through initiation of ring-opening metathesis polymerization from pendant alkene moieties).[25]

Crudden et al. demonstrated that NHCs on Au are more stable than thiolate-based SAMs; monolayers of dodecyl thiolate were partially displaced by iPr_2bimy (see Figure 3.1) through immersion in a solution of the latter, but dodecanethiol was unable to displace iPr_2bimy.[23] In addition, NHC SAMs are found to be resistant to boiling water, organic solvents, alkaline and acidic environments, electrochemical oxidation and reduction, and 1% H_2O_2.[23] The increased stability was attributed to the greater binding energy of NHC–Au (149 and 158 kJ mol^{-1} according to DFT-PBEsol calculations and temperature-programmed desorption measurements respectively for iPr_2bimy[23, 26] compared with thiolate–Au (ca. 125 kJ mol^{-1}).[31-32] Although these studies addressed the packing order, the

ability to graft polymers, and thermal and chemical stabilities of NHC SAMs on gold surfaces, the effect of NHCs on the WF of Au has not, to the best of our knowledge, been studied experimentally. A recent DFT study, however, has suggested the WF of Au modified with 4-(adamantan-1-yl)-1,3-dihydro-2*H*-imidazol-2-ylidene or its *N*,*N*′-diisopropyl analogue would be ca. 3.8 eV.[33]

3.2 N-Heterocyclic Carbenes Studied

Here we report an experimental investigation of the effect of a series of NHCs (Figure 3.1) on the WF of planar Au surfaces in which we measure values as low as 3.3 eV using UPS.

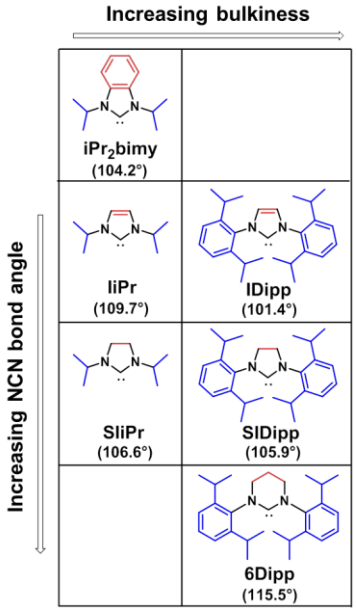

Figure 3.1. Chemical structures of NHCs used in this work to reduce the WF of Au surfaces; red (backbone) and blue (substituents) colored for emphasis. N–C–N bond angles are from gas-phase PBE/cc-pVTZ calculations. Note that the bond-angle difference between **IiPr** and **SIiPr** does not follow the expected trend. (See Table 3.1 for N–C–N bond angles for NHCs bound to gold). The bond-angle calculations were performed by Dr. Alexander Hyla. Reprinted with permission from ref.[34]. Copyright 2017 American Chemical Society.

DFT calculations are used to gain insight into the mechanism of the WF reduction and show qualitative differences between NHCs with relatively small (isopropyl) and bulky (2,6-diisopropylphenyl) N,N′-substituents.

Figure 3.1 shows the NHCs considered in this study; all six compounds were studied computationally, and all except SIiPr were examined experimentally.[35-36] SIiPr and other *N*,*N*′-dialkyl analogues dimerize in solution[35] and so were excluded from the experimental study (but retained in computational work for comparison to SIDipp) to avoid possible complications arising from dimer—Au interactions. NHC dimers are moderately strong one-electron reductants[36] and so might be expected to reduce the WF of Au through an electron-transfer reaction, similar to that between, for example, methyl viologen and Au.[2]

We were interested in varying both the nature of the NHC backbone and the N,N′-substituents. The backbone structure affects the N–C–N bond angle and, thus, the basicity of the NHC lone pair; the molecules in each column of Figure 3.1 are arranged in order of expected increasing bond angle and basicity.[29-30] See Table 3.1 for N–C–N bond angles for NHCs bound to gold.

Table 3.1. Calculated N–C–N Bond Angles (°) for Isolated NHC Molecules[a] and After Interacting with Au(111). These values were calculated by Dr. Alexander Hyla. Reprinted with permission from ref.[34]. Copyright 2017 American Chemical Society.

NHC	Isolated Carbene	Carbene on Gold
iPr$_2$bimy	104.2	106.4
IiPr	109.7	104.5
SIiPr	106.6	108.8
IDipp	101.4	101.5
SIDipp	105.9	105.9
6Dipp	115.5	116.1

Changing the N,N′-substituents can potentially impact both electronic and steric properties; *N*,*N*′-dialkyl NHCs are expected to have higher Brønsted basicities than their *N*,*N*′-diaryl analogues;[29-30] however, because out of plane twisting of aryl moieties can reduce steric interactions with an atom bound to the carbene lone pair, this does not necessarily translate to higher nucleophilicity, Lewis basicity, or electron-donating strength as a ligand.[30, 37] On the other hand, in the present study, 2,6-diisopropylphenyl substituents might be expected to impair the ability of the lone pair to interact with a planar Au surface. We note that iPr_2bimy and IDipp were among the examples used to modify Au by Crudden et al.[23]

3.2.1 XPS Characterization and Molecular Coverage

Since the NHCs have substituents with varying degrees of steric bulk and orientation with respect to the surface, the absolute molecular coverage may vary among the different modified surfaces. Coverage has been shown to play a significant role in the WF modification ability of a surface modifier.[38-39] Plasma-treated Au surfaces were modified under inert atmosphere by dipping in 2 mM THF solutions of the NHC for 24 h, and then the surface composition of the samples was investigated using XPS.

N 1s ionizations are observed for the modified surfaces at binding energies of ca. 400–402 eV, consistent with other reports of NHCs on planar gold,[20, 24-25] In the case of 6Dipp two distinct N signals are seen; the reason for this is unclear, but the lower binding energy signal may arise from NHC molecules that are oriented differently to the majority on the surface, to NHC molecules in a second layer on the surface, and/or from X-ray damage to the surface (since the low cross-section for N 1s ionization and the low nitrogen coverage for these molecules necessitates the use of long acquisition times). The third

possibility is supported by the low-BE feature appearing at similar BE to that of the decomposition product obtained by extensive air exposure of SIDipp-modified Au (see Figure 3.8) and with NHC adhering to the surface. Moreover, the intensity of the N 1s signal (and the N 1s/Au 4f intensity ratio) indicates that the smaller NHCs (a, b) more densely cover the surface than the larger ones (c–e) (Figure 3.2).

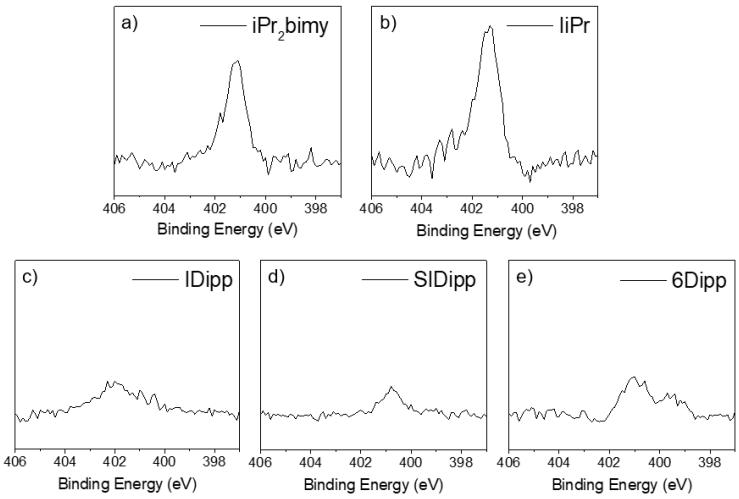

Figure 3.2. Representative XPS N 1s spectra for NHCs on Au. Reprinted with permission from ref.[34]. Copyright 2017 American Chemical Society.

Table 3.2 summarizes the molecular footprint for each geometry-optimized NHC in the calculations, the ideal absolute close-packed, noninteracting coverage value (in molecules cm^{-2}) from the calculated footprint (Figure 3.3b), the experimental absolute coverage as estimated from XPS N/Au ratios (see 3.4.4), and the percentage ideal monolayer values obtained from the comparison of experimental coverage compared to those calculated for a full monolayer. As in the experimental data, the calculated molecular footprints suggest the coverage attainable should depend on the N,N′-substituents, with the

bulkier NHCs with bis(2,6-diisopropylphenyl) substituents being present at one-half to one-third the coverage of the diisopropyl-substituted NHCs.

Table 3.2. Calculated and Experimental Coverages for NHCs on Gold. The calculated values were performed by Dr. Alexander Hyla. Reprinted with permission from ref.[34]. Copyright 2017 American Chemical Society.

NHC	Footprint / Å^2		Coverage / 10^{14} molecule cm^{-2}		
	Calcd	Exptl[a]	Ideal[b]	Exptl[c]	% Ideal Monolayer[d]
iPr_2bimy	29.4	30 ± 6	3.40	3.3 ± 0.6	99
IiPr	29.5	33 ± 6	3.39	3.0 ± 0.5	89
SIiPr	29.5	e	3.39	e	e
IDipp	78.1	65 ± 15	1.28	1.5 ± 0.3	121
SIDipp	83.0	78 ± 11	1.21	1.3 ± 0.2	106
6Dipp	80.7	72 ± 13	1.24	1.4 ± 0.3	112

[a] The experimental footprint given is the reciprocal of the coverage. [b] Estimated as the reciprocal of the calculated footprint. Note that the footprint (Figure 3.3) is based on an ellipse, which cannot be tessellated to fully cover the surface; however, this overlooks the possibility of overlap of the substituents of neighboring ellipses through interlocking of alkyl substituents. [c] Experimental average coverage estimated from XPS data; the error bars are estimated based on spot-to-spot variation of XPS peaks, but do not take into account approximations made in converting XPS ratios to atomic ratios. [d] Percentage ideal monolayer given by 100% × experimental coverage / ideal coverage. [e] Not measured.

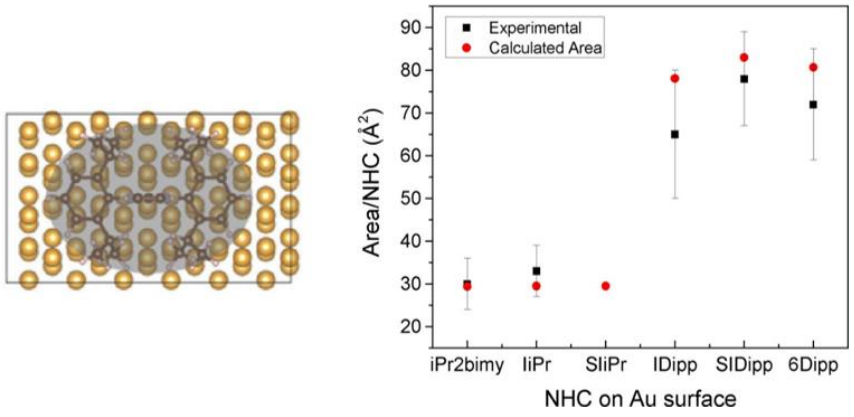

Figure 3.3. Left: Representative footprint of an NHC (IDipp) on a Au(111) surface from DFT calculations. Right: Comparison of experimental and calculated footprints for different NHCs. The left image was made by Dr. Alexander Hyla and the calculated areas in the right plot was provided by Dr. Alexander Hyla as well. Reprinted with permission from ref.[34]. Copyright 2017 American Chemical Society.

The results also show that the experimental estimated coverages are rather close to that estimated for complete monolayers at 89–121% and track fairly linearly (Figure 3.3b). This suggests that the NHCs are tightly packed and, therefore, leave little room for contaminants to interact with the surface. We note that the experimental coverage estimated here for iPr_2bimy is very similar to that previously estimated for a ferrocene-functionalized iPr_2bimy derivative on Au ($(3.5 \pm 0.5) \times 10^{14}$ molecules cm^{-2}) using electrochemistry.[23]

3.2.2 UPS Characterization and Work function Modification

The WFs of bare and NHC-modified Au were measured using UPS in vacuum as well as using KP under nitrogen in ambient pressure conditions.

Table 3.3. Experimental and Calculated Work functions[a] for Gold Surfaces Modified with NHCs (eV). DFT values are from Dr. Alexander Hyla. Reprinted with permission from ref.[34]. Copyright 2017 American Chemical Society.

NHC	UPS		Kelvin Probe		DFT				
	Φ	$\Delta\Phi^b$	Φ	$\Delta\Phi^b$	Φ	$\Delta\Phi^b$	$\Delta V_{\text{int. dip.}}{}^c$	$\Delta V_{\text{geo m.}}{}^c$	$\Delta V_{\text{mol.}}{}^c$
none	5.17 ± 0.13	n/a	5.07 ± 0.11	n/a	5.17	n/a	n/a	n/a	n/a
iPr_2bimy	3.41 ± 0.04	–1.76 ± 0.14	3.98 ± 0.11	–1.09 ± 0.16	3.90	–1.27	–1.00	0.01	–0.27
IiPr	3.29 ± 0.08	–1.88 ± 0.15	3.73 ± 0.12	–1.34 ± 0.18	3.84	–1.33	–0.88	0.01	–0.44
SIiPr	d	d	d	d	3.77	–1.40	–0.90	0.01	–0.51
IDipp	3.30 ± 0.18	–1.87 ± 0.22	3.81 ± 0.17	–1.26 ± 0.20	4.13	–1.04	–0.54	0.01	–0.48
SIDipp	3.52 ± 0.07	–1.65 ± 0.18	3.95 ± 0.15	–1.12 ± 0.19	4.23	–0.94	–0.43	0.01	–0.50
6Dipp	3.42 ± 0.14	–1.75 ± 0.19	3.85 ± 0.12	–1.22 ± 0.18	4.11	–1.06	–0.47	0.01	–0.56

[a] UPS and KP data acquired at the coverages given in Table 1; DFT values calculated at a constant coverage of 5.81 × 1013 molecules cm–2. [b] $\Delta\Phi$ = Φ(mod. Au) – Φ(bare Au). [c] See Equation 3.1 and text for definitions. [d] Not measured.

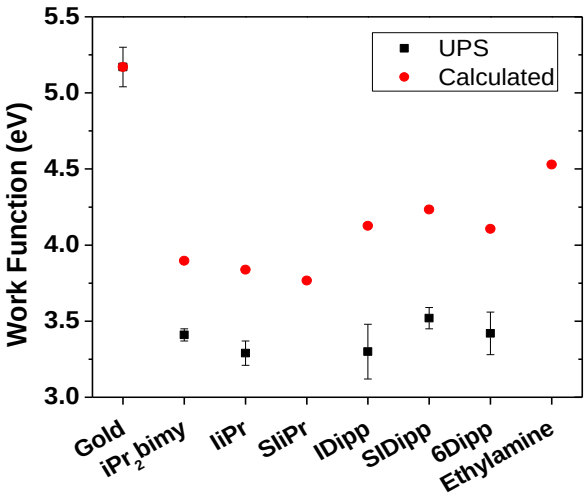

Figure 3.4. Plot showing experimental (UPS) and calculated work functions for bare and NHC-modified Au surfaces. The error bars are the standard deviations of samples over different surfaces. Reprinted with permission from ref.[34]. Copyright 2017 American Chemical Society.

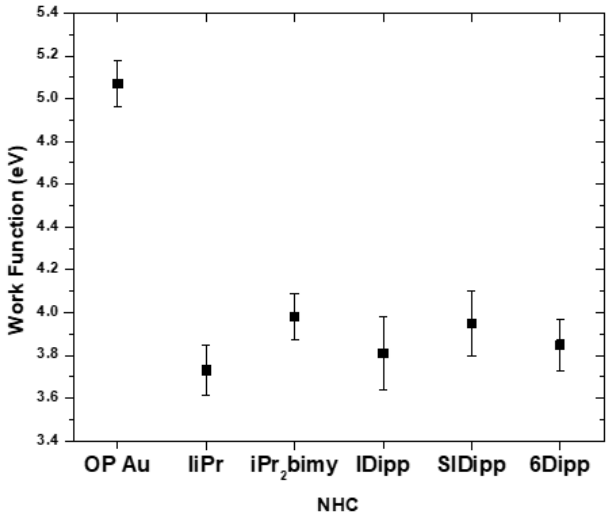

Figure 3.5. Work function values measured by Kelvin Probe under nitrogen for unmodified and NHC-modified Au substrates (modified using same procedure as UPS samples, as described in the experimental section). Reprinted with permission from ref.[34]. Copyright 2017 American Chemical Society.

Both measurement techniques indicate large WF reductions after NHC modification (Table 3.3, Figure 3.4, and Figure 3.5) and that the WF reductions ($-\Delta\Phi$) are

insensitive to the choice of NHC; UPS indicates WF values of ca. 3.3–3.5 eV and KP values of ca. 3.8–4.0 eV for all the NHCs examined.

3.2.3 Air Stability

The WF reductions are larger than those typically obtained using alkanethiolates[8-10] and comparable to those obtained using PEI or PEIE,[6] or solution doping with $(IrCp^*Cp)_2$.[4] Exposure to air leads to an increase in WF; this is not surprising since low-WF surfaces, including those of intrinsically low-WF metals and of dimer-doped ITO and Au,[4-5] but notably not those of PEI- and PEIE-modified substrates,[6] are often air-sensitive, presumably due to electron transfer to atmospheric O_2 and/or water, and since free NHCs are also oxidized in air.[40]

Over 7 days in air the WF of SIDipp-modified gold increases to ca. 4.8 eV, close to that of bare gold. However, after 24 h exposure to air, the WF values for gold modified with various NHCs were only reduced to ca. 4.0 eV according to UPS, i.e., comparable to values for alkanethiolate-modified gold in inert atmosphere[8-10] (Table 3.4).

Table 3.4. Work function Values (eV) for NHC-Modified Surfaces Exposed to Ambient Conditions and Measured Using UPS. Reprinted with permission from ref.[34]. Copyright 2017 American Chemical Society.

NHC	Φ after 4 min air exposure	Φ after 24 h air exposure	$\Phi_{air} - \Phi_{init}$[a]	Φ after 7 d air exposure
none	–	–	–	5.02 ± 0.04
iPr$_2$bimy	–	3.94 ± 0.07	0.53 ± 0.17	–
IiPr	–	3.80 ± 0.13	0.51 ± 0.15	–
IDipp	–	3.94 ± 0.08	0.64 ± 0.26	–
SIDipp	4.00 ± 0.07	3.97 ± 0.02	0.45 ± 0.09	4.77 ± 0.09
6Dipp	–	3.95 ± 0.16	0.53 ± 0.30	–

[a] Difference between WF value measured before exposure to air (from Table 3.3) and that measured after 24 h exposure.

The urea and amide shown in Figure 3.6 are possible products of oxidation and hydrolysis, respectively, of **IiPr** (and are calculated using DFT to result in WF reductions of 1.00 and 0.80 eV vs. bare gold, i.e. higher WFs than **IiPr**).

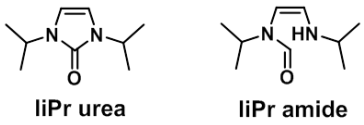

Figure 3.6. Structures of possible NHC decomposition products of IiPr. Reprinted with permission from ref.[34]. Copyright 2017 American Chemical Society.

Figure 3.7 shows XPS spectra of NHC-modified Au before and after air exposure for 4 min. However, no evidence for these species is found using XPS (Figure 3.7) Carbonyl groups are expected to show peaks at around 287.5 eV, at a higher BE than C–C groups.[41]

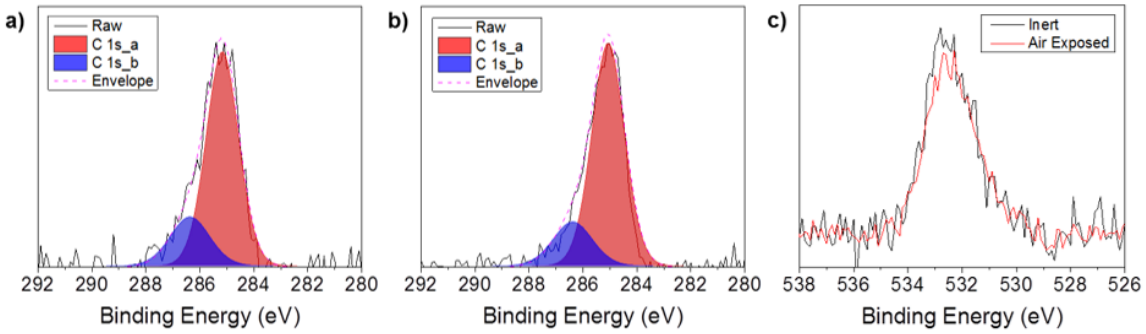

Figure 3.7. XPS spectra of the C 1s peak components for IiPr on Au a) after storage under inert conditions and b) after exposure to ambient conditions for 4 min. The spectra are very similar and were both fitted using two Gaussians (at 285.1 and 286.4 eV); no new component assignable to C=O is observed; c) O 1s peak before and after exposure (presumably due to adventitious O-containing species), which shows a good overlap and no new components attributable to C=O or to additional surface oxide or hydroxide species. Reprinted with permission from ref.[34]. Copyright 2017 American Chemical Society.

The O 1s spectra for before and after also shows no change to the overall peak size as shown by the good overlap of the two trials (Figure 3.7). Thus, the XPS is not sufficiently sensitive enough to enable us to determine the mechanism by which the WF is raised on exposure to air.

Figure 3.8 shows XPS spectra for SIDipp-modified Au before and after *7 days* air exposure; in this case there is a marked change increase in the O 1s signal (also see Table 3.5) and a shift in the O 1s peak to lower BE and a change in the appearance of the N 1s ionization. These data suggest clear chemical changes on air exposure, but both C 1s and O 1s spectra are clearly are again inconsistent with the presence of C=O groups (the O 1s being typically seen at BE values of ca. 533 eV).

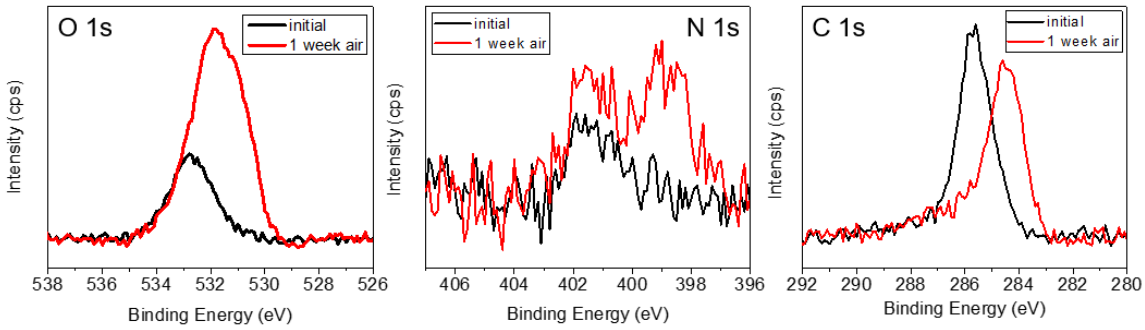

Figure 3.8. XPS spectra of (from left) C 1s, N 1s, and O 1s peaks for SIDipp on Au before and after exposure to ambient conditions for 7 days. All three ionizations shift to markedly lower BE and the O coverage increases; however, these changes are inconsistent with formation of C=O groups. Reprinted with permission from ref.[34]. Copyright 2017 American Chemical Society.

Table 3.5. Quantification of XPS O 1s Peaks Before and After Air Exposure for NHC-Modified Au. Reprinted with permission from ref.[34]. Copyright 2017 American Chemical Society.

NHC	O 1s / Au 4f ratio before air exposure	O 1s / Au 4f ratio after 7 d air exposure
none	0.30 ± 0.04	0.36 ± 0.03
iPr$_2$bimy	0.30 ± 0.09	–
IiPr	0.13 ± 0.04	–
IDipp	0.20 ± 0.09	–
SIDipp	0.18 ± 0.02	0.37 ± 0.03
6Dipp	0.23 ± 0.12	–

On the other hand, the WFs (tested for IDipp-, SIDipp-, and 6Dipp-modified gold) showed only slight increases over 2–7 days of storage in a N_2-filled glovebox (Figure 3.9). Note that the increases may in part have been due to contaminants that may have been present within the glovebox and in part due to repeated handling of the samples for measurement.

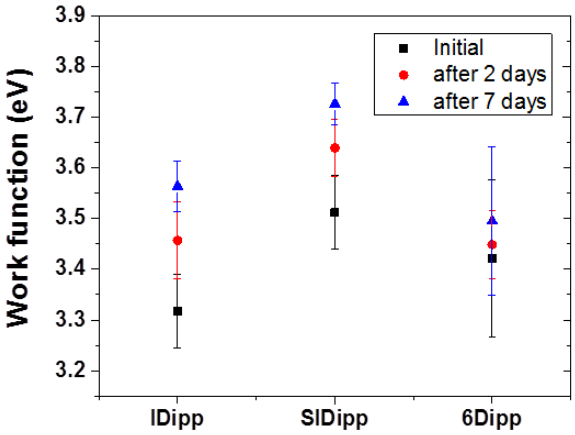

Figure 3.9. WF Retention Test (Using UPS) after 2 Days and 7 Days of Storage under Nitrogen Gas. Reprinted with permission from ref.[34]. Copyright 2017 American Chemical Society.

3.2.4 Comparison with DFT Results

WF values were also calculated using DFT (Figure 3.4 and Table 3.3). The WF of the bare Au(111) surface was calculated to be 5.17 eV, in excellent agreement with the UPS results obtained here and previous values obtained by experiments and calculations in the literature.[3-4, 42-45] The DFT WF values for the NHC-modified gold do not agree so well with experiment as those for bare Au. For IiPr-modified Au, the value at a coverage of 2.32×10^{14} molecules cm^{-2}, close to that found experimentally, is ca. 2.5 eV, i.e., considerably lower than the experimental value; this discrepancy could arise from limitations of the computational method, from effects on the experimental values of impurities in the glovebox atmosphere and/or NHC solution, and/or effects of variations in NHC binding. For the full range of NHCs the WF values shown in Figure 3.4 and Table 3.3 were calculated at one-fourth of this coverage, i.e., 5.81×10^{13} molecules cm^{-2}. These values are higher than the experimental values but are consistent with experiment in that they indicate little dependence of WF on the structure of the heterocyclic core, at least for a given N,N′-substitution pattern.

On the other hand, the calculations suggest that, at equal coverage, the bulkier bis(diisopropylphenyl) species should lead to slightly smaller WF reductions than their diisopropyl analogues, whereas experimentally (where the bulkier examples exhibit lower coverages) little difference is seen; however, as discussed below, $\Delta\Phi$ arises from the interplay of different contributions, the relative importance of which varies between different NHCs. The discrepancy whereby DFT values $\Delta\Phi$ are lower for Dipp than iPr species, but experimental values that are similar may result from limitations in

quantitatively reproducing some of these contributions, but may also result from the different dependencies of these different contributions on coverage (see below).

Table 3.3 also decomposes the contributions to ΔΦ of the NHC-modified Au using a scheme similar to that discussed extensively in our previous work:[39, 46]

$$\Delta\Phi = \Delta V\text{int.dip.} + \Delta V\text{mol.} + \Delta V\text{geom} \qquad \text{Equation 3.1}$$

where $\Delta V_{\text{int dip}}$ is the contribution of the dipole formed at the immediate interface between molecular layer and surface due to charge transfer through coordination of the Lewis basic NHC nonbonding electron pair to the surface, the "cushion" effect[47-48] (corresponding to the push-back of the electronic density spilling from the clean metal surface), and other charge reorganization; ΔV_{mol} is the electrostatic potential energy change across an isolated molecular layer in vacuum; and ΔV_{geom} is the WF change of the bare surface due to the geometric relaxations that take place when interacting with the NHC molecules. The variation in these quantities is discussed in more detail in the following section. Figure 3.4 also includes, as a model for PEI- and PEIE-modified Au,[6] the DFT-calculated WF for Au modified with $EtNH_2$ at the same coverage as the NHCs; this suggests that the WF reduction *per modifier molecule* is larger for NHCs than that for the amine (of course, it must be borne in mind that the density of amines in PEI- or PEIE-modified Au is potentially much higher than that of NHCs in the monolayers studied here).

3.2.4.1 Origin of Work function Modification

The breakdown of DFT-calculated contributions to ΔΦ given in Table 3.3 suggests that ΔV_{geom} is not a significant factor and thus that ΔΦ is dominated by $\Delta V_{\text{int. dip}}$ and ΔV_{mol}. For a given set of N,N′-substituents, the magnitude of ΔV_{mol} increases with the expected N–C–N angle (Figure 3.1) and Brønsted basicity, while variation in $\Delta V_{\text{int dip}}$ is less

straightforward. More interestingly, this breakdown suggests qualitative differences between, on the one hand, the small NHCs, with iPr substituents, for which (at 5.81 × 10^{13} molecules cm^{-2}) the majority of $\Delta\Phi$ is from $\Delta V_{\text{int dip}}$, and, on the other hand, the bulkier NHCs, with Dipp substituents. In the latter cases, the magnitudes of the $\Delta V_{\text{int dip}}$ values are lower, and those of ΔV_{mol} larger than for the iPr species, resulting in approximately equal contributions to $\Delta\Phi$ from interface and molecular dipoles at these coverages. It is worth noting that although the magnitudes of both $\Delta V_{\text{int dip}}$ and ΔV_{mol} are expected to increase with coverage, previous work on other modified surfaces suggests that neither should do so linearly, due to enhanced depolarization effects within densely packed dipole layers;[39] indeed, comparison of two different coverages of IiPr (Table 3.3) shows that ΔV_{mol} is more strongly coverage dependent, being almost tripled when the coverage is increased by a factor of 4, whereas $\Delta V_{\text{int dip}}$ is not even doubled, so that both contributions are approximately equal at near-experimental coverage.

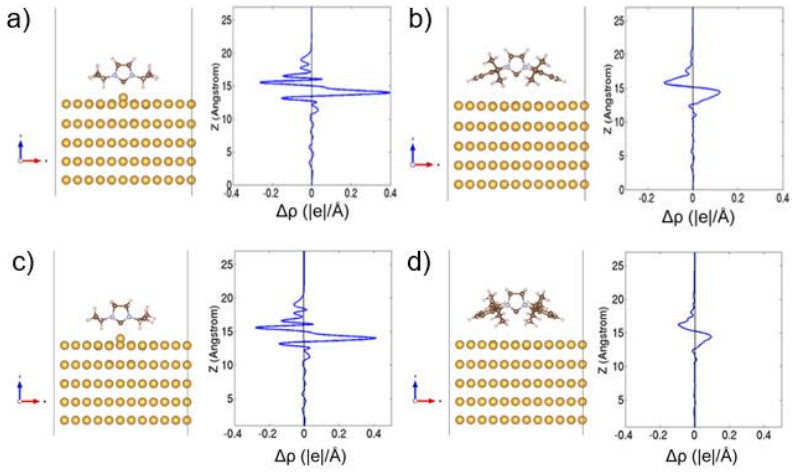

Figure 3.10. Optimized structures and plane-averaged change in charge density ($\Delta\rho$) for (a) IiPr (b) IDipp (c) SIiPr and (d) SIDipp. Negative corresponds to an increased positive charge relative to the bare gold and isolated NHCs, whereas positive corresponds to increased negative charge. These plots were made by Dr. Alexander Hyla. Reprinted with permission from ref.[34]. Copyright 2017 American Chemical Society.

Figure 3.10 shows the plane-averaged electron charge-density difference $\Delta\rho$, for IiPr, IDipp, SIiPr, and SIDipp along with the optimized geometries. The charge-density difference was calculated by subtracting from the charge density of the combined NHC-Au system the charge density of each component (NHC and Au) at the geometry it is calculated to have after interaction with the other component. Each system shows reorganization of charge density at the interface between the top of the gold and the NHC modifier above, but with larger changes in charge density for the IiPr system, consistent with the larger $\Delta V_{\text{int dip}}$ contribution. As mentioned above, this interface dipole results from C_{carbene}–Au bonding, the "cushion" effect, and overall charge re-distribution at the interface. Examination of the optimized geometries of the NHC-modified surfaces, as well as of the evolution of the Bader partial atomic charges,[49] for the carbene carbon atoms on Au and isolated from the surface (considering the same relaxed geometry) explains the much lower magnitudes of $\Delta V_{\text{int dip}}$ for the Dipp NHCs (Table 3.6 and Figure 3.10).

Table 3.6. DFT Calculated Parameters Relating to the Au-NHC Interaction. These calculations were by Dr. Alexander Hyla. Reprinted with permission from ref.[34]. Copyright 2017 American Chemical Society.

NHC	C_{carbene}—Au / Å	C_{carbene} Bader Charge / |e|		NHC—Au Binding Energy / eV	
		NHC on Au	Isolated NHC	Total[a]	Dispersion[b]
iPr_2bimy	2.14	0.41	0.21	-2.84	-1.33
IiPr	2.12	0.40	0.19	-2.87	-1.27
SIiPr	2.14	0.47	0.26	-2.88	-1.30
IDipp	4.11	0.26	0.24	-2.34	-2.51
SIDipp	4.54	0.33	0.32	-1.87	-2.18
6Dipp	5.06	0.33	0.31	-2.04	-2.08

The carbene carbon of the iPr NHCs is clearly coordinated to a Au atom, which, in the relaxed geometry, is slightly displaced from the metal surface; the displacements and the Au–C distances for the iPr series are comparable with those calculated in previous studies of NHC monolayers with similarly sized N,N′-substituents,[23, 27, 33, 50] and are similar to typical bond lengths in NHC Au^{I} complexes.[51-52] On the other hand, the carbene carbons of the bulky Dipp NHCs are located at very long, nonbonded distances from the nearest gold atom. In a previous computational study of comparably bulky NHCs on Au a $C_{carbene}$—Au distance of 2.04 Å was obtained; however, the computational model involved placement of a single Au atom on the Au surface.[25] A very recent work[27] also invokes such "ballbot"-like structures in which the NHC is bound to a single "adatom", not only for bulky NHCs such as IDipp but also for playing a role in the surface diffusion of 1,3-dimethyl-1,3-dihydro-2*H*-imidazol-2-ylidene on Au.

Consistent with the difference in geometries, the Bader charges indicate a significant increase in positive charge density on the carbene carbons of the NHCs with iPr substituents on binding to Au, consistent with charge transfer to the surface; on the other hand, for the NHCs with Dipp substituents, the Bader charges on the carbene carbon atoms are essentially the same as in the isolated molecules, which implies that $\Delta V_{\text{int dip}}$ in the Dipp series arises only from the "cushion" effect[47-48] and charge re-distributions at the interface.

Given (i) the experimental evidence, both in our work and that of others, that bulky carbenes do bind to gold and (ii) the calculated geometries and Bader charges that indicate negligible $C_{carbene}$—Au covalent bonding, we were interested in examining why these carbenes with Dipp substituents even bind to the surface. Calculations show that the dispersion energy gained when Dipp-substituted NHCs bind to gold are, on average, 2.3

eV, whereas the iPr-substituted NHCs only gain 1.3 eV from dispersion interactions on binding to Au (see Table 3.6). Thus, the increased van der Waals interactions in the Dipp-substituted NHCs, presumably arising from the larger substituents, essentially compensate for the stabilization obtained when the iPr NHCs form a covalent bond between the lone pair of the carbene carbon and the surface.

3.2.5 Electrode Behavior

Low-WF materials are generally expected to behave as more effective electron-injecting electrodes than high-WF materials. For example, PEIE-coated Au has previously been shown to afford lower threshold-voltage values and higher electron-mobility values than bare gold when applied as the source and drain electrodes in n-channel organic field-effect transistors.[6] To examine whether NHC-modified Au behaves in a similar way, diode-like devices with the structures Au (150 nm, with or without modification)/C_{60} (100 nm)/MoO_x (10 nm)/Ag (150 nm) were fabricated. SIDipp-modified Au was used for these experiments and, in addition to bare gold, Au modified with spin-coated PEIE was used as a comparison material with similar WF (3.4 eV, UPS).[6] As shown in Figure 3.11 (and Figure 3.12), SIDipp-modified and PEIE-modified devices gave rise to diode-like behavior with a higher rectification, which is indicative of improved electron injection from these electrodes to C_{60} than from the reference, unmodified electrodes.

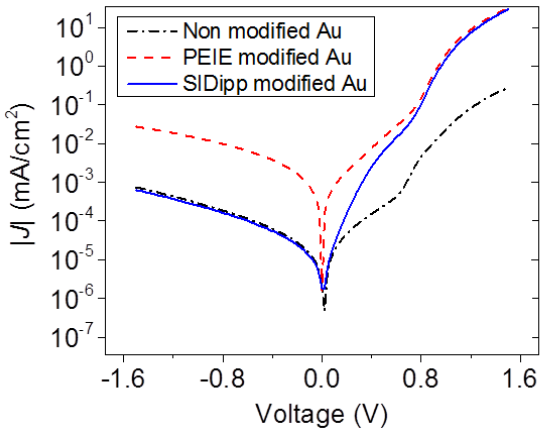

Figure 3.11. Semi-logarithmic plots of J–V characteristics for diodes with Au (150 nm, with or without modification)/C60 (100 nm)/MoO_x (10 nm)/Ag (150 nm). This plot was from Felipe Larrain of the Bernard Kippelen group. Reprinted with permission from ref.[34]. Copyright 2017 American Chemical Society.

The highest rectification ratio (at ±1 V) for a SIDipp-modified device was determined to be 6×10^3. (78: text) The SIDipp–Au devices show less straightforward behavior than the bare Au and PEIE-modified Au devices. The control devices can be reasonably well modeled as the superposition of a leakage current and diode behavior, whereas that of SIDipp-Au devices cannot. The magnitude of the leakage current is expected to be symmetrical for positive and negative voltages, that of the apparent leakage current for the SIDipp devices is not; the reason for this is unclear but may arise from a SIDipp monolayer that is not completely uniform, leading to effectively two diodes in parallel associated with different portions of the electrode surface.

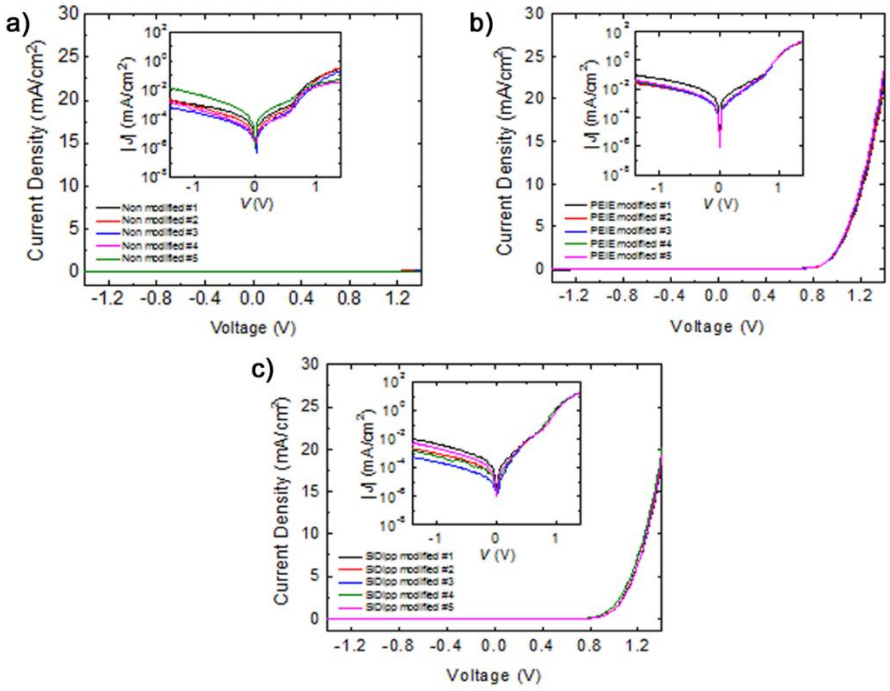

Figure 3.12. Semi-logarithmic plots of *J-V* characteristics showing sample-to-sample variations for devices with structure Au(with or without modification)/C_{60} (100 nm)/MoO_3 (10 nm)/Ag (150 nm) using a) unmodified Au, b) PEIE-modified Au, and c) SIDipp-modified Au. The yield for PEIE modified devices was 93% and for SIDipp modified devices 40%. These plots are from Felipe Larrain of the Bernard Kippelen group. Reprinted with permission from ref.[34]. Copyright 2017 American Chemical Society.

3.3 Conclusions

NHCs are emerging as a flexible tool for materials scientists to impart functionality to metal surfaces,[20] but the accompanying effect of these modifiers on the metal WF has only been so far addressed in one computational study.[33] Here we have experimentally demonstrated that NHC modification of Au surfaces results in large reductions in WF relative to unmodified gold, larger than those achieved with alkanethiolates and comparable to the effects of PEIE or solution-processed reducing organometallic dimers. These reductions are obtained for NHCs with both relatively small (diisopropyl) and bulky (bis(2,6-diisopropylphenyl)) N,N′-substituents.

DFT calculations indicate very different interactions between the carbene and the gold for these two classes of NHCs. For the former, the carbene carbon atom is covalently bound to a gold atom, with the associated charge re-distribution making a significant contribution to the interface dipole. In the latter, the interface dipole is smaller, but, to some extent, compensated by a larger molecular dipole.

In C_{60} diodes, NHC-modified Au acts as an effective electron-injecting electrode, behaving similarly to PEIE-modified Au, albeit with lower air stability. Therefore, NHC-modified Au electrodes may be useful in applications where low-WF electrodes are required, especially when additional functionality, besides low WF, is desired given the synthetic flexibility of NHCs and recent demonstrations of their use in attaching a variety of other species to Au surfaces.[23, 25]

3.4 Experimental

3.4.1 Materials

1,3-Diisopropyl-1,3-dihydro-2*H*-benzo[*d*]imidazol-2-ylidene (iPr_2bimy),[23, 53] 1,3-diisopropyl-1,3-dihydro-2*H*-imidazol-2-ylidene (IiPr),[54] and 1,3-bis(2,6-diisopropylphenyl)-1,3-dihydro-2*H*-imidazol-2-ylidene (IDipp)[55-56] were synthesized according to the literature. 1,3-Bis(2,6-diisopropylphenyl)imidazolidin-2-ylidene (SIDipp) was purchased from Sigma-Aldrich. 1,3-Bis(2,6-diisopropylphenyl)tetrahydropyrimidin-2(1*H*)-ylidene (6Dipp) was synthesized according to adapted literature procedure, using NaHMDS instead of LiHMDS {HMDS = $(Me_3Si)_2N$}.[57] Synthesis and deposition of NHCs were carried out in a nitrogen-filled glovebox (<0.5 ppm water and <0.5 ppm oxygen). Solvents were deoxygenated by freeze-pump-thaw cycles prior to use. All NHCs except

for IiPr were synthesized by Dr. Chelsea Wyss and Abraham Jordan of the Joseph Sadighi group at Georgia Tech.

3.4.2 Au Surface Cleaning and Modification

Commercially available glass:Ti:Au slides (EMF Corp., Ithaca, NY, USA) were cut into 0.5 in. × 0.5 in. squares and sonicated in ethanol for 10 min, dried under a flow of nitrogen, and etched with oxygen plasma (OP) with a PE-50 XL Plasma System for 5 min prior to any additional surface treatment. The samples were transferred into a nitrogen-filled glovebox for modification because both the free NHC and modified surfaces are air-sensitive. Surfaces were immersed in 2 mM solutions of the free NHCs in freeze–pump–thaw deoxygenated dry tetrahydrofuran (THF) for 24 h. They were rinsed with fresh THF (3 × 1 mL) and dried under a flow of nitrogen. Samples were immediately taken for X-ray photoelectron spectroscopy/ultraviolet photoelectron spectroscopy (XPS/UPS) analysis using a Kratos air-sensitive transporter 39-322 that couples with the transfer chamber of the Kratos Axis Ultra DLD XPS/UPS under a positive pressure of nitrogen.

3.4.3 Surface Characterization

3.4.3.1 UPS and XPS and KP

All UPS and XPS measurements were conducted in a Kratos Axis Ultra spectrometer with an average base pressure of 10^{-9} Torr. UPS spectra were collected prior to XPS spectra with a 21.2 eV He (I) excitation and a pass energy of 5 eV using a 27 μm spot size. XPS spectra were collected with a monochromatic Al Kα source using a 400 μm spot size and a pass energy of 160 eV for survey acquisition and 20 eV for high-resolution spectra. XPS was performed with a normal takeoff angle (0°). Data were analyzed using

Vision Processing software 2.2.8. The binding energies of all XPS spectra were calibrated and normalized to the Au 4f line at 84.0 eV. The method for estimating the experimental coverage from XPS data is described in 3.4.4. KP WF data were obtained using a Besocke Delta Phi Kelvin probe system in a nitrogen atmosphere. The measurements were calibrated to a freshly cleaved highly ordered pyrolytic graphite sample with a known WF of 4.50 eV.[58] All XPS, UP, and KP data points represent multiple samples scanned on multiple spots.

3.4.3.2 Calculation Methodology

This methodology detailed in this section was performed by Dr. Alexander Hyla. To describe the Au(111) surface, we used a repeated-slab approach. The lateral dimensions of the unit cells along the $[11\bar{2}]$ and $[1\bar{1}0]$ directions are 17.27 × 9.97 Å^2, values taken from the experimental bulk lattice parameters.[6, 59] We note here that the lattice parameters optimized at the DFT level with the PBE-D3 functional for bulk gold are very close to the experimental values.[60] When one NHC molecule is in the unit cell, the molecular coverage is 5.81×10^{13} molecules cm^{-2}. Each gold slab consists of five atomic layers with the bottom three layers frozen at the optimized crystal structure while the top two layers, and any molecular adsorbate, are allowed to relax over the course of geometry relaxations. The slabs are separated by a vacuum space larger than 20 Å.

All surface calculations were carried out using the Vienna ab Initio Simulation Package (VASP).[61-62] The calculations were performed with plane-wave basis sets with an energy cutoff of 400 eV; the projector augmented wave (PAW) method[63] was used to describe the valence–core electron interactions. We chose the generalized gradient approximation (GGA) exchange-correlation functional of Perdew, Burke, and Ernzerhof

(PBE),[64-65] augmented by the empirical D3 dispersion correction of Grimme et al.[66] in order to describe the nonspecific interactions of the NHCs with the metal surface. While PBE-D3 has deficiencies in describing reaction energies and geometries relative to more calculation-intensive methods,[67] the PBE functional has been used to qualitatively describe charge-transfer systems, such as perylene-3,4,9,10-tetracarboxylicdiimide,[68] perylene-3,4,9,10-tetracarboxylic dianhydride,[69] and C_{60}[70] on ZnO, as well as a charge-transfer complex of a carbazole–phosphonic acid bound to ITO.[71] In these earlier works, the WF change and charge-transfer character were calculated and good agreement with experiments was reported.[68-70]

In order to examine the extent of charge transfer in these NHC systems, Bader charges were evaluated[49] (while it is difficult to assess the accuracy of atomic partial charges, these charges have an estimated error of less than 15%).[72] A 2 × 2 × 1 Monkhorst–Pack *k*-point grid was used for geometry optimizations for the unit cells both with and without NHC molecules, while a 6 × 6 × 1 Monkhorst–Pack *k*-point grid was used for self-consistent total-energy calculations. The Methfessel and Paxton[73] occupation scheme with a smearing of 0.1 eV was used for Brillouin zone integrations in the calculations.

Geometry optimizations were performed using a damped molecular dynamics scheme until the forces were <0.03 eV $Å^{-1}$.[42] To compensate for possible dipole–dipole interactions between the asymmetric slabs, a dipole sheet was inserted into the vacuum gap. WFs (Φ) were calculated using the following definition:

$$\Phi = V_{vac.} - E_F \qquad \text{Equation 3.2}$$

where V_{vac} is the plane-averaged electrostatic potential energy of an electron in the vacuum region away from the slab, at a distance sufficiently far away that the potential energy has reached its asymptotic value, and where E_F denotes the Fermi energy of the system.

Gas-phase calculations of the carbenes were performed in the Gaussian 09 program suite.[74] The carbene geometries were optimized and frequencies were calculated at the PBE/cc-pVTZ level.[75]

3.4.3.3 Electrical Measurements

The electrical measurements in this section were performed by Felipe Larrain of the Bernard Kippelen group. Glass substrates of 1 in. × 1 in. were cleaned in sequential ultrasonic baths (Branson 5510) of deionized water, acetone, and isopropanol (each for 30 min at 30 °C). The Au bottom electrode (150 nm) was evaporated onto 1 in. × 1/2 in. of the glass substrates (with a mask) using a SPECTROS (Kurt J. Lesker) thermal evaporator with substrate rotation. For comparison, devices incorporating Au electrodes modified with PEIE were fabricated: PEIE solution (Sigma-Aldrich, 80% ethoxylated, M_w = 70000 g mol^{-1}, 35–40 wt % in water) was diluted with 2-methoxyethanol to a concentration of 0.4 wt % and magnetically stirred at room temperature (RT) for 12 h prior to use. The solution was dispensed onto the patterned Au substrates through 0.2 μm pore size PTFE filters and then spin-coated at a speed of 5000 rpm for 60 s at an acceleration of 928 rpm s^{-1}. The spin-coated samples were then annealed at 100 °C for 10 min in air. NHC modifications were carried out in the glovebox as described above and transferred to the vacuum thermal evaporation system. The vacuum chamber was pumped down to a base pressure of 8.0 × 10^{-8} Torr. C_{60} (100 nm), MoO_3 (10 nm), and Ag (150 nm) were deposited sequentially through two different shadow masks on the unmodified, PEIE-modified, or NHC-modified

Au substrates, to complete the fabrication of organic diodes. The effective area of the diodes was 10.36 mm^2. Current density–voltage (*J–V*) curves were measured in a nitrogen-filled glovebox by using a Keithley 2400 source meter controlled by a LabVIEW program.

3.4.4 Experimental Coverage Calculation Method

XPS data (taken at normal detection angle) were corrected for photoionization cross-section and detector sensitivity. We assume that the surface N signal is not attenuated and so the intensity of the N 1s signal, corrected as described above, is directly proportional to the number of surface N atoms:

$$I_{\mathrm{N}} = k \cdot N_{\mathrm{N}} \qquad \text{Equation 3.3}$$

and, therefore, that the quantity in which we are interested, N_N/A, the number for N atoms per unit area, is given by:

$$N_{\mathrm{N}}/\mathrm{A} = I_{\mathrm{N}}/(k \cdot A) \qquad \text{Equation 3.4}$$

We also assume that the Au signal is not attenuated by the surface modifier and only by other Au atoms. We furthermore assume that the Au signal is attenuated such that:

$$I_{\mathrm{Au}}(t) = k \cdot N_{\mathrm{Au}}(t) \cdot e^{-t/\lambda_{\mathrm{Au}}} \qquad \text{Equation 3.5}$$

where $I_{Au}(t)/A$ is the contribution to the total Au 4f intensity from the Au atoms at depth *t*, $N(t)$ is the number of Au atoms at depth *t* and λ_{Au} is the mean free path for Au 4f photoelectrons. For Au 4f photoelectrons (for which the binding energy, BE, is ca. 86 eV) using Al Kα radiation ($h\nu$ = 1486 eV), the kinetic energy (KE), is ca. 1400 eV. The mean-free path for photoelectrons with KE > 150 eV can be estimated using the expression

$$\lambda = B(\mathrm{KE})^{0.5} \qquad \text{Equation 3.6}$$

where *B* for Au is 0.054 nm $eV^{-0.5}$,[76] giving a value of 2.02 nm for Au 4f. Since the mean-free path is significantly larger than the lattice parameter of Au ($a = b = c$ = 4.079 Å;

$\alpha = \beta = \gamma = 90°$) it is reasonable to treat Au has having a uniform continuous composition with the same number of Au atoms in any infinitesimal slice δt and thus to write:

$$I_{\mathrm{Au}}(t)/A = kN_{\mathrm{Au}}/V \cdot \delta t \cdot e^{-t/\lambda_{\mathrm{Au}}} \qquad \text{Equation 3.7}$$

where N_{Au}/V is the number of Au atoms per unit volume, which corresponds to 4 per face-centered cubic unit cell, i.e. $4/(4.079)^3$ Å^{-3}. The total Au intensity per unit area will be given integration of (Equation 3.7) from 0 (the surface) to T (the total Au film thickness); for $T >>$ ca. 3λ the value of this integral will very similar to that obtained by evaluating the integral from 0 to ∞.

$$I_{\mathrm{Au(total)}}/A = \int_0^{\infty} k \cdot N_{\mathrm{Au}}/V \cdot e^{-t/\lambda_{\mathrm{Au}}} dt \qquad \text{Equation 3.8}$$

$$I_{\mathrm{Au(total)}}/A = [-\lambda_{\mathrm{Au}} \cdot k \cdot N_{\mathrm{Au}}/V \cdot e^{-t/\lambda_{\mathrm{Au}}}]_0^{\infty} \qquad \text{Equation 3.9}$$

$$I_{\mathrm{Au(total)}}/A = \lambda_{\mathrm{Au}} \cdot k \cdot N_{\mathrm{Au}}/V \qquad \text{Equation 3.10}$$

which, inserting values of λ_{Au} and N_{Au}/V from above gives a value of

$$I_{\mathrm{Au(total)}}/A = k \cdot 1.19\ \text{Å}^{-2} = k \cdot (1.19 \times 10^{16}\ \mathrm{cm}^{-2}) \qquad \text{Equation 3.11}$$

Combining (Equation 3.4) and (Equation 3.11):

$$N_{\mathrm{N}}/A = (I_{\mathrm{N}}/I_{\mathrm{Au(total)}}) \cdot (1.19 \times 10^{16}\ \mathrm{cm}^{-2}) \qquad \text{Equation 3.12}$$

3.5 References

[1] Lindell, L.; Unge, M.; Osikowicz, W.; Stafström, S.; Salaneck, W. R.; Crispin, X.; de Jong, M. P., Integer Charge Transfer at the Tetrakis(Dimethylamino)Ethylene/Au Interface. *Appl. Phys. Lett.* **2008,** *92* (16), 163302.

[2] Bröker, B.; Blum, R. P.; Frisch, J.; Vollmer, A.; Hofmann, O. T.; Rieger, R.; Müllen, K.; Rabe, J. P.; Zojer, E.; Koch, N., Gold Work Function Reduction by 2.2 eV with an Air-Stable Molecular Donor Layer. *Appl. Phys. Lett.* **2008,** *93* (24), 243303.

[3] Li, F.; Zhou, Y.; Zhang, F.; Liu, X.; Zhan, Y.; Fahlman, M., Tuning Work Function of Noble Metals as Promising Cathodes in Organic Electronic Devices. *Chem. Mater.* **2009,** *21* (13), 2798-2802.

[4] Giordano, A. J.; Pulvirenti, F.; Khan, T. M.; Fuentes-Hernandez, C.; Moudgil, K.; Delcamp, J. H.; Kippelen, B.; Barlow, S.; Marder, S. R., Organometallic Dimers: Application to Work-Function Reduction of Conducting Oxides. *ACS Appl. Mater. Interfaces* **2015,** *7* (7), 4320-6.

[5] Akaike, K.; Nardi, M. V.; Oehzelt, M.; Frisch, J.; Opitz, A.; Christodoulou, C.; Ligorio, G.; Beyer, P.; Timpel, M.; Pis, I.; Bondino, F.; Moudgil, K.; Barlow, S.; Marder, S. R.; Koch, N., Effective Work Function Reduction of Practical Electrodes Using an Organometallic Dimer. *Adv. Func. Mater.* **2016,** *26* (15), 2493-2502.

[6] Zhou, Y.; Fuentes-Hernandez, C.; Shim, J.; Meyer, J.; Giordano, A. J.; Li, H.; Winget, P.; Papadopoulos, T.; Cheun, H.; Kim, J.; Fenoll, M.; Dindar, A.; Haske, W.; Najafabadi, E.; Khan, T. M.; Sojoudi, H.; Barlow, S.; Graham, S.; Brédas, J.-L.; Marder, S. R.; Kahn, A.; Kippelen, B., A Universal Method to Produce Low-Work Function Electrodes for Organic Electronics. *Science* **2012,** *336* (6079), 327-32.

[7] Nuzzo, R. G.; Allara, D. L., Adsorption of Bifunctional Organic Disulfides on Gold Surfaces. *J. Am. Chem. Soc.* **1983,** *105*, 4481-4483.

[8] de Boer, B.; Hadipour, A.; Mandoc, M. M.; van Woudenbergh, T.; Blom, P. W. M., Tuning of Metal Work Functions with Self-Assembled Monolayers. *Adv. Mater.* **2005,** *17* (5), 621-625.

[9] Alloway, D. M.; Hofmann, M.; Smith, D. L.; Gruhn, N. E.; Graham, A. L.; Colorado, R.; Wysocki, V. H.; Lee, T. R.; Lee, P. A.; Armstrong, N. R., Interface Dipoles Arising from Self-Assembled Monolayers on Gold: UV−Photoemission Studies of Alkanethiols and Partially Fluorinated Alkanethiols. *J. Phys. Chem. B* **2003,** *107* (42), 11690-11699.

[10] Narasimha, K. T.; Ge, C.; Fabbri, J. D.; Clay, W.; Tkachenko, B. A.; Fokin, A. A.; Schreiner, P. R.; Dahl, J. E.; Carlson, R. M.; Shen, Z. X.; Melosh, N. A., Ultralow Effective Work Function Surfaces Using Diamondoid Monolayers. *Nat. Nanotechnol.* **2016,** *11* (3), 267-272.

[11] Schlenoff, J. B.; Li, M.; Ly, H., Stability and Self-Exchange in Alkanethiol Monolayers. *J. Am. Chem. Soc.* **1995,** *117*, 12528-12536.

[12] Schoenfisch, M. H.; Pemberton, J. E., Air Stability of Alkanethiol Self-Assembled Monolayers on Silver and Gold Surfaces. *J. Am. Chem. Soc.* **1998,** *120*, 4502-4513.

[13] Zenasni, O.; Jamison, A. C.; Lee, T. R., The Impact of Fluorination on the Structure and Properties of Self-Assembled Monolayer Films. *Soft Matter* **2013,** *9* (28), 6356-6370.

[14] Chinwangso, P.; Jamison, A. C.; Lee, T. R., Multidentate Adsorbates for Self-Assembled Monolayer Films. *Acc. Chem. Res.* **2011,** *44* (7), 511-519.

[15] Lin, J. C. Y.; Huang, R. T. W.; Lee, C. S.; Bhattacharyya, A.; Hwang, W. S.; Lin, I. J. B., Coinage Metal−N-Heterocyclic Carbene Complexes. *Chem. Rev.* **2009,** *109* (8), 3561-3598.

[16] Arnold, P. L.; Casely, I. J., F-Block N-Heterocyclic Carbene Complexes. *Chem. Rev.* **2009,** *109* (8), 3599-3611.

[17] Diez-Gonzalez, S.; Marion, N.; Nolan, S. P., N-Heterocyclic Carbenes in Late Transition Metal Catalysis. *Chem. Rev.* **2009,** *109*, 3612-3676.

[18] Samojłowicz, C.; Bieniek, M.; Grela, K., Ruthenium-Based Olefin Metathesis Catalysts Bearing N-Heterocyclic Carbene Ligands. *Chem. Rev.* **2009,** *109* (8), 3708-3742.

[19] Hindi, K. M.; Panzner, M. J.; Tessier, C. A.; Cannon, C. L.; Youngs, W. J., The Medicinal Applications of Imidazolium Carbene−Metal Complexes. *Chem. Rev.* **2009,** *109* (8), 3859-3884.

[20] Zhukhovitskiy, A. V.; MacLeod, M. J.; Johnson, J. A., Carbene Ligands in Surface Chemistry: From Stabilization of Discrete Elemental Allotropes to Modification of Nanoscale and Bulk Substrates. *Chem. Rev.* **2015,** *115* (20), 11503-32.

[21] Vignolle, J.; Tilley, T. D., N-Heterocyclic Carbene-Stabilized Gold Nanoparticles and Their Assembly into 3D Superlattices. *Chem. Commun.* **2009,** (46), 7230-7232.

[22] Roland, S.; Ling, X.; Pileni, M.-P., N-Heterocyclic Carbene Ligands for Au Nanocrystal Stabilization and Three-Dimensional Self-Assembly. *Langmuir* **2016,** *32* (31), 7683-7696.

[23] Crudden, C. M.; Horton, J. H.; Ebralidze, II; Zenkina, O. V.; McLean, A. B.; Drevniok, B.; She, Z.; Kraatz, H. B.; Mosey, N. J.; Seki, T.; Keske, E. C.; Leake, J. D.; Rousina-Webb, A.; Wu, G., Ultra Stable Self-Assembled Monolayers of N-Heterocyclic Carbenes on Gold. *Nat. Chem.* **2014,** *6* (5), 409-14.

[24] Weidner, T.; Baio, J. E.; Mundstock, A.; Grosse, C.; Karthäuser, S.; Bruhn, C.; Siemeling, U., NHC-Based Self-Assembled Monolayers on Solid Gold Substrates. *Aust. J. Chem.* **2011,** *64*, 1177-1179.

[25] Zhukhovitskiy, A. V.; Mavros, M. G.; Van Voorhis, T.; Johnson, J. A., Addressable Carbene Anchors for Gold Surfaces. *J. Am. Chem. Soc.* **2013,** *135* (20), 7418-21.

[26] Crudden, C. M.; Horton, J. H.; Narouz, M. R.; Li, Z.; Smith, C. A.; Munro, K.; Baddeley, C. J.; Larrea, C. R.; Drevniok, B.; Thanabalasingam, B.; McLean, A. B.; Zenkina, O. V.; Ebralidze, I. I.; She, Z.; Kraatz, H.-B.; Mosey, N. J.; Saunders, L. N.; Yagi, A., Simple Direct Formation of Self-Assembled N-Heterocyclic Carbene Monolayers on Gold and Their Application in Biosensing. *Nat. Commun.* **2016,** *7*, 12654.

[27] Wang, G.; Rühling, A.; Amirjalayer, S.; Knor, M.; Ernst, J. B.; Richter, C.; Gao, H.-J.; Timmer, A.; Gao, H.-Y.; Doltsinis, N. L.; Glorius, F.; Fuchs, H., Ballbot-Type Motion of N-Heterocyclic Carbenes on Gold Surfaces. *Nat. Chem.* **2016,** *9*, 152.

[28] Arduengo III, A. J.; Harlow, R. L.; Kline, M., A Stable Crystalline Carbene. *J. Am. Chem. Soc.* **1991,** *113*, 361-363.

[29] Magill, A. M.; Cavell, K. J.; Yates, B. F., Basicity of Nucleophilic Carbenes in Aqueous and Nonaqueous Solvents—Theoretical Predictions. *J. Am. Chem. Soc.* **2004,** *126*, 8717-8724.

[30] Dröge, T.; Glorius, F., The Measure of All Rings—N-Heterocyclic Carbenes. *Angew. Chem. Int. Ed.* **2010,** *49* (39), 6940-6952.

[31] Nuzzo, R. G.; Dubois, L. H.; Allara, D. L., Fundamental Studies of Microscopic Wetting on Organic Surfaces. 1. Formation and Structural Characterization of a Self-Consistent Series of Polyfunctional Organic Monolayers. *J. Am. Chem. Soc.* **1990,** *112*, 558-569.

[32] Lavrich, D. J.; Wetterer, S. M.; Bernasek, S. L.; Scoles, G., Physisorption and Chemisorption of Alkanethiols and Alkyl Sulfides on Au(111). *J. Phys. Chem. B* **1998,** *102*, 3456-3465.

[33] Adhikari, B.; Meng, S.; Fyta, M., Carbene-Mediated Self-Assembly of Diamondoids on Metal Surfaces. *Nanoscale* **2016,** *8*, 8966-8975.

[34] Kim, H. K.; Hyla, A. S.; Winget, P.; Li, H.; Wyss, C. M.; Jordan, A. J.; Larrain, F. A.; Sadighi, J. P.; Fuentes-Hernandez, C.; Kippelen, B.; Brédas, J.-L.; Barlow, S.; Marder, S. R., Reduction of the Work Function of Gold by N-Heterocyclic Carbenes. *Chem. Mater.* **2017,** *29* (8), 3403-3411.

[35] Denk, M. K.; Thadani, A.; Hatano, K.; Lough, A. J., Steric Stabilization of Nucleophilic Carbenes. *Angew. Chem. Int. Ed. Engl.* **1997,** *36* (23), 2607-2609.

[36] Murphy, J. A., Discovery and Development of Organic Super-Electron-Donors. *J. Org. Chem.* **2014,** *79* (9), 3731-46.

[37] Levens, A.; An, F.; Breugst, M.; Mayr, H.; Lupton, D. W., Influence of the N-Substituents on the Nucleophilicity and Lewis Basicity of N-Heterocyclic Carbenes. *Org. Lett.* **2016,** *18* (15), 3566-3569.

[38] Paniagua, S. A.; Li, E. L.; Marder, S. R., Adsorption Studies of a Phosphonic Acid on ITO: Film Coverage, Purity, and Induced Electronic Structure Changes. *Phys. Chem. Chem. Phys.* **2014,** *16*, 2874-2881.

[39] Li, H.; Paramonov, P.; Brédas, J.-L., Theoretical Study of the Surface Modification of Indium Tin Oxide with Trifluorophenyl Phosphonic Acid Molecules: Impact of Coverage Density and Binding Geometry. *J. Mater. Chem.* **2010,** *20* (13), 2630.

[40] Sander, W., Carbonyl Oxides : Zwitterions or Diradicals? *Angew. Chem. Int. Ed. Engl.* **1990,** *29*, 344-354.

[41] Ago, H.; Kugler, T.; Cacialli, F.; Salaneck, W. R.; Shaffer, M. S. P.; Windle, A. H.; Friend, R. H., Work Functions and Surface Functional Groups of Multiwall Carbon Nanotubes. *J. Phys. Chem. B* **1999,** *103*, 8116-8121.

[42] Li, H.; Duan, Y.; Coropceanu, V.; Brédas, J.-L., Electronic Structure of the Pentacene-Gold Interface: A Density-Functional Theory Study. *Org. Electron.* **2009,** *10*, 1571-1578.

[43] Fenwick, O.; Van Dyck, C.; Murugavel, K.; Cornil, D.; Reinders, F.; Haar, S.; Mayor, M.; Cornil, J.; Samorì, P., Modulating the Charge Injection in Organic Field-Effect Transistors: Fluorinated Oligophenyl Self-Assembled Monolayers for High Work Function Electrodes. *J. Mater. Chem. C* **2015,** *3* (13), 3007-3015.

[44] Li, H.; Duan, Y.; Paramonov, P. B.; Coropceanu, V.; Brédas, J.-L., Electronic Structure of Self-Assembled (Fluoro)Methylthiol Monolayers on the Au(111) Surface: Impact of Fluorination and Coverage Density. *J. Electron Spectrosc. Relat. Phenom.* **2009,** *174* (70-77).

[45] Cornil, D.; Cornil, J., Work-Function Modification of the (111) Gold Surface Upon Deposition of Self-Assembled Monolayers Based on Alkanethiol Derivatives. *J. Electron Spectrosc. Relat. Phenom.* **2013,** *189*, 32-38.

[46] Wood, C.; Li, H.; Winget, P.; Brédas, J.-L., Binding Modes of Fluorinated Benzylphosphonic Acids on the Polar Zno Surface and Impact on Work Function. *J. Phys. Chem. C* **2012,** *116*, 19125-19133.

[47] Chen, Y. C.; Cunningham, J. E.; Flynn, C. P., Dependence of Rare-Gas-Adsorbate Dipole Moment on Substrate Work Function. *Phys. Rev. B* **1984,** *30* (12), 7317-7319.

[48] Hwang, J.; Wan, A.; Kahn, A., Energetics of Metal–Organic Interfaces: New Experiments and Assessment of the Field. *Mater. Sci. Eng., R* **2009,** *64* (1), 1-31.

[49] Tang, W.; Sanville, E.; Henkelman, G., A Grid-Based Bader Analysis Algorithm without Lattice Bias. *J. Physics. Condens. Matter.* **2009,** *21*, 084204(1-7).

[50] Rodriguez-Castillo, M.; Laurencin, D.; Tielens, F.; van der Lee, A.; Clement, S.; Guari, Y.; Richeter, S., Reactivity of Gold Nanoparticles Towards N-Heterocyclic Carbenes. *Dalton Trans.* **2014,** *43* (16), 5978-5982.

[51] Wang, H. M. J.; Chen, C. Y. L.; Lin, I. J. B., Synthesis, Structure, and Spectroscopic Properties of Gold(I)−Carbene Complexes. *Organometallics* **1999,** *18* (7), 1216-1223.

[52] de Frémont, P.; Scott, N. M.; Stevens, E. D.; Nolan, S. P., Synthesis and Structural Characterization of N-Heterocyclic Carbene Gold(I) Complexes. *Organometallics* **2005,** *24* (10), 2411-2418.

[53] Huynh, H. V.; Han, Y.; Ho, J. H. H.; Tan, G. K., Palladium(II) Complexes of a Sterically Bulky, Benzannulated N-Heterocyclic Carbene with Unusual Intramolecular C-H Pd and Ccarbene Br Interactions and Their Catalytic Activities. *Organometallics* **2006,** *25*, 3267-3274.

[54] Ryan, S. J.; Schimler, S. D.; Bland, D. C.; Sanford, M. S., Acyl Azolium Fluorides for Room Temperature Nucleophilic Aromatic Fluorination of Chloro- and Nitroarenes. *Org. Lett.* **2015,** *17* (8), 1866-1869.

[55] Hintermann, L., Expedient Syntheses of the N-Heterocyclic Carbene Precursor Imidazolium Salts iPr·HCl, IMes·HCl and IXy·HCl. *Beilstein Journal of Organic Chemistry* **2007,** *3*, 22.

[56] Arduengo, A. J.; Krafczyk, R.; Schmutzler, R.; Craig, H. A.; Goerlich, J. R.; Marshall, W. J.; Unverzagt, M., Imidazolylidenes, Imidazolinylidenes and Imidazolidines. *Tetrahedron* **1999,** *55* (51), 14523-14534.

[57] Kolychev, E. L.; Portnyagin, I. A.; Shuntikov, V. V.; Khrustalev, V. N.; Nechaev, M. S., Six- and Seven-Membered Ring Carbenes: Rational Synthesis of Amidinium Salts, Generation of Carbenes, Synthesis of Ag(I) and Cu(I) Complexes. *J. Organomet. Chem.* **2009,** *694* (15), 2454-2462.

[58] Wilder, J. W. G.; Venema, L. C.; Rinzler, A. G.; Smalley, R. E.; Dekker, C., Electronic Structure of Atomically Resolved Carbon Nanotubes. *Nature* **1998,** *391*, 59.

[59] Owen, E. A.; Yates, E. L., Precision Measurements of Crystal Parameters. *Philos. Mag.* **1933,** *15* (98), 472-488.

[60] Reckien, W.; Janetzko, F.; Peintinger, M. F.; Bredow, T., Implementation of Empirical Dispersion Corrections to Density Functional Theory for Periodic Systems. *J. Comput. Chem.* **2012,** *33* (25), 2023-2031.

[61] Kresse, G.; Furthmüller, J., Efficiency of Ab-Initio Total Energy Calculations for Metals and Semiconductors Using a Plane-Wave Basis Set. *Comput. Mater. Sci.* **1996,** *6* (1), 15-50.

[62] Kresse, G.; Furthmüller, J., Efficient Iterative Schemes for Ab Initio Total-Energy Calculations Using a Plane-Wave Basis Set. *Phys. Rev. B* **1996,** *54* (16), 11169-11186.

[63] Blöchl, P. E., Projector Augmented-Wave Method. *Phys. Rev. B* **1994,** *50* (24), 17953-17979.

[64] Perdew, J. P.; Burke, K.; Ernzerhof, M., Generalized Gradient Approximation Made Simple. *Phys. Rev. Lett.* **1996,** *77* (18), 3865-3868.

[65] Perdew, J. P.; Burke, K.; Ernzerhof, M., Generalized Gradient Approximation Made Simple [Phys. Rev. Lett. 77, 3865 (1996)] Errata. *Phys. Rev. Lett.* **1997,** *78* (7), 1396.

[66] Grimme, S.; Antony, J.; Ehrlich, S.; Krieg, H., A Consistent and Accurate Ab Initio Parametrization of Density Functional Dispersion Correction (DFT-D) for the 94 Elements H-Pu. *J. Chem. Phys.* **2010,** *132*, 154104(1-19).

[67] Goerigk, L.; Grimme, S., A Thorough Benchmark of Density Functional Methods for General Main Group Thermochemistry, Kinetics, and Noncovalent Interactions. *Phys. Chem. Chem. Phys.* **2011,** *13* (14), 6670-6688.

[68] Winget, P.; Schirra, L. K.; Cornil, D.; Li, H.; Coropceanu, V.; Ndione, P. F.; Sigdel, A. K.; Ginley, D. S.; Berry, J. J.; Shim, J.; Kim, H.; Kippelen, B.; Brédas, J.-L.; Monti, O. L. A., Defect-Driven Interfacial Electronic Structures at an Organic/Metal-Oxide Semiconductor Heterojunction. *Adv. Mater.* **2014,** *26* (27), 4711-4716.

[69] Gruenewald, M.; Schirra, L. K.; Winget, P.; Kozlik, M.; Ndione, P. F.; Sigdel, A. K.; Berry, J. J.; Forker, R.; Brédas, J.-L.; Fritz, T.; Monti, O. L. A., Integer Charge Transfer and Hybridization at an Organic Semiconductor/Conductive Oxide Interface. *J. Phys. Chem. C* **2015,** *119* (9), 4865-4873.

[70] Schulz, P.; Kelly, L. L.; Winget, P.; Li, H.; Kim, H.; Ndione, P. F.; Sigdel, A. K.; Berry, J. J.; Graham, S.; Brédas, J.-L.; Kahn, A.; Monti, O. L. A., Tailoring Electron-Transfer Barriers for Zinc Oxide/C60 Fullerene Interfaces. *Adv. Func. Mater.* **2014,** *24* (46), 7381-7389.

[71] Li, H.; Winget, P.; Brédas, J.-L., Surface Modification of Indium-Tin-Oxide Via Self-Assembly of a Donor-Acceptor Complex: A Density Functional Theory Study. *Adv. Mater.* **2012,** *24*, 687-693.

[72] Jacquemin, D.; Tanqui, L. B.; Adamo, C.; Ciofini, I., What Is the 'Best' Atomic Charge Model to Describe through-Space Charge-Transfer Excitations? *Phys. Chem. Chem. Phys.* **2012,** *14* (16), 5383-5388.

[73] Methfessel, M.; Paxton, A. T., High-Precision Sampling for Brillouin-Zone Integration in Metals. *Phys. Rev. B* **1989,** *40* (6), 3616-3621.

[74] Frisch, M. J. T., G. W.; Schlegel, H. B.; Scuseria, G. E.; Robb, M. A.; Cheeseman, J. R.; Scalmani, G.; Barone, V.; Mennucci, B.; Petersson, G. A.; Nakatsuji, H.; Caricato, M.;

Li, X.; Hratchian, H. P.; Izmaylov, A. F.; Bloino, J.; Zheng, G.; Sonnenberg, J. L.; Hada, M.; Ehara, M.; Toyota, K.; Fukuda, R.; Hasegawa, J.; Ishida, M.; Nakajima, T.; Honda, Y.; Kitao, O.; Nakai, H.; Vreven, T.; Montgomery, J. A., Jr.; Peralta, J. E.; Ogliaro, F.; Bearpark, M. J.; Heyd, J.; Brothers, E. N.; Kudin, K. N.; Staroverov, V. N.; Kobayashi, R.; Normand, J.; Raghavachari, K.; Rendell, A. P.; Burant, J. C.; Iyengar, S. S.; Tomasi, J.; Cossi, M.; Rega, N.; Millam, N. J.; Klene, M.; Knox, J. E.; Cross, J. B.; Bakken, V.; Adamo, C.; Jaramillo, J.; Gomperts, R.; Stratmann, R. E.; Yazyev, O.; Austin, A. J.; Cammi, R.; Pomelli, C.; Ochterski, J. W.; Martin, R. L.; Morokuma, K.; Zakrzewski, V. G.; Voth, G. A.; Salvador, P.; Dannenberg, J. J.; Dapprich, S.; Daniels, A. D.; Farkas, Ö.; Foresman, J. B.; Ortiz, J. V.; Cioslowski, J.; Fox, D. J., *Gaussian 09; Gaussian*. Wallingford, CT, USA, 2009.

[75] Kendall, R. A.; Dunning, T. H.; Harrison, R. J., Electron Affinities of the First-Row Atoms Revisited. Systematic Basis Sets and Wave Functions. *J. Chem. Phys.* **1992,** *96* (9), 6796-6806.

[76] Seah, M. P.; A., D. W., Quantitative Electron Spectroscopy of Surfaces: A Standards Data Base for Electron Inelastic Mean Free Path in Solids. *Surf. Interface Anal.* **1979,** *1* (1), 2-11.

CHAPTER 4
REDUCTION OF THE WORK FUNCTION OF GOLD BY PHOSPHINE-SULFIDE PHOSHPINES

4.1 Literature Precedents

4.1.1 Phosphorus Based Surface Modifiers

As described in section 1.3.2, intrinsic dipoles of the interfacial materials and formation of surface interfacial dipoles can lead to vacuum-level shifting at the organic/electrode interface.[1-3] Electron transporting interfacial layers such as non-fullerene oligomers,[4] fullerene derivatives,[5-6] and polymers,[1, 7] typically contain a polar amine, phosphonate, or ethylene glycol group that contribute to the intrinsic and surface dipole. Of these functional groups, PO_3H_2 anchoring group containing SAMs have been widely used as on metal oxides.[8-9] However, phosphine itself has rarely been utilized as a binding group / surface dipole contributor in interfacial layers. In 1998, Chung et al. reported on the use of 20–80 parts per billion (ppb) of phosphine and arsine gas to modify the workfunction of gold thin films.[10] The authors noted a decrease to the workfunction with increased exposure time of the gases, measured by Kelvin Probe, and attribute the change to charge transfer from the hydrides to the gold surface through σ-bonding of the lone-pairs. They believe that little to none of the bonding mechanism is due to π-back donation from the metal because the LUMO of PH_3 is too high to interact efficiently with the d orbital of gold.

4.1.1.1 Phosphine Oxide Based Materials

The first phosphine oxide (PO) based host material was introduced in 2006 for blue phosphorescent organic light emitting diodes (PHOLEDs),[11] and afterwards a series of

phosphine oxide based materials with carbazole and fluorene, among other, cores have been synthesized and utilized as well (Figure 4.1).[12-14] The PO derivatives have been used as electron transport materials in PHOLEDs, OLEDs, and OPVs.[15-20] Incorporating these materials helped to enhance the quantum efficiency and lower the driving voltage of PHOLEDs.

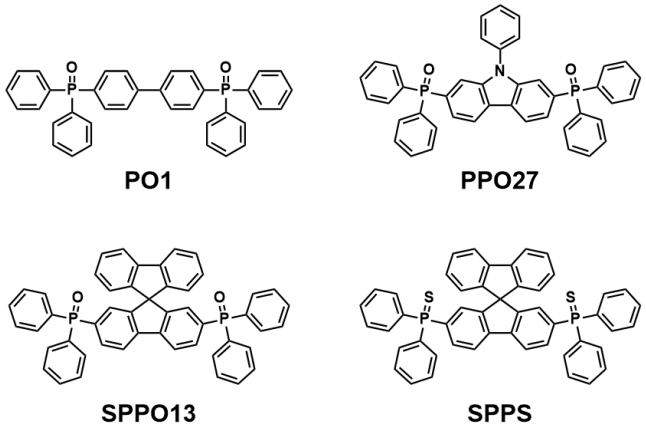

Figure 4.1. Examples of PO and PS based materials used as host and electron transport materials in PHOLEDs and OPVs.[11-13, 21]

4.1.1.2 Phosphine Sulfide Based Materials

Most of the studies on the phosphine-sulfide (PS) unit have been in coordination chemistry as ligand donor atoms in gold, palladium, and other metal complexes.[22-24] The only example of this PS unit used in materials chemistry is by Jeon et al. in SPPS, a spirobifluorene based phosphine sulfide electron injection/collection modification material for OPVs, which slightly improved the efficiency compared with a device without it (Figure 4.1).[21] The authors studied the binding between SPPS and gold by depositing a thin layer (0.2 nm) of Au on SPPS film and analyzing by XPS. They observed two new peak components positioned

at 0.6 eV towards higher binding energy (BE) in the S 2p, in addition to the ones from pure SPPS. They attribute this shift to bond formation, claiming that it is in line with results from thiol adsorbed gold studies. However, it is known that the S 2p BE of alkane thiols on gold actually decreases from 163.5 eV (unbound) to 162 eV (bound).[25-27] A shift in this direction, lower BE, indicates that there is more electron density on the sulfur upon coordination to gold, as would be the case for bond formation as –SH is converted to S^-. They also claim that they observed new peak components shifted towards higher BE in the Au 4f peak. This would imply that Au becomes somewhat oxidized, meaning electron density is transferred to S, but this contradicts their observed shifts in the S 2p BE.

The sulfur from phosphine sulfides are different from thiols/sulfides in that (in general) the former are sp^2 hybridized and the latter are sp^3 hybridized. Therefore, bond formation with the sp^2 electrons from the PS group should lead to less electron density on S, which could explain the observation of Jeon et al. in the higher BE shift.[21] Phosphine sulfides, like phosphine oxides, can also be used to reduce the basicity of phosphines, when installed nearby, because they are strongly inductively withdrawing, which Fahrni and coworkers have demonstrated in a recent study of phosphine-sulfide phosphine (PSP) ligands for probing biological Cu(I).[28] Their ligands are designed to chelate Cu(I) with both the phosphine and PS units in a multidentate fashion, and have shown high binding affinities to copper.[28]

Despite this demonstrated affinity of the PSP ligands to Cu(I), due to the previously reported P=S on planar Au interaction, and their intrinsic chelation ability, PSP ligands were of interest to test their effects on planar Au. PSP ligands (and one fully sulfurized PS

ligand) were synthesized by Dr. Thomas Morgan, referenced above from the Christoph Fahrni group at Georgia Tech and donated for study on planar gold surfaces.[28]

4.2 Selection of Phosphines

Of the selection of published and unpublished PSP ligands that the Fahrni group developed, the simpler aliphatic PSPs were selected for study.

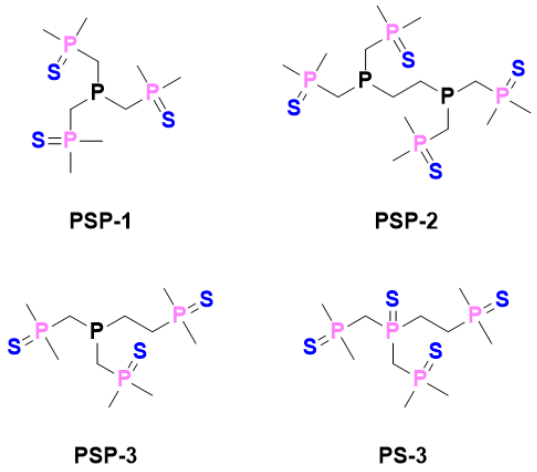

Figure 4.2. Structure of phosphine sulfide phosphines (PSP) and phosphine sulfide (PS) for study. The atoms are color coded.

These include the published PSP-1 and PSP-2, in addition to unpublished PSP-3 and PS-3 (Figure 4.2).[28] PSP-1 is symmetric about the central phosphorus atom with three PS units separated by methylene spacers; the basicity of the phosphine is reduced by three PS units. PSP-2 is an EDTA-like PSP with the basicity of each phosphine reduced by only two PS units. PSP-3, is similar to PSP-1 but has two methylene spacers and one ethylene spacer; the placement of one of the PS units farther away from P would make this compound slightly more basic than PSP-1. Finally, PS-3 is the fully sulfurized version of PSP-3 and consists of only PS units and no phosphine core. This compound was designed

to isolate the activity of phosphine-sulfide in binding and/or work function (WF) modification.

4.3 Analysis of Modified Au Surfaces

4.3.1 Coverage and Work function Analysis of Phosphine-Sulfide Phosphines

This chapter aims to determine the coverage in terms of thickness of modified surfaces under different conditions and the subsequent work function modification, in addition to determining the effect of phosphorus versus phosphine-sulfide in binding and work function change. The details for the determination of thickness are described in 2.4.4. The assumptions in these calculations are that for the overlayer, the inelastic mean free path (IMFP) is 3 nm and density of 1 g/cm^{-3}. Note that if the actual density (or IMFP) is larger than this assumption, then the computed thicknesses in this study have been overestimated (underestimated) and vice versa. The known values used for gold are IMFP of 2.02 nm, density of 19.32 g/cm^{-3}, and MW 196.97 amu. The S/P ratio was used as a metric to determine the accuracy of the background subtraction relative to S and P. The expected ratio for PSP-1 and PSP-3 is 0.75, for PSP-2 is 0.67, and for PS-3 is 1.

Due to the conformational flexibility of the compounds from multiple aliphatic chains, and without calculations to determine the orientation and conformation of binding to planar Au surfaces, elucidation to the binding orientation and footprints were not made. Initial attempts to do so were abandoned and for future work, collaboration with a theoretical chemist who can model the effect of the PSP/PS surface modifiers should be pursued to gain useful information that would bolster this study.

Two methods were utilized to deposit the surface modifiers. In the first section, the results from spin coated substrates will be presented, followed by the results from immersed substrates in terms of thicknesses and work function modification.

4.3.1.1 PSP and PS modified Au from Spin Coating

Several tests were performed to determine whether the phosphine sulfides could form monolayers on the surface of Au. It was originally determined through spin coating from 2 mM solutions of PSPs that there was a change to the WF of Au greater than what would be expected from merely a "push-back" effect (Table 4.1).

Table 4.1. Work function (by UPS), elemental ratios, and thicknesses found by XPS of PSP/PS modified gold surfaces from spin coating in 2 mM chloroform solutions.

Compound	WF (eV)[a]	[P/Au][a]	[S/Au][a]	[S/P][a]	Thickness (nm)[a]
OP Au[b]	4.93 ± 0.03	–	–	–	0
PSP-1	4.30 ± 0.01	0.16 ± 0.01	0.12 ± 0.01	0.75 ± 0.01	2.0 ± 0.1
PSP-2	4.06 ± 0.03	1.16 ± 0.11	0.75 ± 0.07	0.65 ± 0.01	6.1 ± 0.2
PSP-3	4.02 ± 0.01	0.59 ± 0.01	0.44 ± 0.00	0.75 ± 0.01	4.5 ± 0.0
PS-3	4.00 ± 0.01	2.06 ± 0.09	1.98 ± 0.08	0.96 ± 0.00	8.0 ± 0.1

[a] Standard deviations are of sample to sample variations.
[b] OP Au was spin coated with chloroform as a control of the effect of chloroform.

The WF of Au modified with the PSP and PS compounds were reduced by at least 0.63 eV. Au modified with PSP-1 was 4.3 eV but for PSP-2, PSP-3 and PS-3, was 4.0 eV. Not only is PSP-1 presumably the least basic of the three PSP compounds, but it has the least flexibility of the PS groups to simultaneously interact with a planar surface, which was an intentional design for its original purpose, which was to be a metal ion chelator. On planar surfaces however, since the PS groups in PSP-1 are spaced by only a methylene unit, if the PS is contributing to binding and/or work function reducing from a negative dipole towards the surface, then PSP-2, which has an ethylene spacer, would be more

suitable for this type of interaction. This may be the reason for the 0.24 eV difference in measured WF.

Another rationale is that the P/Au ratio for PSP-3 is much higher (0.59) than for PSP-1 (0.16), which implies that PSP-3 coated the surface with a greater thickness than PSP-1, since the volumes of the two compounds are similar (difference of $–CH_2–$). It may be that higher thickness leads to greater reduction in WF. However, PSP-2, PSP-3, and PS-3 had similar WF but different thicknesses. This could imply that after a certain thickness, the orientation of the P and PS groups may be random and lead to depolarization effects, where dipoles cancel and the mere presence of more surface modifier on the surface may not lead to a positive additive effect.

The P 2p and S 2p core level spectra obtained from high resolution scans of the surfaces are displayed in Figure 4.3. P 2p and S 2p have closely spaced spin-orbit components (Δ = 0.87 eV and 1.16 eV, respectively). Thus, the overlapping two peaks in Figure 4.3a at 133.3 eV and 132.4 eV for all spectra correspond to $2p_{1/2}$ and $2p_{3/2}$ and these peaks correspond to the S from the phosphine sulfide unit. The minor peak at 131 eV, most prominent in PSP-2, and not present in PS-3, in turn, corresponds to the phosphine phosphorus. The two peaks in Figure 4.3a at 163.2 eV and 162 eV for all spectra correspond to $2p_{1/2}$ and $2p_{3/2}$ and there is only one type of sulfur in the chemical structure of the surface modifiers. The signals in Figure 4.3 may or may not be representing S interaction with Au, however, due to the thickness of the films, this type of interaction would consist of a small fraction of the total peak intensity. According to these spectra, films of greater than 2 nm, resulted in similar peak positions and shapes for all compounds.

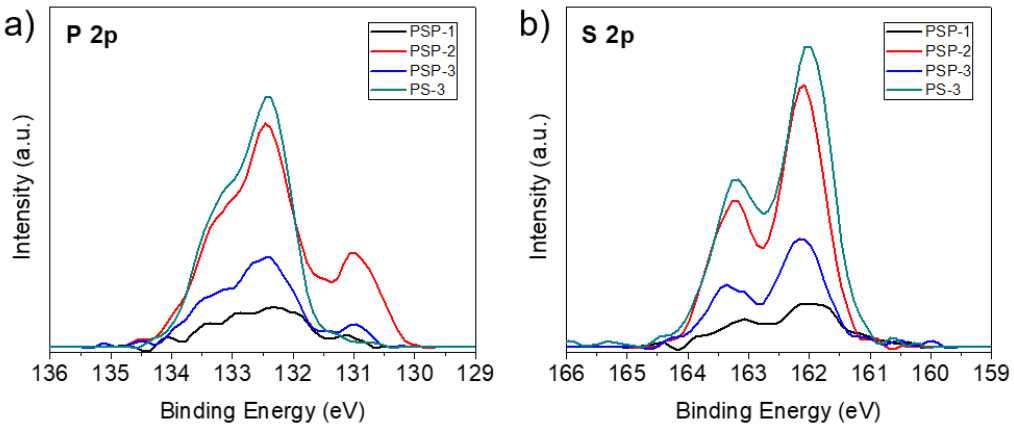

Figure 4.3. Representative XPS spectra of P 2p and S 2p from the modified-surfaces by spin coating from 2 mM solutions in chloroform. The plots were background subtracted and overlapped. The core energy levels are indicated on each plot.

Thus, this first study demonstrate that the work function of gold could be lowered by the PSP and PS compounds, but the robustness of the surface modifiers to washing conditions were not tested and the thicknesses of the films are potentially too thick to be useful as surface modifiers for electronic applications. Therefore, the next section describes investigations of surfaces modified from immersion and washing.

4.3.1.2 PSP and PS modified Au from Immersion

To achieve monolayers, a series of tests were conducted changing solvents, immersion times, and washing conditions. First, chloroform solutions of 2 mM PSP-3 were prepared and used to immerse clean gold substrates for 10 min, 1 h, and 3 h, followed by sonication for 1 min. The work function of all the resulting films, P/Au ratios, and thicknesses were similar at ca. 4.5 eV from these conditions. From the conditions listed in Table 4.1, a P/Au ratio of 0.59 gave rise to a modified-gold WF of 4.0 eV for PSP-3, whereas from the conditions in Table 4.2, a P/Au ratio of 0.06 led to a WF of 4.3 eV. This indicates that even with a tenfold difference in P/Au, the difference in WF is only 0.3 eV.

These results implied that in terms of density of surface modifiers, 10 min of immersion led to similar surface coverage as a 3 h immersion. These quantifications by XPS do not give physical information such as the topology of the surface however and film quality cannot be deduced from here.

Table 4.2. Work function (by UPS), elemental ratios, and thicknesses found by XPS of PSP/PS modified gold surfaces from immersion in 2 mM solutions followed by washing.

2 mM (Solvent)[b]	Immerse Duration	Wash Duration[c]	WF (eV)	[P/Au][a]	[S/Au][a]	[S/P]	Thickness (nm)
PSP-3 (C)	10 min	1 min S	4.34 ± 0.00	0.06	0.04	0.75 ± 0.05	0.9 ± 0.1
PSP-3 (C)	1 h	1 min S	4.39 ± 0.00	0.06	0.04	0.73 ± 0.01	0.9 ± 0.1
PSP-3 (C)	3 h	1 min S	4.37 ± 0.00	0.07	0.05	0.72 ± 0.01	1.0 ± 0.1
PSP-3 (C)	10 min	1 min S	4.29 ± 0.01	0.10	0.08	0.74 ± 0.01	1.5 ± 0.1
PSP-3 (C)	10 min	10 min S	4.16 ± 0.04	0.09	0.07	0.75 ± 0.02	1.3 ± 0.0
PSP-3 (C)	10 min	3x	4.19 ± 0.01	0.08	0.06	0.74 ± 0.04	1.2 ± 0.0
PSP-1 (T)	10 min	1 min S	4.25 ± 0.04	0.05	0.04	0.77 ± 0.03	0.8 ± 0.0
PSP-1 (T)	10 min	10 min S	4.32 ± 0.03	0.05	0.04	0.77 ± 0.02	0.8 ± 0.0
PSP-1 (T)	10 min	3x	4.36 ± 0.04	0.06	0.04	0.79 ± 0.00	0.9 ± 0.0

[a] P/Au and S/Au had sample to sample standard deviations of 0.00–0.01.
[b] For the solvents, T stands for tetrahydrofuran (THF) and C stands for $CHCl_3$.
[c] Washing duration refers to sonication (S) or triple rinse (3x).

Washing conditions were also tested with substrates immersed in 2 mM PSP-3 in chloroform solutions for 10 min followed by sonication in fresh chloroform for 1 min, 10 min, or rinsing three times with fresh solvent. Table 4.2 shows that triple rinse yielded the lowest work function at 4.19 eV and the smallest thickness at 1.2 nm. The difference in P/Au from 1 min of sonication to 10 min of sonication was only 0.01 and the difference in work function between a 10 min sonicated substrate and a triple rinsed substrate was within the standard deviation. Therefore, among the three conditions, 1 min sonication was selected as the optimized condition from these results, based on brevity of time in relation to similarly obtained results in WF and thickness.

Tetrahydrofuran (THF) was considered as a potential solvent but only with PSP-1. Substrates were immersed 10 min followed by the same three washing conditions. In this case, 1 min sonication gave rise to the lowest work function at 4.25 eV. Therefore, though the compounds were very soluble in both chloroform and THF, a preference could not be determined and chloroform was selected due to its earlier use in 4.3.1.1.

From the above optimization studies, an immersion time of 10 min followed by 1 min sonication with chloroform as the solvent was used to modify gold to yield thinner films, potentially monolayers (Table 4.3). First, it should be noted that unlike for the previous results, the S/P ratios, deviated significantly from the expected value for PSP-1 because of poor signal:noise for the S 2p signal. This would imply that for these data, either the sulfur component was underestimated or the phosphorus component was overestimated, if 100% of the compound were still intact and there was no introduction of P or S containing contaminants. Given this caveat, the data in Table 4.3 can be analyzed.

Table 4.3. Work function (by UPS), elemental ratios, and thicknesses found by XPS of PSP/PS modified gold surfaces from immersion for 10 min in 2 mM chloroform solutions followed by sonication for 1 min.

2 mM (Solution)	WF (eV)	[P/Au][a]	[S/Au][a]	[S/P][a]	Expected [S/P]	Thickness (nm)
PSP-1 ($CHCl_3$)	4.57 ± 0.01	0.04	0.01	0.65 ± 0.14	0.75	0.7 ± 0.1
PSP-2 ($CHCl_3$)	4.52 ± 0.10	0.05	0.02	0.69 ± 0.04	0.67	0.8 ± 0.0
PSP-3 ($CHCl_3$)	4.20 ± 0.01	0.05	0.03	0.72 ± 0.05	0.75	0.7 ± 0.1
PS-3 ($CHCl_3$)	4.40 ± 0.03	0.09	0.09	1.00 ± 0.03	1	1.4 ± 0.0

[a] P/Au and S/Au had sample to sample standard deviations of 0.00–0.01.

The PSP compounds have similar P/Au ratios of 0.04–0.05, whereas PS-3 has a P/Au ratio of 0.09. These thin films also resulted in modest WF reductions in the mid-4 eV range. Despite the differences in MW among the compounds, the number of phosphorus per unit weight is similar, which is the variable used to determine thickness, and thus,

similar P/Au values indicate similar thicknesses. Comparing PSP-1, PSP-2, and PSP-3, given similar coverages, PSP-3 modified Au had the lowest WF of 4.2 eV compared with 4.6 and 4.5 eV for PSP-1 and PSP-2, respectively. Although each phosphine in PSP-2 is more basic than one in PSP-3, PSP-3 has the longer and likely more flexible ethylene spacer. In this thinner film, the lower WF for PSP-3 suggests that the dipoles from PSP-3 were collectively directed in the same direction more so than in PSP-1 or PSP-2, leading to a greater overall dipole.

Modification with PSP-3 and PS-3 did not lead to the same thickness under these conditions so the results cannot be directly compared. However, there is twice as much PS-3 on the surface than PSP-3 but the difference in WF is only 0.2 eV with PS-3 at the lower WF of 4.20 eV. Thus, it appears that a compound containing only PS groups may lead to a thicker film, but no drastic improvements to the WF reduction. This would in turn imply that the phosphine functionalities contribute non-trivially to the dipole and that PS units are responsible for binding to the surface.

The plots in Figure 4.4 have not been background subtracted or normalized but rather zoomed in/out to similar peak maxima, so cannot be qualitatively compared as presented. While the shape and position of the P 2p peak is the same for all the compounds in these thinner films (a–d), the position appears to have shifted towards lower BE by 0.3–0.6 eV (position at 131.8–132.1 eV) (compared to in 4.3.1.1). This means that binding to the gold surface caused this shift of the P from the PS unit to have more electron density than before binding. This may be an indication that the metal is donating electron density to the PS group.

The S 2p peaks (Figure 4.4e–h) differ among the compounds and from the films deposited from spin coating (in 4.3.1.1). Here, besides for PS-3, there appears to be another peak at higher BE (located from 172–166 eV). If this peak is not integrated, the S/P ratios are much less than what is expected. Therefore, this region although very noisy, is not noise but represents a signal from the S 2p. The signal is more prominent in PSP-1 and PSP-2 and barely distinguishable in PSP-3. This shift is surprising and is only noticeable in these plots representing thinner films. This may indicate that they were present before but at unnoticeable intensities, or that upon binding to gold, the sulfur exhibits a strongly oxidized character, leading to peaks in the 168–172 eV range, which thiols-Au do not demonstrate.

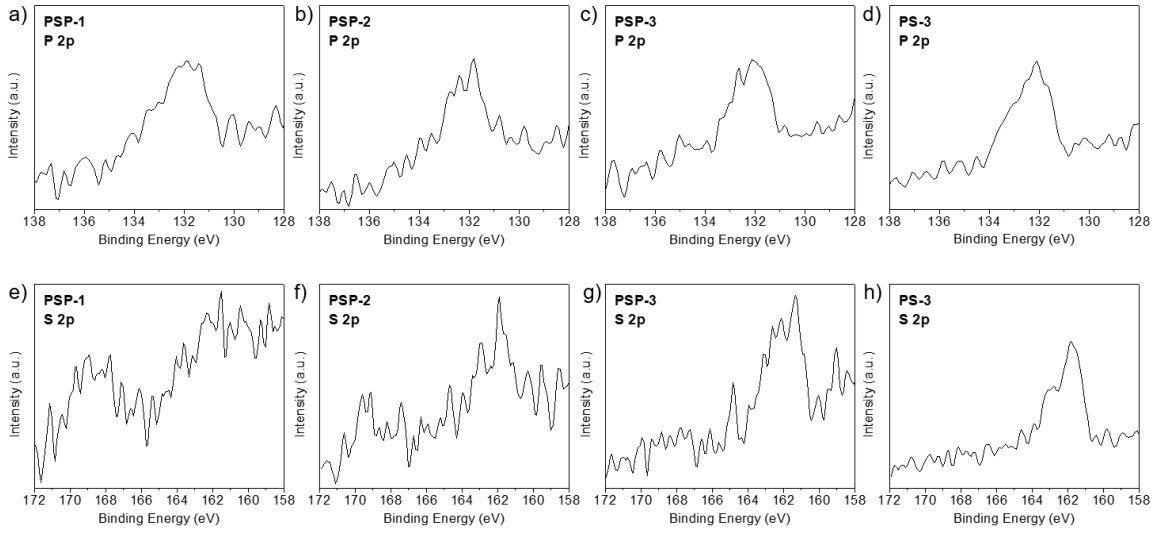

Figure 4.4. Representative XPS spectra of P 2p and S 2p from the modified-surfaces by immersion from 2 mM solutions in chloroform followed by 1 min sonication. The core energy levels are indicated on each plot.

4.3.1.3 Preliminary Copper Surface Modification Results

Although the PSP ligands were designed to and showed strong binding to Cu(I), planar Cu(0) substrates were still tested as substrates for PSP binding. To eliminate the

copper oxides, copper foil was etched according to Chavez et al.[29] The substrates were immediately immersed in either a PSP-1 solution or dI water or fresh tetrahydrofuran. Table 4.4 shows that copper foil that was kept in THF had a WF of 4.40 eV but the WF for the one kept in water was slightly higher at 4.49 eV. The modified copper, however, showed a reduction in WF with 4.11 eV for a surface with a P/Cu ratio of 0.10 and to 3.86 eV for P/Cu ratio of 0.21 eV. From these data, it appears that the presence of PSP-1 at greater concentrations can lower the WF to below 4 eV.

Table 4.4. Work function (by UPS), elemental ratios, and thicknesses found by XPS of PSP-1 modified copper surfaces from immersion in 2 mM THF solutions followed with washing.

2 mM (Solution)	Modification	Wash	WF (eV)	[P/Cu]	[S/Cu]	[S/P]
PSP-1 (THF)	10 min dip	1 min sonic.	4.11 ± 0.05	0.10 ± 0.01	0.07 ± 0.00	0.75 ± 0.01
PSP-1 (THF)	10 min dip	triple rinse	3.86 ± 0.04	0.21 ± 0.06	0.16 ± 0.05	0.76 ± 0.01
H_2O[a]	10 min dip	n/a	4.49 ± 0.01	–	–	–
THF[a]	10 min dip	n/a	4.40 ± 0.01	–	–	–

[a] These were control solvents used with no PSP/PS added.
[b] Standard deviations are of spot to spot variation within the same sample.

Control samples were made to examine the changes in the Cu 2p peaks from exposure to water, which is supposed to increase the presence of copper oxides, and from exposure to THF, to see if during the time that the substrates were immersed in the modifier-solutions (also in THF), whether copper oxides would form. A copper substrate that was not etched but only rinsed in methanol was also prepared and compared.

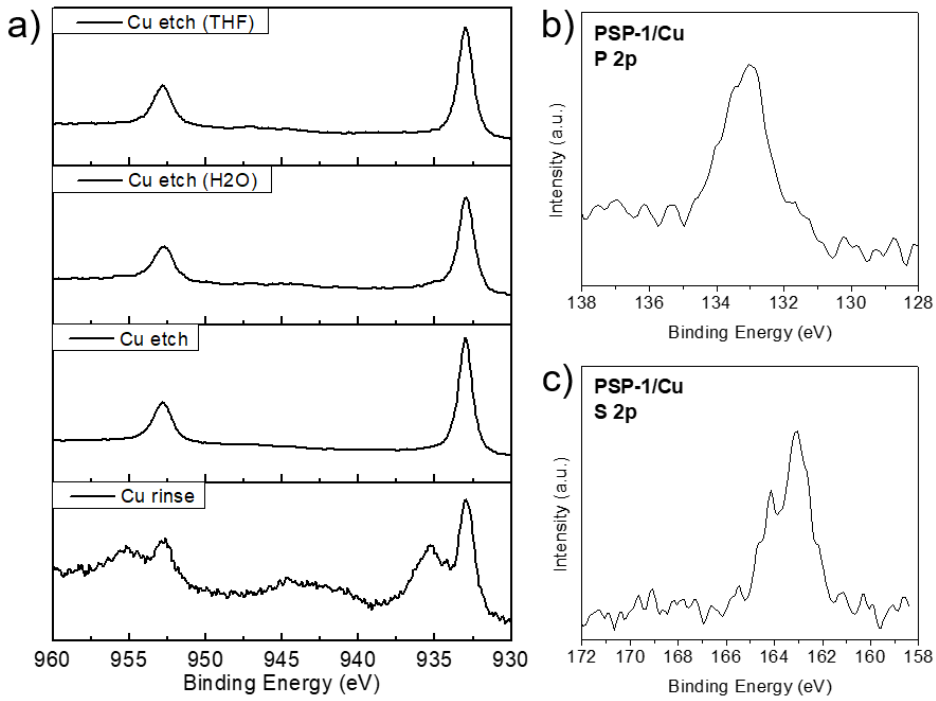

Figure 4.5. Cu 2p (from XPS) of modified gold surfaces with PSP-1 or control solvent washing (a), P 2p (b) and S 2p peaks of PSP-1 on Cu (c). In (a), from top to bottom, the first three spectra show predominantly Cu(0) from the bulk substrate and the last spectrum shows new peaks at 935 and 955 eV from copper oxides.

Figure 4.5a shows the Cu 2p of the modified substrates from modifier-solutions or rinsed from clean solvent. All the Cu etched compounds had similar peak shapes and positions but the Cu that was only rinsed had a clear indication of the presence of copper oxides at higher BE. When the spectra were calibrated to Cu 2p at 933 eV, the resulting S 2p was found at 163 eV and P 2p at 133 eV. These BE are 1.0 and 0.6 eV higher, respectively, than was found on PSP-1 modified Au. This suggests that the sulfur is more electron donating on the copper than it is on the gold.

4.4 Conclusions

Phosphine-sulfide phosphine and phosphine-sulfide ligands were examined on planar gold surfaces to quantify the ability of the surface modifiers to reduce the work

function of gold in addition to determine whether the PS group would form robust bonds to gold. We hypothesized that increased conformational flexibility would allow for the P=S group to better align perpendicularly to the surface, leading to more of the effective dipole in the orientation necessary to reduce the WF. We observed this was the case for PSP-3, with two methylene and an ethylene spacer, which performed the best among the group of compounds in terms of providing the lowest WF surface of 4.2 eV.

When there was half as much PSP-3 than PS-3, its fully sulfurized counterpart, on the surface, PS-3 was only able to lower the WF 0.2 eV more than PSP-3 at half the density. Thus, it was concluded that the phosphorus was necessary to induce dipoles favoring the reduction of the WF. However, the PS groups could withstand 10 min of sonication and thus it is highly likely that the compounds are bound by these groups to the gold. It was observed in an appended study, not recorded here, that a phenyl phosphine was easily washed away from gold by a rinse in polar solvent. However, this was not the case here.

Therefore, although the PSP and PS ligands could only reduce the WF of gold to 4.0 eV, they were robust to sonication and could potentially be used as a new head group for self-assembled monolayers. The compounds can be redesigned to be fit for planar surfaces and other moieties that can contribute to the dipole can be installed in the spacer or tail portions of the compound. Preliminary studies with copper show that PSP ligands may be more suitable to reduce the WF of copper.

4.5 Experimental

4.5.1 Materials

Tris(dimethylphosphorothioylmethyl)phosphine (PSP-1), 1,2-Bis(bis(dimethyl phosphorothioylmethyl)phosphino)ethane (PSP-2), (((2-(dimethylphosphorothioyl)ethyl)

phosphanediyl)bis(methylene))bis(dimethylphosphine sulfide) (PSP-3), and (((2-(dimethylphosphorothioyl)ethyl)phosphorothioyl)bis(methylene))bis(dimethylphosphine sulfide) (PS-3) are all white solids and were synthesized by Dr. Thomas Morgan of the Christoph Fahrni group at Georgia Tech and donated for study. PSP-1 and PSP-2 have been reported and published recently by the Fahrni group and the synthesis is described in the cited work.[28]

4.5.2 Au/Cu Surface Cleaning and Modification

Commercially available copper foil (Sigma-Aldrich) 0.25 mm thickness, 99.98% trace metals basis were cut into 0.5 in. × 0.5 in. squares and etched in glacial acetic acid at 40 °C for 10 min, rinsed with tetrahydrofuran, and dried under a flow of nitrogen. Exposure to air was minimized by immediately immersing the substrate into solutions with surface modifier or fresh solutions as a control.

Commercially available glass:Ti:Au slides (EMF Corp., Ithaca, NY, USA) were cut into 0.5 in. × 0.5 in. squares and sonicated in ethanol for 10 min, dried under a flow of nitrogen, and etched with oxygen plasma (OP) with a PE-50 XL Plasma System for 5 min prior to any additional surface treatment. Substrates were modified by either spin coating freshly prepared solutions (2 mM) in tetrahydrofuran or chloroform at 3000 rpm, 1100 acceleration, for 30 sec or immersing for 1 min–3 h followed by washing in fresh solvent by triple rinse (successive rinsing and drying substrate three times) or sonication (1–10 min) and annealing at 70 °C for 10 min. Samples were immediately taken for X-ray photoelectron spectroscopy/ultraviolet photoelectron spectroscopy (XPS/UPS) analysis.

4.5.3 Surface Characterization

4.5.3.1 UPS and XPS

All UPS and XPS measurements were conducted in a Kratos Axis Ultra spectrometer with an average base pressure of 10^{-9} Torr. UPS spectra were collected prior to XPS spectra with a 21.2 eV He (I) excitation and a pass energy of 5 eV using a 27 μm spot size. XPS spectra were collected with a monochromatic Al Kα source using a 400 μm spot size and a pass energy of 160 eV for survey acquisition and 20 eV for high-resolution spectra. XPS was performed with a normal takeoff angle (0°). Data were analyzed using CasaXPS processing software. The binding energies of all XPS spectra were calibrated to the Au 4f line at 84.0 eV (or Cu 2p line at 933 eV) and processed with a Shirley background subtraction and Savitzky-Golay smoothing unless otherwise stated. All UPS and XPS data points represent multiple samples scanned on multiple spots; the standard deviation reported reflects variation among different samples.

4.6 References

[1] Zhou, Y.; Fuentes-Hernandez, C.; Shim, J.; Meyer, J.; Giordano, A. J.; Li, H.; Winget, P.; Papadopoulos, T.; Cheun, H.; Kim, J.; Fenoll, M.; Dindar, A.; Haske, W.; Najafabadi, E.; Khan, T. M.; Sojoudi, H.; Barlow, S.; Graham, S.; Brédas, J.-L.; Marder, S. R.; Kahn, A.; Kippelen, B., A Universal Method to Produce Low-Work Function Electrodes for Organic Electronics. *Science* **2012,** *336* (6079), 327-32.

[2] Lee, B. H.; Jung, I. H.; Woo, H. Y.; Shim, H. K.; Kim, G.; Lee, K., Multi-Charged Conjugated Polyelectrolytes as a Versatile Work Function Modifier for Organic Electronic Devices. *Adv. Func. Mater.* **2013,** *24* (8), 1100-1108.

[3] Kang, R.; Oh, S. H.; Kim, D. Y., Influence of the Ionic Functionalities of Polyfluorene Derivatives as a Cathode Interfacial Layer on Inverted Polymer Solar Cells. *ACS Appl. Mater. Interfaces* **2014,** *6* (9), 6227-36.

[4] Zhang, Z.-G.; Qi, B.; Jin, Z.; Chi, D.; Qi, Z.; Li, Y.; Wang, J., Perylene Diimides: A Thickness-Insensitive Cathode Interlayer for High Performance Polymer Solar Cells. *Energy Environ. Sci.* **2014,** *7* (6), 1966-1973.

[5] Zhang, Z.-G.; Li, H.; Qi, Z.; Jin, Z.; Liu, G.; Hou, J.; Li, Y.; Wang, J., Poly(Ethylene Glycol) Modified [60]Fullerene as Electron Buffer Layer for High-Performance Polymer Solar Cells. *Appl. Phys. Lett.* **2013,** *102* (14), 143902.

[6] Zhang, Z.-G.; Li, H.; Qi, B.; Chi, D.; Jin, Z.; Qi, Z.; Hou, J.; Li, Y.; Wang, J., Amine Group Functionalized Fullerene Derivatives as Cathode Buffer Layers for High Performance Polymer Solar Cells. *J. Mater. Chem. A* **2013,** *1* (34), 9624-9629.

[7] Huang, F.; Wu, H.; Wang, D.; Yang, W.; Cao, Y., Novel Electroluminescent Conjugated Polyelectrolytes Based on Polyfluorene. *Chem. Mater.* **2004,** *16* (4), 708-716.

[8] Pawsey, S.; Yach, K.; Reven, L., Self-Assembly of Carboxyalkylphosphonic Acids on Metal Oxide Powders. *Langmuir* **2002,** *18* (13), 5205-5212.

[9] Paniagua, S. A.; Hotchkiss, P. J.; Jones, S. C.; Marder, S. R.; Mudalige, A.; Marrikar, F. S.; Pemberton, J. E.; Armstrong, N. R., Phosphonic Acid Modification of Indium−Tin Oxide Electrodes: Combined XPS/UPS/Contact Angle Studies. *J. Phys. Chem.* **2008,** *112* (21), 7809-7817.

[10] Chung, Y. S.; Evans, K.; Glaunsinger, W., Work Function Response of Thin Gold Film Surfaces to Phosphine and Arsine. *Appl. Surf. Sci.* **1998,** *125* (1), 65-72.

[11] Burrows, P. E.; Padmaperuma, A. B.; Sapochak, L. S.; Djurovich, P.; Thompson, M. E., Ultraviolet Electroluminescence and Blue-Green Phosphorescence Using an Organic Diphosphine Oxide Charge Transporting Layer. *Appl. Phys. Lett.* **2006,** *88* (18), 183503.

[12] Jeon, S. O.; Yook, K. S.; Joo, C. W.; Lee, J. Y., Theoretical Maximum Quantum Efficiency in Red Phosphorescent Organic Light-Emitting Diodes at a Low Doping

Concentration Using a Spirobenzofluorene Type Triplet Host Material. *Org. Electron.* **2010,** *11* (5), 881-886.

[13] Kim, B. S.; Lee, J. Y., Phosphine Oxide Type Bipolar Host Material for High Quantum Efficiency in Thermally Activated Delayed Fluorescent Device. *ACS Appl. Mater. Interfaces* **2014,** *6* (11), 8396-8400.

[14] Jeon, S. O.; Lee, J. Y., Phosphine Oxide Derivatives for Organic Light Emitting Diodes. *J. Mater. Chem.* **2012,** *22* (10), 4233-4243.

[15] Jeon, S. O.; Yook, K. S.; Lee, J. Y.; Park, S. M.; Won Kim, J.; Kim, J.-H.; Hong, J.-A.; Park, Y., Mechanism for the Direct Electron Injection from Al Cathode to the Phosphine Oxide Type Electron Transport Layer. *Appl. Phys. Lett.* **2011,** *98* (7), 073306.

[16] Jeon, S. O.; Jang, S. E.; Son, H. S.; Lee, J. Y., External Quantum Efficiency above 20% in Deep Blue Phosphorescent Organic Light-Emitting Diodes. *Adv. Mater.* **2011,** *23* (12), 1436-1441.

[17] Jiang, W.; Duan, L.; Qiao, J.; Dong, G.; Wang, L.; Qiu, Y., Tuning of Charge Balance in Bipolar Host Materials for Highly Efficient Solution-Processed Phosphorescent Devices. *Org. Lett.* **2011,** *13* (12), 3146-3149.

[18] Jiang, W.; Cui, P.; Ban, X.; Sun, Y., Bis(Phosphine Oxide)/Triphenylamine Based Material for Solution-Processed Blue Electrofluorescent and Green Electrophosphorescent Devices. *RSC Adv.* **2015,** *5* (60), 48654-48658.

[19] Chakravarthi, N.; Aryal, U. K.; Gunasekar, K.; Park, H.-Y.; Gal, Y.-S.; Cho, Y.-R.; Yoo, S. I.; Song, M.; Jin, S.-H., Triazine-Based Polyelectrolyte as an Efficient Cathode Interfacial Material for Polymer Solar Cells. *ACS Appl. Mater. Interfaces* **2017,** *9* (29), 24753-24762.

[20] Chakravarthi, N.; Park, H.-Y.; Aryal, U. K.; Kim, J.; Gal, Y.-S.; Song, M.; Cho, Y.-R.; Jin, S.-H., Phosphine Oxide and Amino N-Oxide Functionalized Phenylquinoline-Based Small Molecules: New Cathode Interfacial Layers for High-Performance Inverted Organic Solar Cells. *Org. Electron.* **2018,** *58*, 111-118.

[21] Jeon, S. O.; Lee, J. Y., Improved Device Performances of Organic Solar Cells with Au Cathode Using a Phosphine Sulfide Type Cathode Modification Layer. *Electrochem. Solid-State Lett.* **2011,** *14* (10), B93-B95.

[22] Ahmad, S.; Isab, A. A.; Perzanowski, H. P.; Hussain, M. S.; Akhtar, M. N., Gold(I) Complexes with Tertiary Phosphine Sulfide Ligands. *Trans. Metal Chem.* **2002,** *27* (2), 177-183.

[23] Aizawa, S.-i.; Majumder, A.; Yokoyama, Y.; Tamai, M.; Maeda, D.; Kitamura, A., Air-Stable, Recyclable, and Regenerative Phosphine Sulfide Palladium(0) Catalysts for C−C Coupling Reaction. *Organometallics* **2009,** *28* (20), 6067-6072.

[24] Dilworth, J. R.; Wheatley, N., The Preparation and Coordination Chemistry of Phosphorus Sulfur Donor Ligands. *Coord. Chem. Rev.* **2000,** *199* (1), 89-158.

[25] Castner, D. G.; Hinds, K.; Grainger, D. W., X-Ray Photoelectron Spectroscopy Sulfur 2p Study of Organic Thiol and Disulfide Binding Interactions with Gold Surfaces. *Langmuir* **1996,** *12*, 5083-5086.

[26] Sun, F.; Grainger, D. W.; Castner, D. G.; Leach-Scampavia, D. K., Adsorption of Ultrathin Films of Sulfur-Containing Siloxane Oligomers on Gold Surfaces and Their in Situ Modification. *Macromol.* **1994,** *27* (11), 3053-3062.

[27] Nuzzo, R. G.; Zegarski, B. R.; Dubois, L. H., Fundamental Studies of the Chemisorption of Organosulfur Compounds on Gold(111). Implications for Molecular Self-Assembly on Gold Surfaces. *J. Am. Chem. Soc.* **1987,** *109* (3), 733-740.

[28] Morgan, M. T.; Yang, B.; Harankhedkar, S.; Nabatilan, A.; Bourassa, D.; McCallum Adam, M.; Sun, F.; Wu, R.; Forest Craig, R.; Fahrni Christoph, J., Stabilization of Aliphatic Phosphines by Auxiliary Phosphine Sulfides Offers Zeptomolar Affinity and Unprecedented Selectivity for Probing Biological Cu(I). *Angew. Chem. Int. Ed.* **2018,** *57*, 9711-9715.

[29] Chavez, K. L.; Hess, D. W., A Novel Method of Etching Copper Oxide Using Acetic Acid. *Journal of the Electrochemical Society* **2001,** *148* (11), G640-G643.

CHAPTER 5
REDUCTION OF THE WORK FUNCTION OF GOLD BY N-HETEROCYCLIC THIONES AND SELONES

5.1 Literature Precedents

5.1.1 Thiourea Characteristics

Thioureas have been used as ligands to form complexes with a variety of metals for over a century.[1-4] They have a similar structure as urea, but the oxygen atom is replaced with sulfur. Although they are known to have three coordination modes, through the N, S, and C=S, coordination through the S is favored on gold.[5] A typical thiourea is not cyclic, but when the two N atoms are connected to form a heterocyclic core, the thiourea is called a N-heterocyclic thione (NHT), and a selenium derivative is called N-heterocyclic selone (NHSe).

Crystallographic data indicate 1,3-dimethyl-imidazoline-2-thione (an NHT) has a C–S bond length of 1.68 Å, which is between that of a conventional C–S bond (1.81 Å) and a C=S bond (1.56 Å) (referring to an isolated C=S bond and not a thiourea).[6] In addition, infrared studies of thiourea versus thiourea-metal complexes indicated appreciable $^{+}$N=C–S character from shifts in the absorption peaks with N–C–N antisymmetric stretch towards higher frequency and C=S stretch towards lower frequency in the complexes.[7] These results imply that the sulfur of the NHT could coordinate well to electron deficient atoms. The zwitterionic nature of NHTs and NHSe is depicted in Figure 5.1. Comparing thiourea to NHT, the latter is expected to have a greater zwitterionic contribution due to the aromatic stabilization of that resonance contributor.

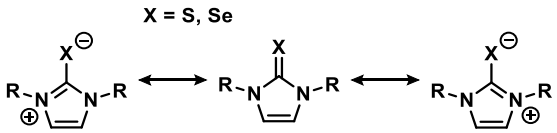

Figure 5.1. Zwitterionic resonance contributors of a generic NHT/NHSe.

Song et al. demonstrated the electron-donating effects of thioureas through density functional calculations (Figure 5.2).[8] They showed that the nitrogen atoms in thiourea donate electrons to the sulfur atom, which increases the HOMO (p) and HOMO-1 (π) energy levels compared to those in thioformaldehyde. Upon coordination of the thiourea to the metal with the HOMO, the HOMO-1 interacts favorably with the metal d orbital and leads to an increase in d–π back donation between the metal and ligand C=S π*. Therefore, thioureas demonstrated electron-donating properties. As indicated earlier by the zwitterionic nature of NHT/NHSe, the electrostatic potential map also supports the presence of higher negative charge density on the sulfur due to the nitrogen atom donation than without Figure 5.2. Note that thioacetone would have been a more fair comparison in place of thioformaldehyde.

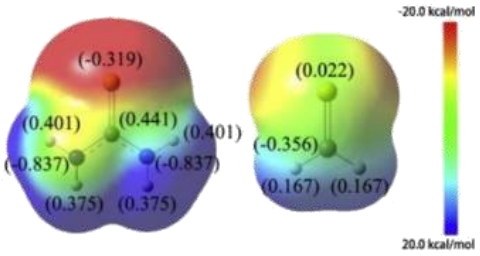

Figure 5.2. Electrostatic potential and total natural population analysis charge of thiourea (left) and thioformaldehyde (right) calculated by the RHF method using the cc-pVTZ basis set. Reprinted with permission from ref.[8]. Copyright 2014 Elsevier.

Furthermore, the stronger electron-donating nature of the thiourea unit in comparison with sulfide and higher polarizability in comparison with oxygen enables the thiourea to be make more stable bonds with gold. Therefore, these units may be thiol alternatives when used as a surface modifier.

5.1.2 N-Heterocyclic Thiones and Selones

NHTs and NHSes have been utilized to stabilize metal complexes,[9-11] nanoparticles,[12-15] and nanocrystals.[16] These ligands serve to control the reactivity and physical properties, among others, of the complexes. In addition, the coordination of NHSe variants on gold(I) species,[17] and catalysis by NHT ligands, including structures that are included in this thesis, have been studied in detail.[14, 18-20]

As mentioned earlier, the preferential binding coordination of NHTs/NHSes are through the S/Se atoms and examples of crystal structures of ligands coordinated to gold atoms are shown in Figure 5.3.[11, 17]

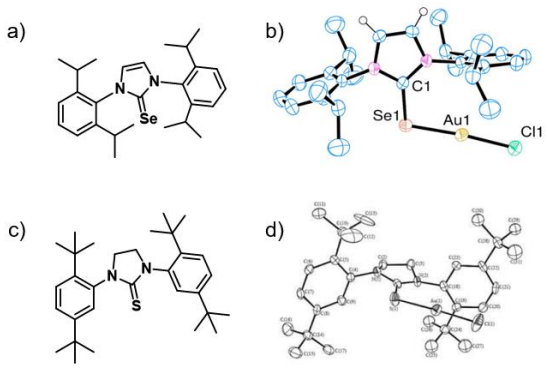

Figure 5.3. Structure and X-ray crystal structures with 50% probability thermal ellipsoids of Se(IPr) (a) Au–Se(IPr) –Cl complex (b), S(*t*Bu) (c), and Au–S(*t*Bu) –Cl complex (d). Most H atoms are excluded for clarity. Se(IPr) refers to 1,3-bis(2,6-diisopropylphenyl)-1,3-dihydro-2H-imidazole-2-selenone and S(tBu) refers to 1,3-bis(2,5-di-tert-butylphenyl)imidazolidine-2-thione. Crystal structures are reprinted with permission from ref.[11, 17]. Copyright 2014 American Chemical Society and copyright 2015 Royal Society of Chemistry.

Pan et al. reports the Au–S–C bond angle to be 111.70° upon coordination, which demonstrates that if these ligands were bound on the surface, they would not be upright but most likely be tilted in this manner.[11]

N-heterocyclic thiones and selones have been primarily studied in coordination and inorganic chemistry and have not been explored in materials chemistry in respect to deposition on planar surfaces. They have demonstrated the ability to coordinate to metal atoms such as Au and Cu, and theoretical calculations show higher electron density on the S (results can most likely be translated to Se as well). Due to these factors, we wanted to study the ability of NHT and NHSe to bind to planar gold and explore the modified-surface properties to determine whether these classes of compounds would be interesting head groups and whether the work function (WF) of the modified-surface would be reduced and to what extent under various conditions.

5.2 Selection of NHTs and NHSes

NHTs and NHSes with typical bulky side groups of diisopropylphenyl and mesityl and a small methyl group (one example for NHT) were synthesized by Abraham Jordan of the Joseph Sadighi group and members of Daniel Rabinovich group at UNC Charlotte, and are shown in Figure 5.4.

In this study, we wanted to compare the effect of the side groups (Dipp, Mes, and Me) and the effect of the head group (sulfur and selenium) on the surface coverage of the deposited films and the effect of the work function of the surface of gold. Although the bulky side groups would, all else being equal, reduce the relative density of coverage compared to a compound with a small side group, as in the case of the NHCs (CHAPTER 3) the density of coverage may or may not affect the relative change in work function.

Despite Dipp (1,3-bis(2,6-diisopropylphenyl) and Mes (mesityl) both being bulky groups, they may have different dihedral angles with the core upon binding to the surface, which could affect the packing as well. Therefore, these compounds were selected for study.

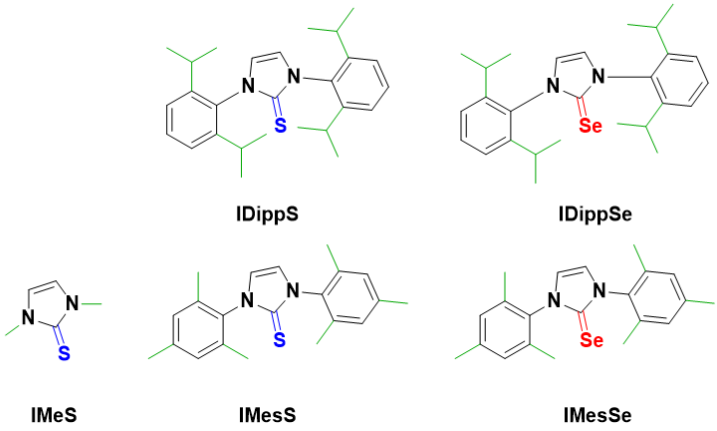

Figure 5.4. Structures of the N-heterocyclic thiones and selones under study. Atoms and bonds were colored to highlight the differences between the compounds.

5.2.1 Calculated Dipole Moments

To determine the dipole moment vectors of each of the NHTs and NHSes in their ground-state conformations, DFT calculations with B3LYP/6-31G** were performed. The sign of the dipole is indicated as positive when it is in the direction of the surface and negative when away from the surface. Although there is a slight tilt of the dipole moment vector in IMeS with respect to the central axis (along the C=S bond), the values were not corrected for this tilt and they are compared as is. In addition, despite the expected binding mode of the compounds to be tilted towards the surface in ~110° as reported by Pan et al.[11] for ligand-Au complexes, because calculations of the optimized geometry of the compounds on the surface were not carried out, the dipole moments were not corrected for

this tilt either. Depending on the bulkiness of the side groups however, the distance and angle of binding would differ between a metal atom and metal surface, with the latter inducing relatively limited flexibility. These values, however, can still provide a sense of direction and magnitude of electron density and resulting dipole on the surface. It is expected that positive dipole moments (negative dipole towards surface) should lead to a decrease in the work function.

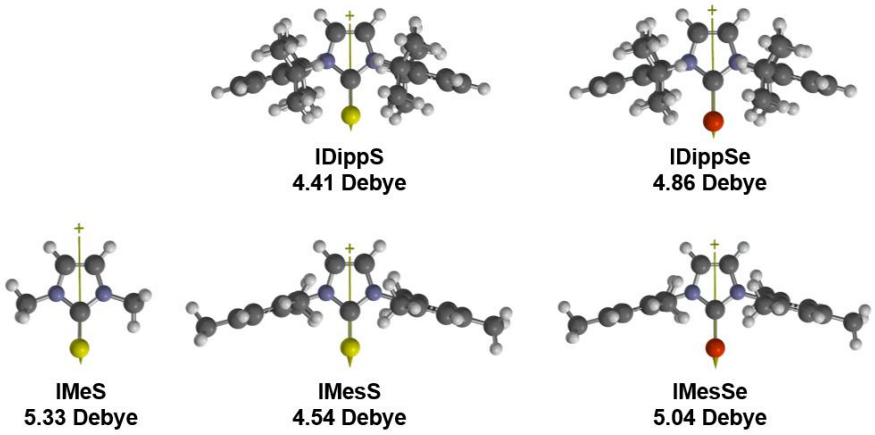

Figure 5.5. Calculated dipole moments for NHT and NHSe compounds. The projected dipole is depicted by the arrowhead from the positive to negative direction, but the value is given a positive sign to indicate that in this orientation, the negative dipole is pointing towards the surface.

According to the results, the smallest, IMeS has the largest dipole moment among all the compounds (5.33 D) and IDippS has the smallest (4.41 D). Depending on the binding orientation on the surface however, as mentioned earlier, these may not be the final dipoles normal to the surface, not to mention to the contribution from the bond dipole. However, when comparing IDippS and IDippSe, the selenium compound has a slightly larger dipole moment (by 0.45 D) and the same trend for the IMesS and IMesSe is evident with an increase of 0.50 D when replacing the sulfur for selenium. Since in these sets, the

side groups are the same, the differences in binding (distance to the surface or orientation), if any, would occur depending on the head group, sulfur versus selenium.

To draw more meaning from these values however, the effective dipole moment normal to the surface and the optimized geometry upon binding need to be calculated. However, without these prerequisites, the footprints of the compounds were unable to be estimated and subsequent coverage in terms of percent monolayer were not attained. In place of this metric, thickness measurements and element ratios were utilized instead.

5.3 Analysis of Modified Au Surfaces

The main studies in this chapter focus on determining the coverage in terms of thickness of modified surfaces under different conditions and the subsequent work function modification. The details to the determination of thickness is described in 2.4.4. The assumptions in these calculations are that for the overlayer, the IMFP is 3 nm and density is 1 g/cm^{-3}. Note that if the actual density (or IMFP) is larger than this assumption, then the computed thicknesses in this study have been overestimated (underestimated) and vice versa. The known values used for gold are IMFP of 2.02 nm, density of 19.32 g/cm^{-3}, and MW 196.97 amu.

Two methods were utilized to deposit the surface modifiers. In the first section, the results from spin coated substrates will be presented, followed by the results from immersed substrates in terms of thicknesses and work function modification.

5.3.1 Coverage Analysis of NHTs and NHSes from Spin coating

5.3.1.1 Data Processing Note

Peak areas were corrected with the respective relative sensitivity factors to scale the measured intensities and account for the different ionization cross-sections. The core

levels with high ionization cross-sections were used to quantify the presence of modifier relative to surface (Au 4f, S 2p, Se 3p, N 1s). Au 4f has a high cross-section and strong signal intensity in XPS. Therefore, taking background subtractions is straightforward because of the high signal/noise (S/N) ratio. On the other hand, nitrogen, sulfur, and selenium have similar and lower cross-sections and resulting weaker signal intensities. Thus, adjusting the background binding energy (BE) range by a few tenths of a eV can lead to drastic changes in corrected peak areas depending on the noise.

Consequently, the ratio of the head group (sulfur or selenium) to nitrogen was used as a metric to determine the accuracy of the background subtraction relative to S/Se and N. The expected ratio is 1N/2S or Se (0.5) for all compounds in this chapter. While this metric can help align the peak intensities within a compound, one must be careful to not over/underestimate both N and S/Se together, which would over/underestimate the amount of modifier present. In certain cases, the S 2p or Se 3p signals were indistinguishable from noise (due to low coverage) and the ratios containing these elements were omitted from the table. In these situations, the backgrounds for these N 1s signals were unable to be cross-checked with the ones from S 2p or Se 3p, but care was taken to apply the same overall background across modified-surfaces.

5.3.1.2 Optimization

To optimize the conditions used to deposit the surface modifiers on planar gold, two different concentrations were used with the mesityl substituted IMesS and IMesSe and methyl substituted IMeS. Tetrahydrofuran (THF) was selected as the solvent due to the good solubility of the compounds and two extremes of dilute and concentrated solutions were made (2 mM and 10 mM). The surfaces were modified according to the experimental

and not rinsed or washed post modification. The coverage results of these conditions measured by XPS are recorded in Table 5.1 and representative peaks from each of the modified-surfaces are presented in Figure 5.6 and Figure 5.7.

Table 5.1. Elemental ratios and thicknesses found by XPS of IMesS and IMesSe modified gold surfaces from spin coating in THF solutions.

Compound (conc. in THF)	[S or Se/N][b]	[N/Au][b]	[S or Se/Au][b]	Thickness (nm)[b]
IMeS (2 mM)	0.48 ± 0.01	0.33 ± 0.03	0.16 ± 0.01	2.6 ± 0.1
IMesS (2 mM)	0.50 ± 0.02	0.09 ± 0.00	0.05 ± 0.00	2.1 ± 0.1
IMesSe (2 mM)	—[a]	0.21 ± 0.01	—[a]	3.9 ± 0.1
IMesS (10 mM)	0.49 ± 0.00	0.57 ± 0.11	0.28 ± 0.05	5.9 ± 0.5
IMesSe (10 mM)	0.50 ± 0.00	0.40 ± 0.05	0.20 ± 0.03	5.4 ± 0.3

[a] The Se 3d region was measured and did not provide quantifiable signal.
[b] All standard deviations represent sample to sample variations.

Films deposited from 2 mM solutions gave thinner thicknesses (< 4 nm) than the ones from 10 mM solutions (> 5 nm), but they all led to quantifiable amounts of surface modifier on the surface from these treatment conditions (Table 5.1). This indicates that a concentration of 2 mM is sufficient to provide at least a monolayer, assuming uniform coverage. The spot to spot variations (not listed) and sample to sample variations are within a few angstroms in terms of thickness. Therefore, the uniformity across the sample is assumed to be good by XPS, but may be rougher at a smaller length scale given that the spot size for XPS is 400 μm.

The issues stated above with ionization cross-section is evident in Figure 5.6 with the best signals from the Au 4f core levels and similarly poor signals from the N 1s and S 2p core levels. By calibrating with the Au 4f peak, shifts in the N 1s peaks are evident among the different compounds, with N 1s for IMeS at 402.1 eV, IMesS at 400.5 eV, and

IMesSe at 401.2 eV (Figure 5.6b,e,h). The high N 1s BE of 402 eV is usually reported for species that are protonated such as ammonium and protonated free amines can range from 400.9–401.7 eV.[21-22] Thus, it is evident that there is strong iminium character for the nitrogens in each compound.

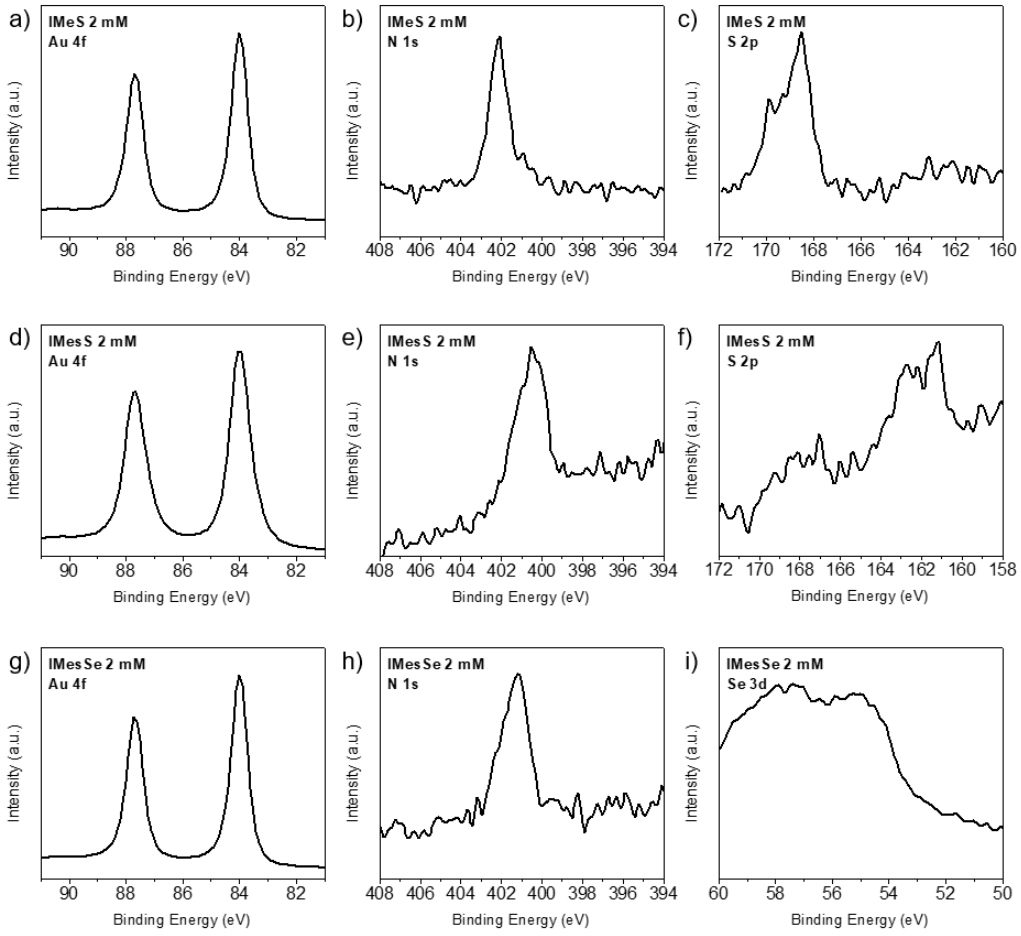

Figure 5.6. Representative XPS spectra of Au 4f, N 1s, and S 2p from the modified-surfaces by spin coating from 2 mM solutions in THF with IMeS (a–c), IMesS 2 mM (d–f), IMesSe (g–i). The core energy levels are indicated on each plot.

Compared to N-heterocyclic carbenes (NHCs) discussed in CHAPTER 2, which had N 1s peaks at ca. 401 eV, the one for IMeS was slightly higher, IMesS was slightly

lower, and IMesSe was similar. The reason why the N 1s in IMesS was so much lower may be because when the NHT has perpendicular aryl groups, the repulsion between the aryl and S is reported to increase the C(S)–N bond length. This would result in slightly higher electron density retained on the nitrogen atoms in IMesS compared with IMeS where this repulsion is not present.[8]

It is known that the S 2p BE of alkane thiols on gold decreases from 163.5 eV (unbound) to 162 eV (bound).[23-25] A shift in this direction, lower BE, indicates that there is more electron density on the sulfur upon loss of a hydrogen atom and coordination to gold. Another group compared the S 2p BE for bound alkane thiols versus thioureas (to gold) and found that the latter had lower BE at 160.9 eV compared to bound thiol (162.3 eV).[26] According to a study by Srinivasan et al. of thioureas coordinated to Co, Ni, and Cu complexes, the S 2p of uncoordinated thiourea was measured to be 162.4 eV and upon coordination to the various metals all shifted to higher BEs by 0.3 to 0.6 eV.[27] It is evident that the typical S 2p BEs for thiols and thioureas are in the lower 160 eV range. The types of sulfur that exhibit S 2p BEs in the upper 160 eV range are sulfoxides (S=O) and sulfones (O=S=O), when the sulfur is at a higher oxidation state.

The S 2p peaks in Figure 5.6c,f between the methyl and mesityl NHT compounds are drastically different. Whereas IMeS has a peak maximum at 168.5 eV, IMesS has one at 161.2 eV and a smaller one at 167.0 eV. When comparing with the spectrum of S 2p in a thicker film of IMesS (Figure 5.7c), there is only one main component at 162.0 eV. In addition, thiols and thioureas typically have S 2p peaks around 162 eV as mentioned earlier. Therefore, the higher BE component found in IMesS in a thinner film may be from new interactions with the gold surface (though the shift of 5 eV is very significant) or may

be a residue of contamination from IMeS. The high BE of IMeS however cannot be explained. It is possible that the compound may have oxidized to a higher order sulfur oxidation species, whose S 2p peaks by XPS do appear in this region. However, this was not further investigated.

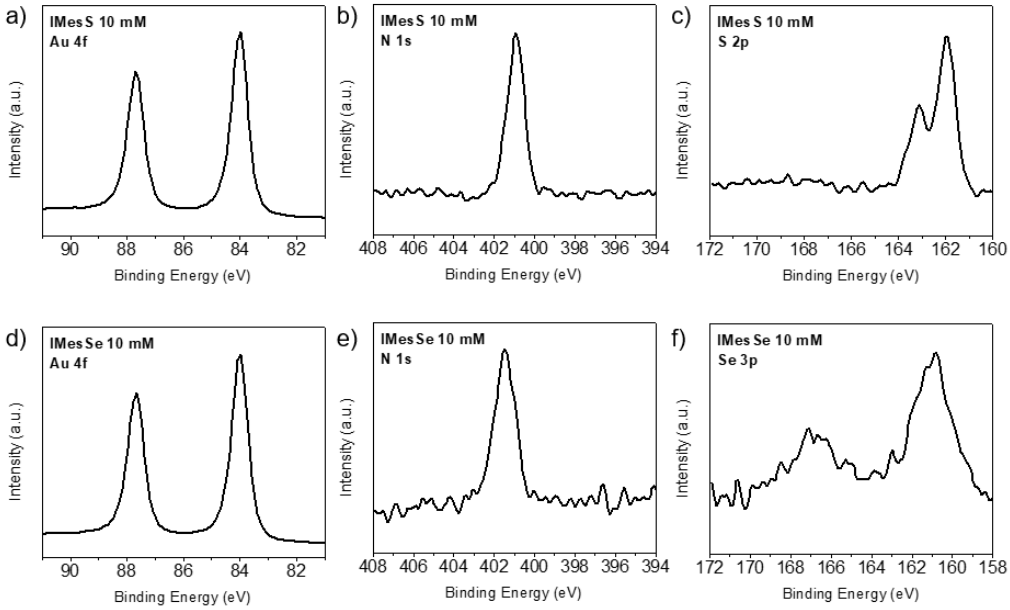

Figure 5.7. Representative XPS spectra of Au 4f, N 1s, Se 3p, and Se 3d from the modified-surfaces by spin coating from 10 mM solutions in THF with IMesS (a–c), IMesSe (d–f). The core energy levels are indicated on each graph.

As for selenium, no appropriate reference peaks can be found in the literature but the peaks (peak splitting) exhibited in Figure 5.7f are in the correct range for Se 3p and are similar to the peaks from elemental Se.[28] The two peaks (160.8 eV and 167.1 eV) correspond to the peak splitting of Se $3p_{3/2}$ and Se $3p_{1/2}$, respectively and were evaluated together as one Se 3p peak for quantification.

According to Table 5.1, as expected, the films deposited from more concentrated solutions gave rise to larger thicknesses. However, these thicknesses are above what would

be typically ideal for “thin” films. Therefore, for the next optimization test, 2 mM solutions were used and a different solvent, methanol, was tested to determine which was a better solvent and whether solvent plays a role in film formation.

The coverage results of these conditions measured by XPS are recorded in Table 5.2 and representative peaks from each of the modified-surfaces are presented in Figure 5.8 and Figure 5.9. When comparing the sulfur containing compounds, IMeS had two sets of peaks at 168.1 eV and 162.4 eV. Unlike the case for Se 3p, these do not correspond to spin-orbit peak splitting, but to different chemical environments. Nonetheless, the strongest peak corresponds to the higher BE one, which is the same as previous (Figure 5.6c) and the lower BE one may be insignificant. No conclusions can be reached at this point.

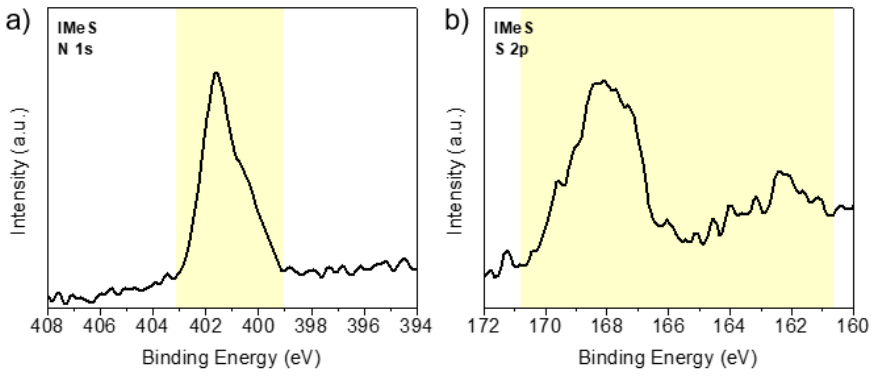

Figure 5.8. Representative XPS spectra of N 1s and S 2p from the modified-surfaces by spin coating from 2 mM solutions in methanol with IMeS (a, b).

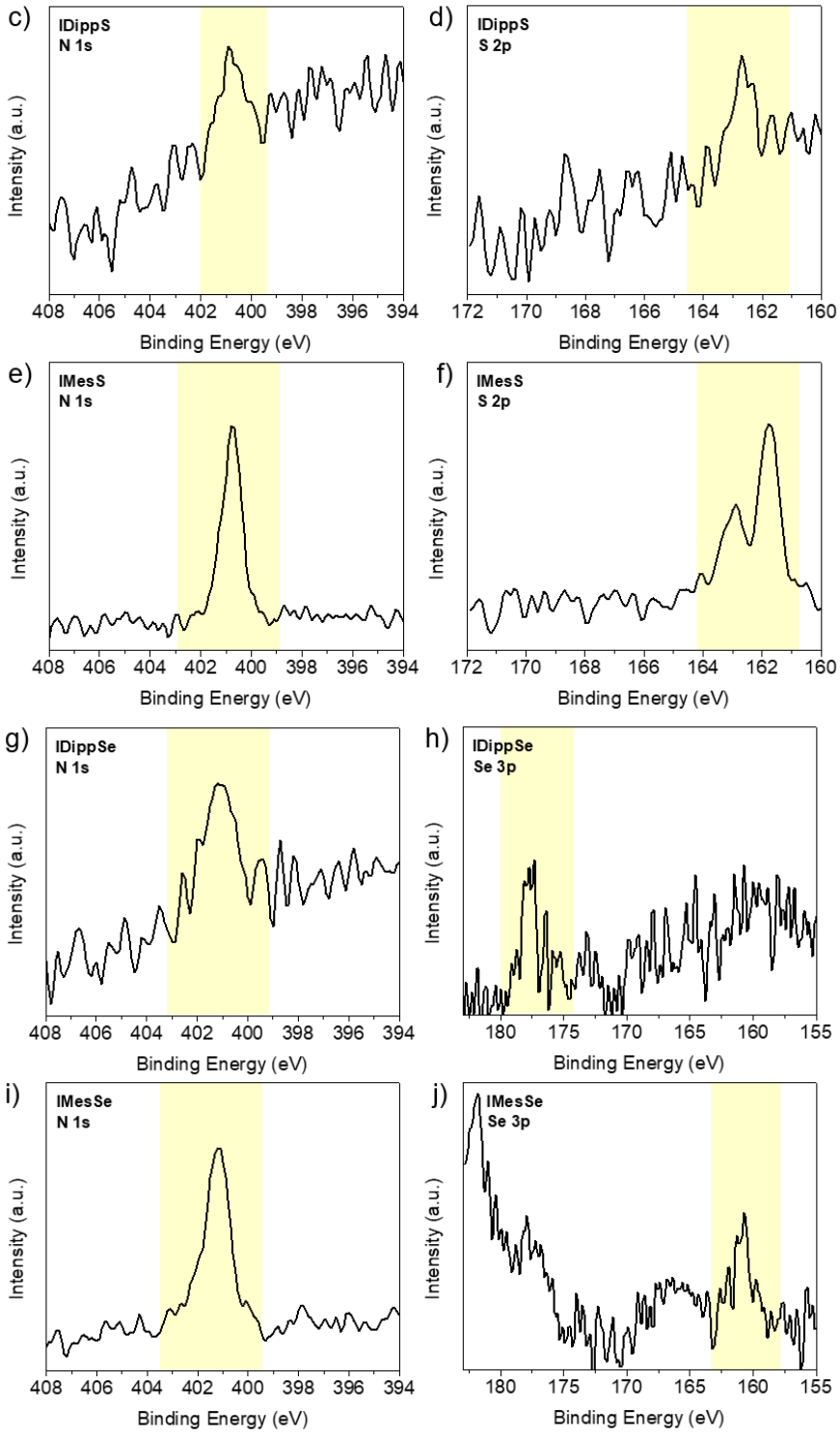

Figure 5.9. Representative XPS spectra of N 1s, S 2p, and Se 3p from the modified-surfaces by spin coating from 2 mM solutions in methanol with IDippS (c, d), IMesS (e, f), IDippSe (g, h), IMesSe (i, j). The core energy levels are indicated on each graph and regions indicating the peak area boundaries are highlighted in yellow.

Table 5.2. Elemental ratios and thicknesses found by XPS of NHT and NHSe modified gold surfaces from spin coating in 2 mM methanol solutions.

Compound (2 mM in MeOH)	[S or Se/N][a]	[N/Au] [a]	[S or Se/Au] [a]	Thickness (nm)
IMeS	0.44	0.36	0.16	2.8 ± 0.1
IDippS	0.50	0.02	0.01	0.7 ± 0.0
IMesS	0.49	0.11	0.05	2.3 ± 0.4
IDippSe	0.49	0.06	0.03	1.9 ± 0.3
IMesSe	0.48	0.18	0.09	3.7 ± 0.4

[a] All standard deviation (sample to sample variation) were within 0.1 eV.

According to Table 5.2, both the mesityl compounds (IMesS and IMesSe) gave higher N/Au ratios than the Dipp compounds (IDippS and IDippSe) under the same spin coating conditions. This may be a result of the differences in bulk between Mes and Dipp. The Dipp compounds are relatively bulkier around the head group than are the Mes compounds (Figure 5.10).

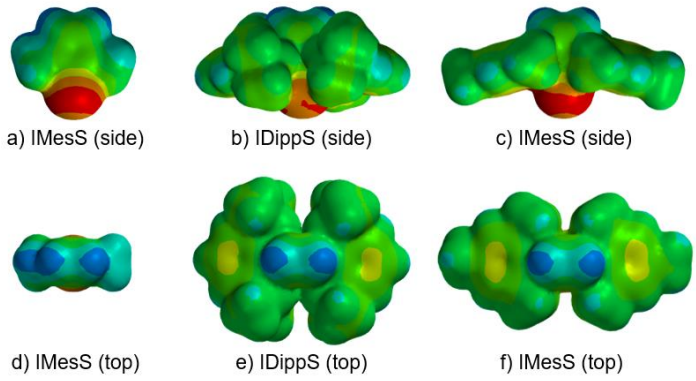

Figure 5.10. Electrostatic charge density surfaces for the NHTs with side (a–c) and top (d–f) views. These were produced from the same calculations in 5.2.1. Red represents negative charge density and blue represents positive charge density with the exact magnitude not quantified in the image.

Therefore, these N/Au ratio differences may be an indication of the ability of the compounds to form multilayers. Without the need to consider the mode of binding of the

first monolayer, the more accessible dipoles from the less hindered Mes compounds may enable multilayer formation better than the Dipp compounds can. As mentioned in 5.2.1, having footprint calculations and insight into how the compounds are laying on the surface would aid in the interpretation of these data.

Since comparing results among samples with different coverages is scientifically irrelevant, monolayers were attempted to be formed from the next set of experiments.

5.3.2 Coverage Analysis of NHTs and NHSes from Immersion

5.3.2.1 Optimization

Forming monolayers involves immersing a substrate into a solution for a given amount of time, followed by rinsing to ensure the removal of physisorbed material. IMesSe was diluted in methanol to perform the following tests involving changing the time of immersion and type of washing condition.

Methanolic solutions of 2 mM IMesSe were prepared and clean gold surfaces were immersed for 1 min and 1 h to determine the appropriate length of time for film formation, followed by the same rinsing procedure (triple rinse described in 5.5.2) (Table 5.3). Although again due to the lack of estimated footprints, the N/Au ratio that indicates a monolayer was unknown, the N/Au ratio doubled from 1 min immersion to 1 h immersion. The same substrates that were measured from immersion for 1 h were stored for one week in ambient conditions and sonicated in fresh methanol for 3 minutes prior to remeasuring. The N/Au ratio of these substrates were reduced to the same amount as for the 1 min immersed samples. Therefore, an immersion time of 1 min was deemed sufficient over 1 h and sonication is more reliable to remove excess modifiers.

Table 5.3. Elemental ratios and thicknesses found by XPS of IMesSe modified gold surfaces from immersion in 2 mM methanol solutions for different times followed by washing.

Compound-#	Modification condition	[N/Au][a]	Thickness (nm)[a]
IMesSe-1	Immerse 1 min 2 mM MeOH; triple rinse	0.03 ± 0.01	0.8 ± 0.2
IMesSe-2	Immerse 1 h 2 mM MeOH; triple rinse	0.05 ± 0.02	1.8 ± 0.3
IMesSe-3	Store "IMesSe-2" substrates 1 week Sonicate 3 min and remeasure	0.03 ± 0.00	1.0 ± 0.0

[a] All standard deviations represent sample to sample variations.

However, it must be noted that 1 min or 1 h may not have been sufficient time to form robust monolayers and an elongated annealing time at elevated temperatures may have been necessary. Therefore, the optimization procedure has room for improvement and using spectroscopic techniques to image the surface to verify monolayers would provide an added measure of confidence for future studies.

5.3.2.2 Thin Layer Formation

From the previous tests, both methanol and THF as solvents gave rise to films from spin coating. However, all compounds were more soluble in THF than in methanol, which was observed during the solution making process. Therefore, the best conditions from the current optimization data in terms of thin layer formation were immersion for 1 min in 2 mM followed by 1 min sonication. Modified substrates from each of the five NHT and NHSes were prepared as such and the coverage results of these conditions measured by XPS are recorded in Table 5.4 and representative peaks from each of the modified-surfaces are presented in Figure 5.11. The S 2p signals in all modified substrates, except for IMeS-modified Au suffered from poor signal:noise. Therefore, the resulting S/N ratios were unable to be used as a metric, though they are listed in Table 5.4.

Table 5.4. Elemental ratios and thicknesses found by XPS of NHT and NHSe modified gold surfaces from immersion in 2 mM THF solutions for 1 min followed by sonication for 1 min.

Compound (2 mM in THF)	[S/N]	[N/Au]	[S/Au]	Thickness (nm)
IMeS	0.42 ± 0.04	0.22 ± 0.07	0.09 ± 0.02	2.0 ± 0.5
IDippS	0.42 ±0.06	0.02 ± 0.00	0.01 ± 0.00	0.9 ± 0.1
IMesS	0.48 ±0.02	0.02 ± 0.00	0.01 ± 0.00	0.5 ± 0.0
IDippSe	0.26 ± 0.11	0.02 ± 0.01	0.00 ± 0.00	0.8 ± 0.2
IMesSe	0.36 ± 0.11	0.02 ± 0.00	0.01 ± 0.00	0.7 ± 0.1

The bulky modifiers all had N/Au ratios of 0.02 and thicknesses below 1 nm. Although this ratio is much smaller than observed previously for the spin coated substrates, this may be an indication of a monolayer formation. IMeS, the least bulky modifier of the set, had a much higher N/Au ratio of 0.22 and a thickness at least twice as large as the others. According to the thickness however, more than a monolayer may have formed. Given that this compound regardless of binding mode would still have the smallest footprint, it should also correlate with the highest packing density, which we observe here. The plots in Figure 5.11 have been background subtracted to eliminate the slope and to accentuate the observed peaks. The N 1s peak for IMeS is prominent while the ones for the other compounds are similar in shape and intensity. As observed in the other substrates modified with IMeS, the N 1s peak is asymmetric with indication of at least another peak component at slightly lower BE. The identity of these peak components has not been further probed.

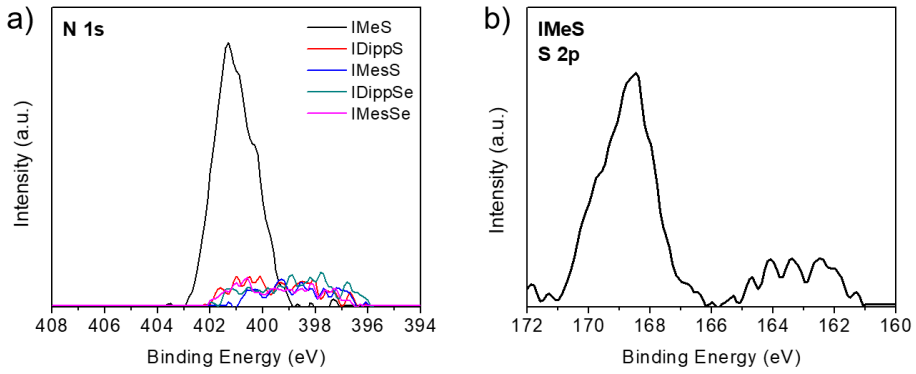

Figure 5.11. Representative XPS spectra of N 1s, S 2p, and Se 3p from the modified-surfaces by immersion from 2 mM solutions in THF, followed by sonication, with IMeS (a, b), IDippS (c, d), IMesS (e, f), IDippSe (g,h), IMesSe (i, j). The core energy levels are indicated on each graph. These spectra were background subtracted.

Several conditions were utilized to determine the thickness of films formed under spin coating and by immersion. The ability of NHT and NHSe compounds to form films that are quantifiable by XPS has been demonstrated in this section. The effect of the modifiers to the work function will be discussed next.

5.3.3 Workfunction Modification of Au with NHT/NHSe

5.3.3.1 Experimental UPS Results

All the WF values obtained in this section were from the same substrates that were used to quantify the amount of modifier on the surface. A table summarizing the results is shown in Table 5.5 ordered by compound. To better visualize the effect of the change in WF per compound, the WF was plotted against the thicknesses listed in the tables in previous sections (Figure 5.12). In general, thicker films gave rise to lower WF among all compounds, and within the same compound, as there is negative slope from a linear regression of the data points.

Table 5.5. Work function modification of planar gold surfaces with NHTs and NHSes measured by UPS.

Compound	Modification type	Conc. solvent	Wash	WF (eV)
OP gold	n/a	n/a	n/a	5.07 ± 0.13
IMethylS	Spin coat	2 mM THF	None	3.64 ± 0.04
IMethylS	Immerse	2 mM THF	Sonication	4.24 ± 0.05
IDippS	Spin coat	2 mM MeOH	None	4.02 ± 0.02
IDippS	Immerse	2 mM THF	Sonication	4.50 ± 0.08
IMesS	Spin coat	10 mM THF	None	3.82 ± 0.09
IMesS	Spin coat	2 mM MeOH	None	4.05 ± 0.02
IMesS	Immerse	2 mM THF	Sonication	4.78 ± 0.01
IDippSe	Spin coat	2 mM MeOH	None	3.86 ± 0.05
IDippSe	Immerse	2 mM THF	Sonication	4.69 ± 0.09
IMesSe	Spin coat	2 mM THF	None	3.76 ± 0.12
IMesSe	Spin coat	10 mM THF	None	3.79 ± 0.11
IMesSe	Spin coat	2 mM MeOH	None	3.79 ± 0.04
IMesSe	Immerse 1 h	2 mM MeOH	Triple rinse	4.07 ± 0.11
IMesSe	Immerse	2 mM MeOH	Triple rinse	4.29 ± 0.01
IMesSe	Immerse	2 mM THF	Sonication	4.61 ± 0.07

[a] The durations imply 1 min for immersion and 1 min for sonication unless otherwise listed.

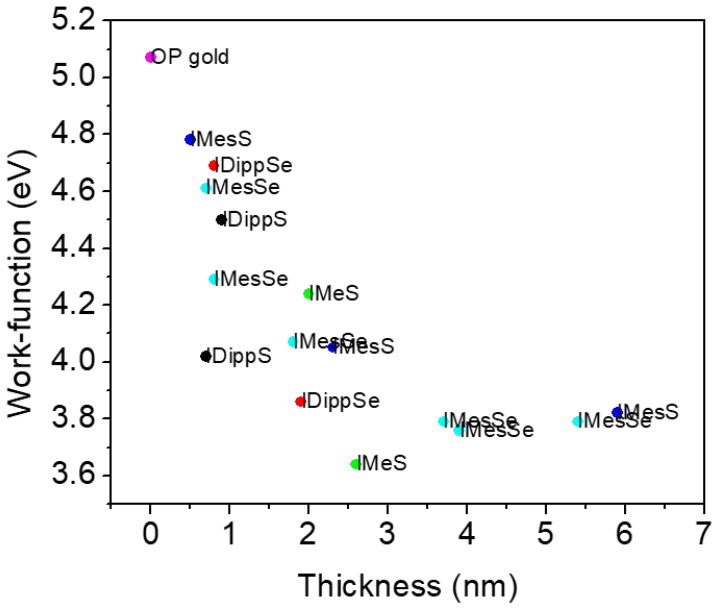

Figure 5.12. Plot of work function (by UPS) versus thickness of all the NHTs and NHSes. The data points are color coded by compound with OP gold (magenta), IMeS (green), IDippS (black), IMesSe (turquoise), IDippSe (red).

The lowest WFs were obtained for the spin coated substrates, which also had the highest N/Au ratios. This implies that even though there may be multilayers of surface modifier present, the dipoles are collectively in the direction that lowers the WF of gold. IMeS had the lowest WF at 3.64 eV and thickness of 2.6 nm. IDippSe, IMesSe, and IMesS also could reach low WFs from 2–6 nm thick films.

Per unit area, assuming close packing, there should be more IMeS than any of the other compounds, meaning IMeS most likely has a higher packing density (cmpd/unit area) than the others. This means that for films of the same thickness, IMeS would be more densely packed than IMesS. Taking the data points for IMeS at 2.6 nm and IMesS at 2.3 nm for example, if the WFs were the same, then this would imply that IMesS is more WF reducing per molecule than IMeS. However, the data show that this relation does not hold for these data points because the WF for the IMeS deposited film was measured to be 3.64 eV and the one for IMesS to be 4.05 eV. This may imply the opposite, that IMeS is more reducing than IMesS or that they may be similar.

The thinner films processed from immersion had higher WFs, some of which did not differ much from oxygen plasma (OP) treated gold. For these films the WFs were similar for the bulky compounds and within 0.2 eV. IMeS, which had the thickest film from this condition as mentioned in the previous section, also had the lowest WF at 4.24 eV. Whether this thickness is an overestimation, referring to the assumptions in 5.3, or whether the 1 min sonication was not sufficient to strip the surface of physisorbed modifier is not known at this point and would require modeling (to determine the footprint and associated monolayer coverage) in conjunction with further washing tests (longer durations) to determine if there are multilayers.

In terms of the differences between the headgroups, sulfur and selenium, no conclusions can be drawn from the work function data. Although the selenium compounds have a larger dipole moment than the sulfur compounds (except for IMeS), the correlation with the work function and thickness is unclear from these data. For the mesityl compounds however, at the lower thickness regime (0.5–0.8 nm), the IMesSe modified surface had a lower WF (4.29 eV) than the IMesS modified (4.78 eV). Thus, this may be the result of the dipole moment difference with IMesSe having a larger dipole moment at 5.04 D than IMesS at 4.54 D. This molecular dipole however, is only one of the dipole contributions to the overall change in work function and the bond dipole from covalent bond linkage between the sulfur/selenium to Au would need to be evaluated to provide a more complete story of the factors leading to the overall WF change.

5.4 Conclusions

In this chapter, five different N-heterocyclic thiones and selones were examined as surface modifiers to gold. Three of the compounds had sulfur as the head group and two of them had selenium. For the side groups, methyl, mesityl, and Dipp were examined. We hypothesized that the surface modifier that was able to bind to the surface in an orientation that allowed for the greatest effective dipole would lead to the greatest reduction in WF.

Films of varying thicknesses, not exceeding 6 nm were processed by solution immersion and spin coating techniques. Spin coating provided films of greater thicknesses than solution immersed films, implying the formation of multilayers in the former condition. The work function of the modified substrates were lower for thicker films than for thinner films. The differences between the Dipp and Mes side groups were evident in the spin coated films with the Mes compounds achieving thicker films under the same

concentration as Dipp. This gave an implication that although from a top view the Dipp compounds may constitute a larger area than the Mes compounds, the crowding of the head group in the Dipp compounds may be a barrier to achieving proximity to the surface, which could affect the surface dipole.

The significantly higher S 2p BE for IMeS compared with IMesS, with IMeS having values typical for more oxidized sulfur, is an interesting result worth exploring. The XPS peaks were quantified but were not deconvoluted for components, which could help determine the binding mode on the surface. Overall, the NHT and NHSe could reduce the work function of gold and demonstrated robustness to the surface based on their presence post-sonication. They may be useful head groups for surface modifiers if the bulkiness of the side groups were reduced.

5.5 Experimental

5.5.1 Materials

1,3-bis(2,6-diisopropylphenyl)-1,3-dihydro-2H-imidazole-2-thione (IDippS), 1,3-dimesityl-1,3-dihydro-2H-imidazole-2-thione (IMesS), 1,3-bis(2,6-diisopropylphenyl)-1,3-dihydro-2H-imidazole-2-selenone (IDippSe), 1,3-dimesityl-1,3-dihydro-2H-imidazole-2-selenone (IMesSe), and 1,3-dimethyl-1,3-dihydro-2H-imidazole-2-thione (IMeS) are all white solids and were synthesized by Abraham Jordan of the Joseph Sadighi group at Georgia Tech and by the Daniel Rabinovich group at UNC Charlotte and donated for study.

5.5.2 Au Surface Cleaning and Modification

Commercially available glass:Ti:Au slides (EMF Corp., Ithaca, NY, USA) were cut into 0.5 in. × 0.5 in. squares and sonicated in ethanol for 10 min, dried under a flow of

nitrogen, and etched with oxygen plasma (OP) with a PE-50 XL Plasma System for 5 min prior to any additional surface treatment. Substrates were modified by either spin coating freshly prepared solutions (2 or 10 mM) of NHT/NHSe in dry tetrahydrofuran or methanol at 3000 rpm, 1100 acceleration, for 30 sec or immersing for 1 min–1 h followed by washing in fresh solvent by triple rinse (successive rinsing and drying substrate three times) or sonication (1–3 min) and annealing at 70 °C for 10 min. Samples were immediately taken for X-ray photoelectron spectroscopy/ultraviolet photoelectron spectroscopy (XPS/UPS) analysis.

5.5.3 Surface Characterization

5.5.3.1 UPS and XPS

All UPS measurements were conducted in a Kratos Axis Ultra XPS with an average base pressure of 10^{-8} Torr. UPS spectra were collected prior to XPS spectra with a 21.2 eV He (I) excitation and a pass energy of 5 eV using a 27 μm spot size. All XPS measurements were conducted in either a Kratos Axis Ultra XPS or a Thermo K-Alpha XPS with an average base pressure of 10^{-8} Torr. XPS spectra were collected with a monochromatic Al Kα source using a 400 μm spot size and a pass energy of 160 eV (200 eV) for survey acquisition and 20 eV (50 eV) for high-resolution spectra (parenthesis refers to Thermo K-Alpha conditions). XPS was performed with a normal takeoff angle (0°) and the samples were flooded with low energy electrons using the flood gun to compensate for surface charging. Data were analyzed using CasaXPS processing software. The binding energies of all XPS spectra were calibrated to the Au 4f line at 84.0 eV and processed with a Shirley background subtraction and Savitzky-Golay smoothing unless otherwise stated. All UPS

and XPS data points represent multiple samples scanned on multiple spots; the standard deviation reported reflects variation among different samples.

5.6 References

[1] Rosenheim, A.; Loewenstamm, W., Über Die Thiocarbamidverbindungen Einwertiger Metallsalze. *Z. Anorg. Chem.* **1903,** *34* (1), 62-81.

[2] Raper, E. S., Complexes of Heterocyclic Thionates. Part 1. Complexes of Monodentate and Chelating Ligands. *Coord. Chem. Rev.* **1996,** *153*, 199-255.

[3] Akrivos, P. D., Recent Studies in the Coordination Chemistry of Heterocyclic Thiones and Thionates. *Coord. Chem. Rev.* **2001,** *213* (1), 181-210.

[4] Spicer, M. D.; Reglinski, J., Soft Scorpionate Ligands Based on Imidazole-2-Thione Donors. *Eur. J. Inorg. Chem.* **2009,** *2009* (12), 1553-1574.

[5] Bernard, M.; Delbecq, F.; Fache, F.; Sautet, P.; Lemaire, M., Dithiourea Ligands in the Rhodium-Catalyzed Hydride-Transfer Reduction of Ketones − a Theoretical and Experimental Approach. *Eur. J. Org. Chem.* **2001,** *2001* (8), 1589-1596.

[6] Kushi, Y.; Fernando, Q., The Crystal and Molecular Structure of Dehydrodithizone. *J. Chem. Soc. D* **1969,** (21), 1240b-1241.

[7] Schafer, M.; Curran, C., Infrared Spectra of Complexes of Metal Halides with Tetramethylurea and Tetramethylthiourea. *Inorg. Chem.* **1966,** *5* (2), 265-268.

[8] Song, L.; Lei, Y.; Yang, Z.; Lan, Y., Theoretical Study of the Electron-Donating Effects of Thiourea Ligands in Catalysis. *J. Mol. Struct.* **2014,** *1074*, 527-533.

[9] Raper, E. S., Complexes of Heterocyclic Thione Donors. *Coord. Chem. Rev.* **1985,** *61*, 115-184.

[10] Kimani, M. M.; Brumaghim, J. L.; VanDerveer, D., Probing the Antioxidant Action of Selenium and Sulfur Using Cu(I)-Chalcogenone Tris(Pyrazolyl)Methane and -Borate Complexes. *Inorg. Chem.* **2010,** *49* (20), 9200-9211.

[11] Pan, J.-H.; Yang, M.; Gao, Q.; Zhu, N.-Y.; Yang, D., Bulky Thioureas as New Ligands for Gold(I)-Catalyzed Cyclization of Acetylenic 1,3-Dicarbonyl Compounds. *Synthesis* **2007,** *2007* (16), 2539-2544.

[12] Srinivas, K.; Naga Babu, C.; Prabusankar, G., Linear Cu(I) Chalcogenones: Synthesis and Application in Borylation of Unsymmetrical Alkynes. *Dalton Trans.* **2015,** *44* (35), 15636-15644.

[13] Moraes, L. C.; Lacroix, B.; Figueiredo, R. C.; Lara, P.; Rojo, J.; Conejero, S., Stabilisation of Gold Nanoparticles by N-Heterocyclic Thiones. *Dalton Trans.* **2017,** *46* (26), 8367-8371.

[14] Alvarado, E.; Badaj, A. C.; Larocque, T. G.; Lavoie, G. G., N-Heterocyclic Carbenes and Imidazole-2-Thiones as Ligands for the Gold(I)-Catalysed Hydroamination of Phenylacetylene. *Chem. Eur. J.* **2012,** *18* (38), 12112-12121.

[15] Kimani, M. M.; Watts, D.; Graham, L. A.; Rabinovich, D.; Yap, G. P. A.; Brumaghim, J. L., Dinuclear Copper(I) Complexes with N-Heterocyclic Thione and Selone Ligands: Synthesis, Characterization, and Electrochemical Studies. *Dalton Trans.* **2015,** *44* (37), 16313-16324.

[16] Liu, X.; Duan, X.; Peng, P.; Zheng, W., Hydrothermal Synthesis of Copper Selenides with Controllable Phases and Morphologies from an Ionic Liquid Precursor. *Nanoscale* **2011,** *3* (12), 5090-5095.

[17] Nelson, D. J.; Nahra, F.; Patrick, S. R.; Cordes, D. B.; Slawin, A. M. Z.; Nolan, S. P., Exploring the Coordination of Cyclic Selenoureas to Gold(I). *Organometallics* **2014,** *33* (13), 3640-3645.

[18] Paas, M.; Wibbeling, B.; Fröhlich, R.; Hahn, F. E., Silver and Rhodium Complexes of Stable, Monomeric Imidazolidin-2-Ylidenes: Synthesis, Reactivity and Decomposition Pathway. *Eur. J. Inorg. Chem.* **2005,** *2006* (1), 158-162.

[19] Matsumura, T.; Nakada, M., Preparation of Imidazolinium Salts by the Pd-Catalyzed Reduction of Thioureas with Triethylsilane and Trialkylsilyl Triflate. *Tetrahedron Lett.* **2014,** *55* (8), 1412-1415.

[20] Yang, D.; Chen, Y. C.; Zhu, N. Y., Sterically Bulky Thioureas as Air- and Moisture-Stable Ligands for Pd-Catalyzed Heck Reactions of Aryl Halides. *Org. Lett.* **2004,** *6* (10), 1577-1580.

[21] Wilson, K.; Lee, A., Applications of Xps to the Study of Inorganic Compounds. In *Spectroscopic Properties of Inorganic and Organometallic Compounds: Techniques, Materials and Applications*, The Royal Society of Chemistry: 2010; Vol. 41, pp 72-86.

[22] Graf, N.; Yegen, E.; Gross, T.; Lippitz, A.; Weigel, W.; Krakert, S.; Terfort, A.; Unger, W. E. S., XPS and NEXAFS Studies of Aliphatic and Aromatic Amine Species on Functionalized Surfaces. *Surf. Sci.* **2009,** *603* (18), 2849-2860.

[23] Castner, D. G.; Hinds, K.; Grainger, D. W., X-Ray Photoelectron Spectroscopy Sulfur 2p Study of Organic Thiol and Disulfide Binding Interactions with Gold Surfaces. *Langmuir* **1996,** *12*, 5083-5086.

[24] Sun, F.; Grainger, D. W.; Castner, D. G.; Leach-Scampavia, D. K., Adsorption of Ultrathin Films of Sulfur-Containing Siloxane Oligomers on Gold Surfaces and Their in Situ Modification. *Macromol.* **1994,** *27* (11), 3053-3062.

[25] Nuzzo, R. G.; Zegarski, B. R.; Dubois, L. H., Fundamental Studies of the Chemisorption of Organosulfur Compounds on Gold(111). Implications for Molecular Self-Assembly on Gold Surfaces. *J. Am. Chem. Soc.* **1987,** *109* (3), 733-740.

[26] Ning, Y.; Xie, H.; Xing, H.; Deng, W.; Yang, D., Comparison of Self-Assembled Monolayers of N-Alkanethiols and Phenylthioureas on the Surface of Gold. *Surf. Interface Anal.* **1996,** *24* (9), 667-670.

[27] Srinivasan, V.; Walton, R. A., X-Ray Photoelectron Spectra of Inorganic Molecules.: Xx. Observations Concerning the Sulfur 2p Binding Energies in Metal Complexes of Thiourea. *Inorg. Chim. Acta* **1977,** *25*, L85-L86.

[28] Hagström, A. L.; Fahlman, A., The Electronic Structure of PbSe and its Interaction with O2 Adsorbate Layers. *Phys. Script.* **1977,** *16* (5-6), 432.

CHAPTER 6
CONCLUSIONS AND OUTLOOK

6.1 Conclusions

This thesis described the design, synthesis and study of new surface modifier materials on metal oxide and metal surfaces. The overarching goal was to develop compounds that could reduce the work function of relatively high work function materials to be used as electrodes in organic and optoelectronic devices, through systematic studies that could separate multiple factors to be examined closely individually. This thesis describes investigations of dipolar compounds incorporating N, O, P, and/or S atoms as monolayers and multilayers on ITO and Au.

Chapter 2 discusses the ability of aliphatic amine *N*-oxides to reduce the work function of ITO, with the reduction depending on thickness of the film. The goal of this chapter was to determine the effect of an *N*-oxide group, which had been used in literature as side groups on conjugated material. Although the films could be removed with polar solvents, 1.5 nm was sufficient to reduce to WF to 3.8 eV. The *N*-oxide group, which is very polar, induced large surface dipoles, and led to better adhesion to ITO than amines. The next step for this project would be to translate the material into devices to test its effectiveness in performing as a surface modifier on electron selective electrodes. In addition, probing the physical surface with methods such as atomic force microscopy (AFM) would be useful in giving surface morphological data to determine whether there is uniform coverage or the presence of islands. The presence of islands would lead to detrimental effects in a device and this is a critical question that must be answered prior to device fabrication in case of introducing unwanted pinholes.

Chapter 3 discusses the role of a series of N-heterocyclic carbenes as surface modifiers to planar Au. The collaborative work has already been cited ten times since its publication in April 2017. Most of the compounds were synthesized by the Sadighi group, electrical measurements performed by the Kippelen group, and critical computations by Dr. Alexander Hyla and the Brédas group. The experimental work function of all NHC-modified gold surfaces showed low WF of less than 3.5 eV by UPS and calculations helped elucidate the mode of binding among the compounds. We determined that an NHC with a bulky Dipp substituent bound differently and had different work-function reducing contributions compared with a smaller iPr substituted NHC. The NHC surface modifiers were also incorporated in devices and demonstrated diode-like behavior. Further work in this chapter would examine the work function reduction of other metals. The NHC-Au robustness, stability and work function reducing ability have been characterized and the utility of NHC in other systems is worth exploring.

Chapter 4 discusses the role of phosphine sulfide phosphines and a phosphine sulfide, all of which were synthesized by Dr. Thomas Morgan of the Christoph Fahrni group. These ligands demonstrated high selectivity and binding affinity towards Cu(I) in biological studies. However, they were explored on planar gold surfaces in this chapter, to determine whether the PSPs could reduce the work function of gold and whether they were bound robustly. Thick films (ca. 5–8 nm) of PSPs could reduce the WF of gold to 4.0 eV. Although this is not as low as for NHCs studied in Chapter 3, the films were robust to 10 min of sonication, washing away multilayers but still resulting in thin films. It was deduced that the phosphine and phosphine sulfides are responsible for reducing the WF of gold, but the PS are necessary to form robust bonds to gold (not conclusively drawn from this study

but from inference). A preliminary study using Cu surfaces demonstrated that PSPs may be more suitable surface modifiers for Cu, the modified-surface of which had a WF of 3.86 eV (clean Cu has a reported WF of 4.4 eV). Although there has been one example in the literature of a PS derivative utilized as an electron selective interfacial layer (the compound was processed on top of the active layer in OPV device architecture with the Au evaporated on top), they did not measure the work function of the modified metal. This chapter demonstrates the first reported work function values for PSP modified gold. The outlook for this chapter will be discussed collectively with that for Chapter 5.

Chapter 5 discusses the role of N-heterocyclic thiones and selones, all of which were synthesized by Abraham Jordan of the Joseph Sadighi group and members of the Daniel Rabinovich group at UNC Charlotte, who donated their compounds to the Sadighi group, who in turn donated them for this study. Similar to the previous conclusions, the NHT and NHSes reduced the work function of modified gold to as low as 3.64 eV measured by UPS, but this value varies depending on the thickness of the films. Films with thicknesses roughly consistent with monolayer coverage resulted in moderate reductions to the WF (ca. 4.5 eV), and a difference in N/Au ratios was observed between the Mes and Dipp compounds, with the C=X (X = S, Se) in the Mes compounds possibly being more accessible to the surface (not necessarily limited to the metal surface but a modified-surface as well) than in the Dipp compounds, which in turn leads to thicker multilayer formation for the Mes compounds given the same processing conditions. Although thiourea has been used as surface modifiers and been characterized on surfaces, N-heterocyclic thiones and selones have been limited to the field of coordination chemistry. Therefore, this was also the first demonstration of quantifying the reduction to the work function of planar gold

surfaces with NHTs and NHSe derivatives. The prospects for this chapter will be discussed below collectively with Chapter 4.

Chapter 4 and Chapter 5 both introduced new ligands that are typically used for binding to metal atoms or nanoparticles. The PSPs had P=S groups that were of interest and the NHTs/NHSes had N–C=S/Se groups that were of interest. As indicated in the introduction, sulfur and polarizable atoms bind strongly to metals, and in this case gold. Both were expected to form strong dipoles in one direction (negative pole towards the S/Se atom) and thus make a large contribution to the molecular dipole. In both cases, thin films could be achieved through removal of excess physisorbed material by sonication. However, to quantify the percent monolayer formed, and to utilize better optimization conditions, first, collaboration with a theoretical chemist who can model the preferred binding geometry of surface modifiers on the surface should be pursued. This type of collaboration was realized for Chapter 3, but not for the other studies.

With accurate footprints and packing density of the surface modifiers, one can use the N/Au or S/Au ratios from the XPS more effectively especially for optimization conditions to determine whether a monolayer has formed and when washing, whether multilayers were washed away only, or whether surface bound modifiers were removed as well. The first optimization that should be performed is with at least 24 h of immersion and possibly annealing at higher temperatures for longer durations to complete binding. Since an appreciable amount of surface modifier remains on the surface after washing, the remainder of the compounds are likely chemisorbed. Therefore, kinetic studies to determine the rate of binding should be pursued for both the PSPs and NHT/NHSe's since they are new binding groups to materials chemistry.

Although the shifts in the XPS were used to determine which direction the net charge flowed upon binding of the surface modifier to the metal, a powerful tool that is described in CHAPTER 1, called IRRAS, can be used to determine binding modes. IRRAS is a surface IR technique that detects shifts in the vibrational energy between neat compound and surface-confined compound. The position of the P=S to lower frequencies is indicative binding from the S of the PS group.[1-3] This has been reported for gold complexes with the frequency of the P=S band in $Ph_3P=S$ shifting from 638 cm^{-1} to 589 cm^{-1} in a $R_3P=S–Au–Br$ complex.[4] Unfortunately, this could not be carried out due to the lack at Georgia Tech of an instrument capable of detecting absorption in the required spectral range. For the NHTs, Schafer and Curran's study of tetramethylthiourea complexes can be referenced, which show that the antisymmetric NCN stretch shifts toward higher frequency (from 1504 cm^{-1} to 1544 cm^{-1} in $ZnCl_2(tmtu)_2$ complexes) and C=S stretch shifts towards lower frequency (from 1126 cm^{-1} to 1104 cm^{-1}).[5] The shifts in the IR are more noticeable than in the XPS and this technique would give insight to whether the groups are bound as expected and how different that shift is compared to just a phosphine or just a thiourea.

Stability tests to time, temperature, and washing cycles should be performed to verify the robustness of the modified surfaces to these treatment conditions. Examples of these types of tests are thoroughly demonstrated in Zhou et al.[6] The binding strength can be tested by immersing a modified substrate in water and measuring the effect of stirring or sonication (for prolonged periods up to 1 h) on the work function. Thermal stability can be tested by annealing a modified substrate on a hot plate at increasingly elevated temperatures for a set period of time to measure the effect of temperature on the work

function. Modified surfaces can also be remeasured for the work function repeatedly over the course of a month or year.

The modified surfaces should also be characterized by scanning tunneling microscopy (STM). For Chapters 4 and 5, STM can provide a picture of the packing arrangement on the surface to determine the ordering and possible voids of the monolayers, as was done by Crudden et al. with NHCs on gold, which are similar in size to NHTs/NHSes.[7] Contact angle can be used to determine to determine monolayer formation (by comparing the contact angle of the modified-surface with the known value expected from a monolayer), and also be used to calculate surface energy and wettability. This is important to verify that a modified electrode will be compatible with an active layer in the case of OPVs that is solution cast or evaporated on top of the modified surface. These types of measurements, however, may be less reliable when the surface modifier is not covalently bound and can dissolve in the probe liquid.

Finally, if the ligands prove to be stable, robust, and work function reducing, they should progress to the next step, which is incorporation in devices. Since work function reducing compounds are sought to reduce the work function of electrodes to be used in devices, it is critical to provide evidence that these surface modifiers were effective electron selective electrodes. Depending on the properties of each surface modifier, the suitable device and architecture may differ. There may also be a tradeoff in work function reduction and sufficiently thin films for tunneling. For example, thin films may allow for charge tunneling but result in less WF reduction than thick films, which may result in large work function changes but are too insulating. Therefore, designing effective surface modifiers would require finding a balance between these two measurables.

6.2 References

[1] Zingaro, R. A., Phosphine Sulfides and Selenides: The Phosphorus-Sulfur and Phosphorus-Selenium Stretching Frequencies. *Inorg. Chem.* **1963,** *2* (1), 192-196.

[2] Chremos, G. N.; Zingaro, R. A., Correlation of Metal-Chalcogen Stretching Frequencies of Some Trialkyl Group Va Chalcogenides. *J. Organomet. Chem.* **1970,** *22* (3), 647-651.

[3] Kincaid, J.; Nakamoto, K.; Tiethof, J. A.; Meek, D. W., Vibrational Spectra of Some Phosphine Sulfides and Their Cu(I) Complexes. *Spectrochim. Acta Mol. Spectr.* **1974,** *30* (11), 2091-2101.

[4] Ahmad, S.; Isab, A. A.; Perzanowski, H. P.; Hussain, M. S.; Akhtar, M. N., Gold(I) Complexes with Tertiary Phosphine Sulfide Ligands. *Trans. Metal Chem.* **2002,** *27* (2), 177-183.

[5] Schafer, M.; Curran, C., Infrared Spectra of Complexes of Metal Halides with Tetramethylurea and Tetramethylthiourea. *Inorg. Chem.* **1966,** *5* (2), 265-268.

[6] Zhou, Y.; Fuentes-Hernandez, C.; Shim, J.; Meyer, J.; Giordano, A. J.; Li, H.; Winget, P.; Papadopoulos, T.; Cheun, H.; Kim, J.; Fenoll, M.; Dindar, A.; Haske, W.; Najafabadi, E.; Khan, T. M.; Sojoudi, H.; Barlow, S.; Graham, S.; Brédas, J.-L.; Marder, S. R.; Kahn, A.; Kippelen, B., A Universal Method to Produce Low-Work Function Electrodes for Organic Electronics. *Science* **2012,** *336* (6079), 327-32.

[7] Crudden, C. M.; Horton, J. H.; Ebralidze, II; Zenkina, O. V.; McLean, A. B.; Drevniok, B.; She, Z.; Kraatz, H. B.; Mosey, N. J.; Seki, T.; Keske, E. C.; Leake, J. D.; Rousina-Webb, A.; Wu, G., Ultra Stable Self-Assembled Monolayers of N-Heterocyclic Carbenes on Gold. *Nat. Chem.* **2014,** *6* (5), 409-14.

APPENDIX A
RESEARCH COLLABORATIONS

A.1 CCHF FUNDED WITH KAIST IN SOUTH KOREA

This work can be found at Gwon, D., Hwang, H., Kim, H. K., Marder, S. R., Chang, S., Synthesis of 8-Aminoquinolines by Using Carbamate Reagents: Facile Installation and Deprotection of Practical Amidating Groups. *Chem. Eur. J.* **2015**, *21*, 17200–17204. DOI: 10.1002/chem.201503511.

This work was an international collaboration funded by the NSF funded Center for Selective C-H Functionalization (CCHF). As part of the Science Across Virtual Institutes (SAVI) program the CCHF has helped establish the Virtual Institute for C–H Functionalization (VICHF). This allows student and scholar exchange from the US to Japan, South Korea, Germany, and the United Kingdom and vice versa.

Abstract: Described herein is the development of practical routes to 8-aminoquinolines by using readily installable and easily deprotectable amidating reagents. Two scalable procedures were optimized under Rh(III)-catalyzed conditions: i) the use of pre-generated chlorocarbamates and ii) a two-step one-pot process that directly employs carbamates. Both approaches are highly convenient for the gram-scale synthesis of 8-aminoquinolines under mild conditions. Facile deprotection of the synthetically versatile amidating groups was achieved under the Pd-catalyzed transfer hydrogenation conditions with simultaneous deoxygenation of quinoline *N*-oxides, thus yielding 8-aminoquinolines in excellent overall efficiency.

A.2 NSF IGERT FUNDED WITH PEERS AT GEORGIA TECH

This work can be found at Tervo, E., Agbim, K., DeAngelis, F., Hernandez, J., Kim, H. K., Odukomaiya, A. An Economic Analysis of Residential Photovoltaic Systems with Battery Storage in the United States. *Renew. Sust. Energ. Rev.* **2018**, *94*, 1057–1066. DOI: 10.1016/j.rser.2018.06.055.

This work was an interdisciplinary collaboration across two IGERT cohorts with students in Mechanical Engineering and Chemistry at Georgia Tech. IGERT was an NSF funded fellowship program titled Integrative Graduate Education and Research Traineeship where students learned about the economics and science of sustainable energy technology.

Abstract: Residential photovoltaic systems can reduce reliance on grid electricity, which may be desirable for numerous reasons. However, the economic viability of such systems is dependent on effective use of excess electricity generation, most often through net or bi-directional metering. With recent cost reductions in residential-scale lithium ion battery storage systems, these may be a practical alternative. In this work, we model the lifetime performance and economics of residential photovoltaics with lithium ion batteries across all 50 states in the U.S. We investigate in detail how photovoltaic size and battery capacity affect performance and cost metrics in California, Georgia, and Massachusetts. We find that with appropriate sizing, photovoltaic-battery systems can be more affordable than photovoltaics alone. We demonstrate that these systems may be competitive with grid prices when the federal investment tax credit and favorable financing terms are used, and we calculate the sell-back price required for bi-directional metering to reach cost parity with photovoltaic-battery systems in every state.